CHALMERS

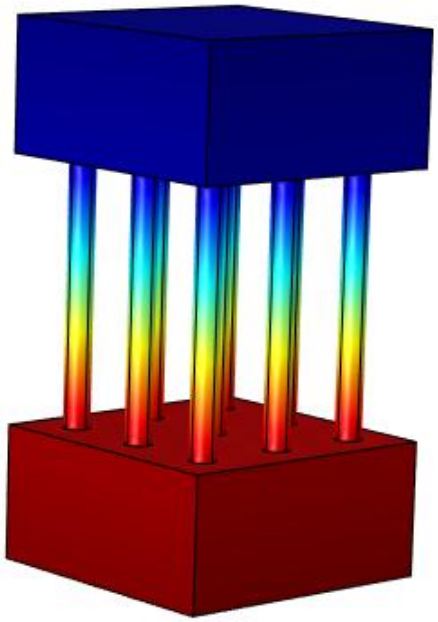

Modelling mass and heat transfer in a porous structure

Microclimate in a hygiene product

Master's Thesis within the Innovative and Sustainable Chemical Engineering programme

EMMA PERSSON

Department of Chemistry and Chemical Engineering
Division of Chemical Engineering
CHALMERS UNIVERSITY OF TECHNOLOGY
Göteborg, Sweden 2015
Master's Thesis 2015

MASTER'S THESIS

MODELLING MASS AND HEAT TRANSFER IN A POROUS STRUCTURE

MICROCLIMATE IN A HYGIENE PRODUCT

Master's Thesis within the Innovative and Sustainable Chemical Engineering programme

EMMA PERSSON

SUPERVISORS
Per Bergström
Charlotta Hanson

EXAMINER
Derek Creaser

Department of Chemistry and Chemical Engineering
Division of Chemical Engineering
CHALMERS UNIVERSITY OF TECHNOLOGY
Göteborg, Sweden 2015
Master's Thesis 2015

Modelling mass and heat transfer in a porous structure
Microclimate in a hygiene product
EMMA PERSSON

Department of Chemistry and Chemical Engineering
Division of Chemical Engineering
Chalmers University of Technology
Göteborg, Sweden
+46 (0)31-772 1000

Cover: 3D diffusion model, vapor concentration profile

Göteborg, Sweden, 2015

Abstract

The aim of this thesis was to build a model and analyze the microclimate in a diaper worn by a baby at dry state. In optimization process of product design, simulation models can often be helpful as they are versatile in parameters and geometry and not very time consuming in the analysis. To build the models used for this thesis, COMSOL Multiphysics software was used. Three different models were created; one micro model analyzing the heat transfer and fluid flow in the product, one diffusion model investigating the effect of diffusion through the outer layer on the product and one larger macro model combining the two previous models. The results show significant effects on the microclimate due to convection and radiation. As the convection occurring in the system is natural, the velocity will be low. Nevertheless, both heat and mass transfer showed clear effects when the phenomenon was disconnected resulting in a warmer and more moist product. The radiative effect could be observed in the temperature profile but would not affect the concentration of vapor in the system.

The analysis showed that the convective effects in the microclimate would benefit from a material with a high porosity. The permeability properties in the material would increase as a result of a higher porosity, resulting in a better convective flow. This is however only valid during the period the product is still dry and will need to be investigated further for liquid phases.

The surface area ratio between a 20µm thick outer film of the product and the micro pores covering the layer could be observed to $2.14 \cdot 10^{-2}$ % in order to diffuse 1000g H_2O/m^2day. The model only demonstrates an ideal situation in the film with vertical cylindrical shaped channels. To approximate a more reality like situation with longer pathways through the film, the length of the channels can be extended and the ratio may be observed for any length. In order to make this process easier for the user, an application app of the model was built allowing the user to insert new parameters of the film without any extensive knowledge about the software used.

Keywords: microclimate, COMSOL modelling, porous media, breathable films, thermal radiation, convection, conductivity, gas diffusion

Acknowledgements

I would first like to express my gratitude to my supervisors at SCA for letting me take on this project. Without the great input I received from Charlotta Hanson in the theoretical part of the project including the analysis, I would not have been able to achieve such clear results. The help and support I received by Per Bergström whenever I got stuck creating the models proved to be very helpful, as I don't think I would have gotten this far in the limited amount of time without his input. Special thanks go to my examiner Derek Creaser who always seemed to find time to look through my written text and answer any question I might have. I would also want to thank Björn Jedvik at COMSOL support team, whom I could always call or text with both practical and theoretical questions concerning the software. My understanding of the software would not be as good as it is today without all the help I received from you. Finally, I want to thank my family who has always supported me and become my rock through all my years of studies.

Nomenclature

Roman upper-case letters

$C_{p,i}$	Specific heat at constant pressure ($J \cdot kg^{-1} \cdot K^{-1}$)
D_{ij}	Effective diffusion constant for the *ij* gas system in clear fluid ($m^2 \cdot s^{-1}$)
F_{ij}	View factor from element *i* to *j*.
$\boldsymbol{F}$	Volume force ($N \cdot m^{-3}$)
J_i	Molecular flux of component *i* ($mol \cdot m^{-2} \cdot s^{-1}$)
Ra	Rayleigh number
RH	Relative humidity
T	Temperature (K)

Roman lower-case letters

c_i	Concentration of component *i* ($mol \cdot m^{-3}$)
$\boldsymbol{g}$	Gravitational constant ($m \cdot s^{-2}$)
k	Thermal conductivity ($W \cdot m^{-1} \cdot K^{-1}$)
p	Pressure (Pa)
q_c	Conductive thermal energy flux ($W \cdot m^{-2}$)
q_r	Net radiative thermal energy flux ($W \cdot m^{-2}$)
$\boldsymbol{u}$	Darcy's velocity of the fluid ($m \cdot s^{-1}$)
x_i	Mole fraction of component *i*

Greek letters

σ	Stefan-Boltzmann constant (5.67×10^{-8} W K^{-4} m^{-2})
β	Volumetric thermal expansion coefficient of fluid (K^{-1})
β_s	Absorption constant of fiber
μ	Dynamic viscosity of fluid (Pa·s)
$\bar{\mu}$	Effective dynamic viscosity of fluid (Pa·s)
ε	Surface emissivity of fiber
ϵ_p	Porosity of fiber material
ψ	Porous media factor
ρ_i	Density of material *i* ($kg \cdot m^{-3}$)
φ_i	Volume fraction of material
κ	Permeability of material (m^2)
τ	Tortuosity of fiber

Content

1

Introduction

The amount of studies conducted on heat and mass transfer in porous media has increased significantly during the last three decades. These studies are of great importance as they can be used for a wide range of applications; typically for various sorts of clothing, insulation materials and drying of food products [1]. An understanding of the fundamental mechanisms inside a specific media will allow models to be used for evaluation and optimization of product design. A large number of studies have been conducted on saturated porous media with a fluid flow, commonly liquid. However, less is known about the gas transport in a dry material and what physical phenomena are of primary importance in such situations [1].

SCA is a leading global hygiene and forest products company. The group develops and produces a number of products for personal care, tissues and forest products and is conducting sales under a number of leading global names such as TENA and Tork. The products are under constant development, and to further understand what areas in the product are most interesting for the development stage an analysis of the product's microclimate could be proven helpful.

1.1 Background

Knowledge of the microclimate in a hygiene product worn close to the human body is of importance for the functionality and comfort of the wearer. To achieve the desired properties in the product, a well-designed structure for mass and heat transport is necessary. As the microclimate formed within the product is determined by the body of the wearer, the construction of the product as well as the heat and mass transfer in the system are all factors that need to be considered in order to optimize the product. With many different factors to consider, a very large quantity of data will be necessary to analyze in order to reach optimization. This can often be proven difficult to manage when carrying out an analysis experimentally. Computing a model of the system is therefore preferable as the amount of inputs can be substantial and a graphical solution is possible.

1.2 Purpose & Goals

The aim of this thesis is to create a model of the microclimate in a porous structure, to be applied in a diaper worn by a baby.

As the main focus of the study is to observe the gas and heat transfer, any potential liquid flow will be neglected as well as a potential liquid phase adsorption/desorption within the porous structure.

Some primary questions to be investigated are the following:

- When is the effect of convection essential for the modelling of the microclimate?
- Is the effect of heat radiation in the microclimate of importance?
- What surface area ratio between pores and film would be desired for an ideal outer film of the product?

To answer the questions, COMSOL Multiphysics software will be used. A smaller extendable part of the diaper will be observed in the study, as a sub-model to determine the appropriate conditions for the whole product. This model will analyze the effects of convection, radiation and conduction through the structure. A second micro model will be used to investigate the diffusivity of the outer layer of the diaper, before building one macro model of the product with diffusivity included.

1.3 Assumptions & simplifications

During the modelling several assumptions and simplifications will be made:

The system of the product will be a simplified to a 2D geometry. This is a reasonable assumption as the properties of the diaper cross section are close to uniform throughout the whole product, and can therefore easily be applied in a 3D product.

The fiber structure is assumed to be isotropic in fiber arrangement and material properties as well as homogenous throughout the structure.

Any complex skin models of the body surface will be neglected, the emitted heat and vapor concentration from the body will be viewed as constant.

In order to observe the full potential of the product itself, no isolating material such as clothes will be applied as an outer boundary.

The initial air outside the product is set to be stagnant.

2

Theory

This theory chapter will provide a description of the main transport phenomena for heat and gas transfer in a porous structure, as well as a mathematical analysis of the interactions occurring.

2.1 Theoretical background

2.1.1 Product analysis

Hygiene products such as diapers are commonly used across the globe. The product can come in many different sizes and shapes, but the cross section is in general the same.

As shown in Figure 2.1, the diaper consists of four distinctive layers: One thin non-woven layer of fiber material close to the body (1) usually made by synthetic fibers such as polypropylene. One thicker layer made out of synthetic fibers (2) on top of one or two layers of the main pulp material (3). The porosity of the pulp layers can vary as well as the content and thickness. If there are two pulp layers one is generally much thicker than the other and includes some super absorbent polymers (SAP) for improved absorption properties. In addition, there is one polymer film on the outer surface of the product towards the surrounding air (4). This film will keep the main part of liquid within the product and prevent it from leaking out to the surrounding [2]. The figure depicts the approximate relative thickness of each layer in the model, although layer 3 can vary significantly depending on the product.

Figure 2.1, Diaper cross section

2.1.2 Porous medium

A porous medium is a medium typically filled with structures such as granular solids, foams or fibers. Typically when fibers are used the porosity of the media is increased to over 90%. Such high porosity is mainly due to the complex surface chemistry and the irregular form of the fibers [3]. The medium usually undergoes some changes due to condensation of vapor, swelling in the fibers or other deformations but will be viewed as a rigid structure in this analysis.

As can be seen in Figure 2.2, describing the fibers as uniform can be viewed as almost impossible as the exact shape and size distribution is highly irregular through the medium. This is a common problem in natural materials such as pulp. Since there rarely is any information regarding the consistency of properties in the material, various parameters are usually set as constant in a porous medium. As the material for the analysis is only observed in a macro scale, the medium can be seen as close to homogenous, thus regarding properties as constant is a valid assumption.

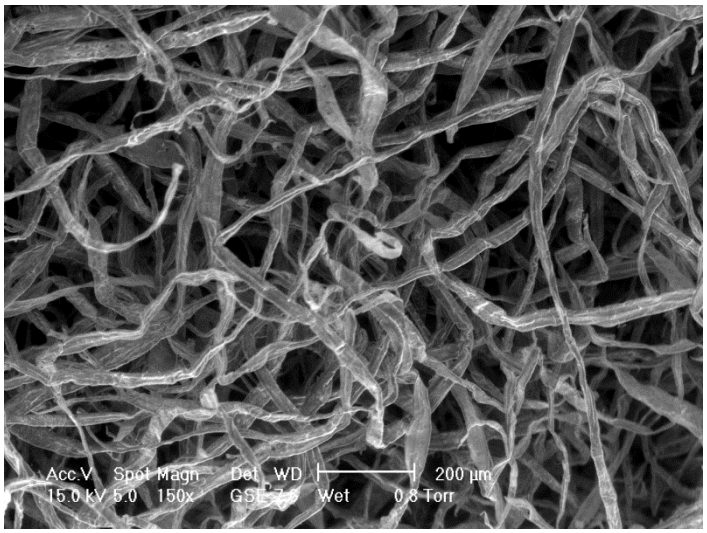

Figure 2.2 Pulp fiber [2]

2.1.3 Outer film

The thin outer-layer of the product consists of a breathable microporous film. This film consists of solid man-made polymers such as polyethylene or polypropylene with additional inorganic fillers. One of the most common fillers is calcium carbonate ($CaCO_3$) [2, 4]. As the polymers are man-made, their shape and position are more uniform than in the case of natural fibers and can more easily be chosen after desired properties [5].

Breathable microporous films usually contain billions of small pores. Many of the micro pores are connected to each other creating channels through the film. The main function of the film is, in addition to keep the main layers of the product in place, to stop any leaking of liquid to occur. It is however of importance that vapor is able to transport through the film, in order to allow it to be breathable. Therefore the size of the pores needs to be much larger than the vapor molecules, but small enough to prevent any penetration of liquid [4].

To form the pores in the film, the plastic usually undergoes stress cracking by stretching the material mechanically. Due to the presence of fillers, the stretching can be done under normal ambient conditions and become more controlled [4]. Even though the polymers are more uniform than in natural fibers, the shape and size of the pores generally varies a lot as the channels created takes different paths through the layer. This will result in different distances for the moist air to travel in the medium and a uniform transport time cannot be guaranteed. Figure 2.3 shows a typical polymer-$CaCO_3$ structure with some possible paths for the vapor to travel.

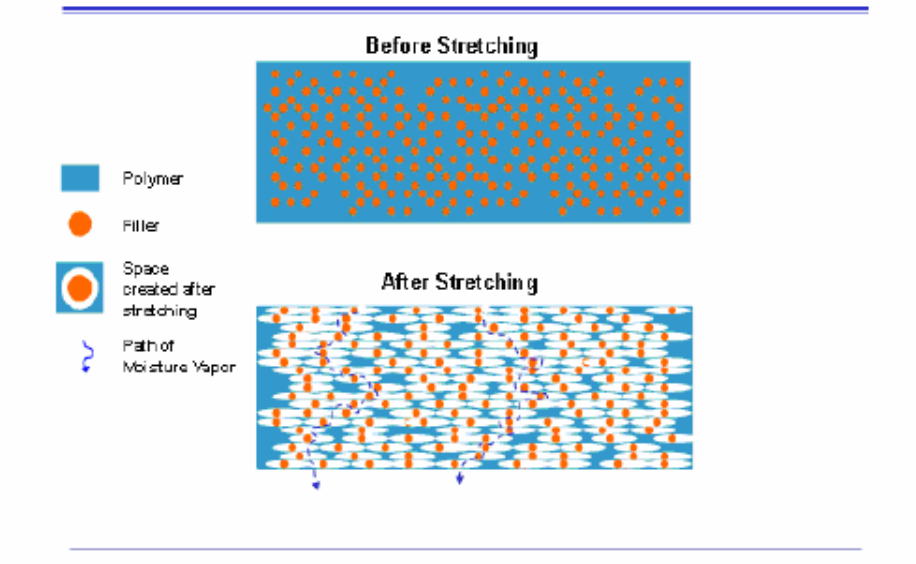

Figure 2.3 Migration of moisture vapor through a microporous film [4]

2.2 Gas Transport Mechanisms

The fluid moves through the porous structure mainly due to convection and diffusion induced by pressure and concentration gradients. Due to the fact that condensation is not observed, the vapor will in this case be regarded as a regular gas without any phase changes.

The free fluid flow is defined by the Navier-Stokes (or Stokes) equation and is the fundamental expression for the motion of fluids [5]. For a compressible Newtonian fluid, it is defined as

$$\underbrace{\rho_f \frac{\partial \boldsymbol{u}}{\partial t} + \rho_f \boldsymbol{u}\nabla \cdot \boldsymbol{u}}_{1} = \underbrace{-\nabla p\boldsymbol{I}}_{2} + \underbrace{\nabla \cdot (\mu(\nabla \boldsymbol{u} + (\nabla \boldsymbol{u})^T) - \frac{2}{3}\mu(\nabla \cdot \boldsymbol{u})\boldsymbol{I})}_{3} + \underbrace{\boldsymbol{F}}_{4} \tag{2.1}$$

With inertial forces (1), pressure forces (2), viscous forces (3) and external forces applied on the fluid (4).

2.2.1 Convective mass transfer

Convective transport processes can exist both for mass and heat processes (see section 2.3.1) and are classified according to the nature of the flow. If an external source to the flow is present, such as a fan or a pump, then the convection is forced. If however, the fluid is allowed to flow freely only driven by temperature differences in the domain the convection is regarded natural [6]. The following two sub-sections will show the fundamentals of convective mass transfer.

2.2.1.1 Darcy's law

Flow of fluids through a porous medium can be explained by Darcy's law if it is laminar (low Reynolds number). As natural flows through porous structures generally are laminar, the correlation is commonly used [6]. The equation states that the velocity is directly proportional to the pressure gradient (∇p) of the gas phase.

$$\boldsymbol{u} = -\frac{\kappa}{\mu}\frac{\partial p}{\partial x} = -\frac{\kappa}{\mu}\nabla p \tag{2.2}$$

Rearranged

$$\nabla p = -\frac{\mu}{\kappa}\boldsymbol{u} \tag{2.3}$$

Where $\boldsymbol{u}$ is the Darcy's velocity of the fluid, μ the dynamic viscosity of the fluid and κ the permeability of the bed defining the resistance of fluid flow through the medium.

This equation is a different form of the momentum equation from the Navier-Stokes (Equation 2.1), with the assumption of a continuum media [7].

2.2.1.2 Brinkman extension

Darcy's law is only applicable in regions without any boundary shear flow, such as away from walls. Since porous structures consist of a considerable amount of wall surfaces, an extension including the wall effects needs to be added to the momentum equation. The Brinkman extension of Darcy's law can be used for this, as defined in equation 2.4 [6].

$$\nabla p = -\frac{\mu}{\kappa}\boldsymbol{u} + \bar{\mu}\nabla^2\boldsymbol{u} \tag{2.4}$$

As can be seen in the Brinkman's equation, there are two viscous terms. The first is identified as the Darcy's term (Equation 2.3) and the second is a Laplacian term that is normally included in the Navier-Stokes equation (Equation 2.1). By using this extension the sheer stress will be accounted for, as a relationship between the permeability and the porosity is formed. This approximation by Brinkman has been analyzed in several studies and it has been concluded that it is only valid for highly porous media ($\epsilon_p > 0.6$). One main reason for the limited validity is that in Equation 2.4 the effective viscosity coefficient $\bar{\mu}$ is set equal to the gas viscosity μ. This is usually not the case in reality as the relationship depends on the geometry of the medium [5]. With a high porosity, the volume of material is low and therefore the error will be limited enough for the equation to be valid.

2.2.2 Gas-phase diffusion

To investigate the transport of certain species in a fluid, diffusion needs to be regarded. In a porous media, the transport consists of ordinary diffusion as well as free-molecule diffusion. When calculating the diffusion in clear fluids, Fick's law is generally used [6].

For one dimension: Two dimensions or more:

$$\boldsymbol{J_i} = -D_{ij}\frac{\partial c_i}{\partial x} \qquad \boldsymbol{J_i} = -D_{ij}\nabla c_i \tag{2.5}$$

$$\frac{\partial c_i}{\partial t} = D_{ij}\frac{\partial^2 c_i}{\partial x^2} \qquad \frac{\partial c_i}{\partial t} = D_{ij}\Delta c_i \tag{2.6}$$

Where $\boldsymbol{J_i}$ is the molecular flux and x the position (length) of the medium. To apply this on a porous structure, a porous media factor is needed, here defined as ψ [8].

$$D_{ij,eff} = \psi D_{ij} \tag{2.7}$$

$$\psi = \varepsilon \cdot \tau \tag{2.8}$$

Where $D_{ij,eff}$ is the effective diffusion coefficient for the *ij* gas system in a porous media, D_{ij} the effective diffusion coefficient for the *ij* gas system in a clear fluid and τ the tortuosity of the porous media. The tortuosity factor is defined as a ratio between the length of a straight line through the porous media and the length of the tortuous path, and is only used for calculating diffusion [6]. There are several different models for calculating the tortuosity factor for a dry porous media, with the correlation made by Millington [8] being one of the most common:

$$\tau = \varepsilon^{-1/3} \tag{2.9}$$

For a fluid that is between clear ($\tau = 1$) and all gas ($\tau = 0$).

The free-molecule diffusion, also called Knudsen diffusion occurs when the pore diameter of the porous media is of the same order as the mean free path of the gas molecules. With an increased porosity and/or larger pore size in the medium, the Knudson diffusion becomes less important. As the walls in the porous media will influence the diffusion, the porous media will be accounted for without the need of an extra factor [6].

2.2.2.1 Convection coupled diffusion

The interaction between diffusion and convection has historically often been neglected but can sometimes be of great significance for the transport of species [6]. Steam has a lower molecular weight than air, as a consequence the velocity of vapor will be higher and diffusion will occur faster than for the more dense air. The main species to regard in transport equations will therefore be the water vapor.

As most vapor molecules are transported through the volume of air inside the porous material, the pressure of the air will increase. Increasing the pressure will cause the formation of convection in the gas phase; hence diffusion and convection are directly connected.

The complete transport of species in a porous media is defined as

$$\underbrace{\frac{\partial}{\partial t}\left(\epsilon_p c_i\right)_s + \frac{\partial}{\partial t}\left(\rho C_{P,i}\right)_f + \frac{\partial}{\partial t}\left(\alpha_v c_i\right)_g}_{1} + \underbrace{\boldsymbol{u}\nabla c_i}_{2} = \underbrace{\nabla \cdot \left[\left(D_i + D_{i,eff}\right)\nabla c_i\right]}_{3} + \underbrace{R_i + S_i}_{4} \tag{2.10}$$

$$\alpha_v = \epsilon_p - \varphi \tag{2.11}$$

Where (1) accounts for accumulations of species in solid, liquid and gas phases, (2) is the convection occurring in the medium and (3) explains the spreading of species *i* due to dispersion, diffusion and any possible volatilization in the gas phase. The two last terms (4) describes production and/or consumption of species *i* with R_i being the reaction rate and S_i the arbitrary source term.

2.3 Heat Transfer Mechanisms

Heat is transferred by convection of the gas, conductivity in gas and solids and radiation from surface to surface of the porous material. To define the over-all heat transfer equation for a porous material, a mathematical combination of the heat transfer in solid and gas is made [7].

Energy equation in fluid:

$$(\rho C_p)_f \frac{\partial T}{\partial t} + (\rho C_p)_f \nabla \cdot (\boldsymbol{u} T) = k_f \nabla^2 T \quad (2.12)$$

Energy equation in solid:

$$(\rho C_p)_s \frac{\partial T_s}{\partial t} = k_s \nabla^2 T_s \quad (2.13)$$

Using average values in a defined volume and assuming the heat transfer in both phases are parallel (no net heat transfer between phases), the equation becomes

$$(\rho C_p)_{eff} \frac{\partial T}{\partial t} + (\rho C_p)_f \boldsymbol{u} \cdot \nabla T = \nabla \cdot \left(k_{eff} \nabla T\right) + q_{eff} \quad (2.14)$$

Where q_{eff} is the production of heat per unit volume.

2.3.1 Convective heat transfer

As mentioned in section 2.2.1, convection is a significant contributor to the heat transfer equation. In heat transfer terms, natural convection is the phenomena of heat transport processed by fluid motion. Energy is transferred by the fluid due to temperature differences in the fluid and the medium [6]. Natural convection heat transfer is occurring solely due to the formation of buoyancy forces in the fluid caused by the density differences as the temperature changes in the medium. As a result, the buoyancy forces will create a force field as a function of the gravitational force and the density variations [5].

Natural convection is often divided in two branches; external and internal natural convection. External natural convection defines the fluid motions occurring along the surface of a medium due to heat transfer from the surface out to a large reservoir. Internal natural convection however, is the convection inside enclosures caused by the interactions from all surfaces containing the fluid [6].

When analyzing convective heat transfer, Rayleigh number (Ra) is used to characterize the transition between stable and unstable flow of natural convection [5].

$$Ra = Pr \cdot Gr = \frac{\rho^2 \boldsymbol{g} \beta C_p \Delta T \cdot L^3}{\mu \cdot k_f} \quad (2.15)$$

For air in porous media, the critical Rayleigh number is usually around 10^5. When Ra $\geq 10^5$ instability sets in and thermal convection needs to be included in the over-all heat transfer. When Ra $<10^5$ the convection is negligible and the heat transfer is assumed to occur mainly by thermal conductivity [9]. An approximate value of critical Rayleigh in free flowing air domains with a rigid and free boundary is in the magnitude of 10^3 [10].

2.3.2 Conductive heat transfer

Conductive heat transfer defines the heat transfer in all phases within the medium. When defining a one dimensional flow, the heat flux by thermal conductivity (q_c) can be defined as

$$q_c = -k\frac{\partial T}{\partial L} \tag{2.16}$$

The thermal conductivity k is influenced by a number of factors in the material observed, and even more so in polymers as the orientation of chain segments and level of crystallinity are of high importance [11]. This makes an exact value of k hard to define and can often be seen varying in literature. Due to the effect of porosity in the polymer material, an effective thermal conductivity k_{eff} is used rather than the conductivity for solids.

$$k_{eff}(x,t) = (1-\varphi)k_f + \varphi k_s \tag{2.17}$$

Where k_f and k_s are the conductivity of fluid and solid respectively

The conductivity of polymers such as pulp is generally much lower than for ceramics or metals, and can therefore be used as an effective thermal insulator [12]. The low conductivity potential is however an indication that regarding only conductivity will not be sufficient for prediction of the heat transport. This is an indication that thermal radiation and convection will be very important to include in the heat equation for a fibrous material.

2.3.3 Thermal radiation

Heat is radiated from the human body through the system and further out to the surrounding environment. A common way to view thermal radiation is as a 'radiative conductivity' where the radiation flux is proportional to the temperature gradient in the system. This is generally a valid approach when the penetration of radiation in the material is small compared to the thickness of the medium [13]. To ensure that this is the case, the medium can be defined as opaque prescribing no penetration possible [14].

Radiative heat transfer rate is generally defined as in equation 2.18

$$\frac{\partial q_{r(x)}}{\partial x} = \frac{\partial q_r^+(x)}{\partial x} - \frac{\partial q_r^-(x)}{\partial x} \tag{2.18}$$

With

$$\frac{\partial q_r^+(x)}{\partial x} = \beta_s(q_r^+(x) - \sigma T^4(x)) \tag{2.19a}$$

$$\frac{\partial q_r^-(x)}{\partial x} = -\beta_s(q_r^-(x) - \sigma T^4(x)) \quad (2.19b)$$

Where $q_r(x)$ is the net radiative thermal energy flux at the position x and $q_r^+(x)$, $q_r^-(x)$ are the radiative thermal energy flux from hot and cold surface, respectively. σ denotes the Stefan–Boltzmann constant and β_s the absorption constant.

The general equation for radiation with component *i* is defined as:

$$J_i = \varepsilon_i \sigma T_i^4 + (1 - \varepsilon_i) \sum_{j=1}^{N} F_{ij} J_j \quad (2.20)$$

Where F_{ij} is the view factor from element *i* to *j*.

As Equation 2.19ab and 2.20 show, radiation is a function of T^4. Therefore the largest differences in thermal radiation flux will be in the outer and inner layer of the media, as this is where the temperature reaches its minimum and maximum, respectively. As the same layers also dominate the convection/conductivity flux, it will be of great importance to investigate the microclimate in the outer layer of the product.

2.3.4 Parameters

Different parameters have proven to be of different significance in gas and heat transfer, it will therefore be essential to investigate some of the different effects when computing the model.

2.3.4.1 Porosity

The porosity (ϵ_p) of a material is defined as the fractional void of a total volume, thus $1 - \epsilon_p$ is defined as the fraction of solids.

$$\epsilon_p = 1 - \varphi \tag{2.21}$$

According to Nield, Bejan [5], the surface porosity (porosity in a typical cross section) for an isotropic porous material can be assumed to be equal to ϵ_p. As shown in a study made by Wu, Fan [15], increasing the fiber fractional volume (φ) will increase the effect of thermal conductivity but decrease the energy flux of thermal radiation. As thermal conductivity is dependent on the orientation of chain segments it is natural that the change in porosity will generate a change in the conductivity as well.

2.3.4.2 Relative humidity

As the body emits both heat and moisture, the water content in the air will affect various properties in gas and solids. The content of water is commonly defined as the relative humidity (*RH*) of a gas. RH is defined as the ratio between vapor partial pressure of the air and the saturation vapor pressure, as can be seen in Equation 2.22.

$$RH = \frac{p_w}{p_w^{sat}} \ [\%] \tag{2.22}$$

By assuming a constant pressure, RH can be simplified in to the amount of vapor in dry air [17]. Data for such simplification with a total pressure of 1bar can be seen in Appendix A2.

2.3.4.3 Permeability

Determining the permeability in pulp fibers has been proven difficult as pulp fibers swell when wetted and collapse with added pressure [16]. A theoretical permeability may be determined by the correlation between Darcy's law and Hagen Poiseuilles' equation, seen in Appendix A1.

With the permeability defined as follow

$$\kappa = \frac{(1-\epsilon_p)\cdot d_p^2}{32} \tag{2.23}$$

It can be seen that the permeability of the porous media is dependent on the diameter *dp* of the pores or channels inside the media. Assuming that the porosity will stay constant in the medium, this pore diameter will be proven to be a very important parameter in convection of the fluid.

By using Equation 2.23 a solely theoretical value of permeability is obtained. The numerical approximate value used for the simulations will be provided by SCA. As the porous media is assumed to be isotropic, the permeability will be scalar for each simulation.

3

Model 1 – Sub model

As mentioned in section 1.2, three different models will be created in COMSOL. The first model will be a smaller section of the product, investigating the convective flow and heat transport.

3.1 Model definition

From Figure 2.1 four different layers in the product cross section were identified. Due to the simplification of a homogenous porous structure pulp layer (layer 3 in Figure 2.1), the model will only observe one large layer. It was decided to exclude product layer 1 and 2, as a simplification in the modelling. The layers could be added on to the system in future research if required. The outer film (layer 4) of the product will not be modelled as a domain, as the meshing would be too small and inconsistent when performing simulations. This film will therefore be set as a boundary on the outer surface of the pulp material.

Considering all changes from the product cross section to a working model in COMSOL, the sub-model will consist of three different domains; a 3 mm layer of air between the product inner layer and the body surface (1), one 15 mm thick main layer of pulp (2) and one outer layer of air defining 30 mm of the environment (3). The model showcasing a 5cm piece of the product can be seen in Figure 3.1.

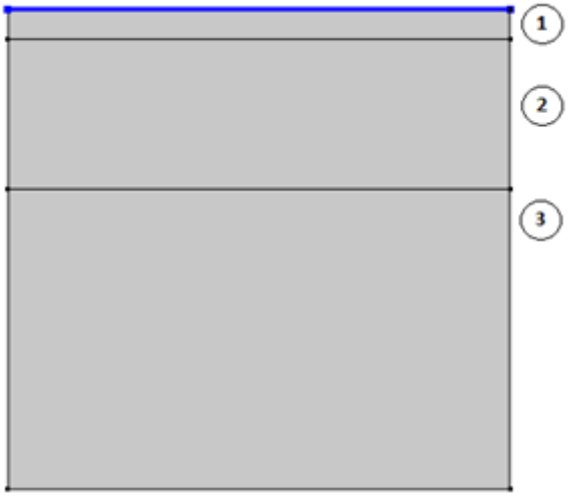

Figure 3.1 Simplified sub-model

Natural convection, thermal radiation as well as conductivity will be included in the model. The skin is simplified to have a constant temperature and concentration of steam on the upper boundary of layer 1, marked blue in Figure 3.1.

3.2 Material data

The polymer used for the porous domain and the outer surface of the product has been approximated to consist of pure pulp. Material data for pulp was obtained by a literature search and can be seen below (Table 3.1). Due to the fact that pulp can be made out of various raw materials, the values may change depending on the location of the production.

Table 3.1 Constant material properties

Material	ρ [kg/m^3]	k [W/(m·K)]	Cp [J/(kg·C)]	ε [-]
Pulp	900[17]	0.07[11]	1500[17]	0.95[17]

For the fluids in the model, air and nitrogen gas could be found as already defined in COMSOL. Any additional literature search was therefore not necessary.

The value of permeability was changed between $3.75 \cdot 10^{-11}$ to $3.75 \cdot 10^{-9}$ m^2, which can be viewed as reasonable values for the material used in the products [2].

3.3 Fluid flow

To calculate the fluid flow (convective mass transfer) through the media in Model 1, the Brinkman extension for flow in porous regions (layer 2) and the Navier-Stokes equation for flow in open regions (layer 1 and 3) are combined in COMSOL's *Free and Porous Media Flow Interface* module. In this way the same velocity and pressure fields are created throughout the whole model and the flow becomes continuous. This interface is well suited for the model as the transition between the different velocity flows in the porous media and the open surrounding regions are already accounted for [18].

The fluid flow is defined in COMSOL as shown in equations 3.1 and 3.2:

Free flowing fluid

$$\rho \frac{\partial \boldsymbol{u}}{\partial t} + \rho(\boldsymbol{u} \cdot \nabla)\boldsymbol{u} = \nabla \cdot [-p\boldsymbol{I} + \mu(\nabla \boldsymbol{u} + (\nabla \boldsymbol{u})^T)] + \boldsymbol{F} \quad (3.1)$$

$$\rho \nabla \cdot \boldsymbol{u} = 0$$

Porous media

$$\frac{\rho}{\epsilon_p}\left((\boldsymbol{u} \cdot \nabla)\frac{\boldsymbol{u}}{\epsilon_p}\right) = \nabla \cdot \left[-p\boldsymbol{I} + \frac{\mu}{\epsilon_p}(\nabla \boldsymbol{u} + (\nabla \boldsymbol{u})^T) - \frac{2\mu}{3\epsilon_p}(\nabla \cdot \boldsymbol{u})\boldsymbol{I}\right] - \left(\mu\kappa^{-1} + \beta_F|\boldsymbol{u}| + \frac{Q_{br}}{\epsilon_p^2}\right)\boldsymbol{u} + \boldsymbol{F} \quad (3.2)$$

$$\rho \nabla \cdot \boldsymbol{u} = Q_{br}$$

The equations can be identified as rearrangements of the Navier-Stokes (equation 2.1) and Brinkman (Equation 2.4) equations, where $\boldsymbol{F}$ is defined as the volume force of the regions, ϵ_p the porosity of the porous material and Q_{br} an optional source term that accounts for any possible mass deposits/creations within the regions [18]. The effect of adsorption/desorption in the porous media will not be accounted for in the model and Q_{br} will therefore not be included (=0).

3.3.1 Volume force

Since the convection occurring is natural, a gravitational term $\rho_f \boldsymbol{g}$ will need to be added on the right side of the momentum equations as an external force applied on the fluid [5]. Therefore a volume force $\boldsymbol{F}$ was defined over the whole system

$$\boldsymbol{F}_x = 0$$

$$\boldsymbol{F}_y = \rho \boldsymbol{g} \beta (T - T_{ref}) \tag{3.3}$$

In this expression, β is the volumetric thermal expansion coefficient of the fluid ($3.43 \cdot 10^{-3}$ K^{-1} for air). The addition of a gravitational term is commonly called the Boussinesq buoyancy approximation. Just as for an incompressible fluid, this reduces the equation of continuity to $\nabla \cdot \boldsymbol{u} = 0$ (conservation of mass) [5]. The Boussinesq buoyancy approximation is commonly used in problems including both natural convection and thermal surface radiation due to the complexity of the mathematical models. The simplification is valid provided that the difference in fluid density is much lower than the starting density of the fluid, as well as ΔT is insufficient to cause any significant changes of the mean values for various properties of the solid and fluid [5]. In the study conducted by Montiel Gonzalez, Hinojosa Palafox [19] it could also be concluded that the approximation is valid for $\varphi \leq 0.167$. This was determined by comparing the approximate values with the different variable properties for different Rayleigh numbers (Ra) [19]. As the study was done with the same temperature difference as for this thesis, the outcome can be assumed to be valid for this case as well.

The volume force depends on the temperature profile in the model and is iterated by the software. The temperature will therefore be defined as variable T. By defining the volume force as a Boussinesq buoyancy approximation the force becomes dependent on the temperature change. The pressure changes in the model can therefore be excluded from calculations. As the density of the fluid is dependent on the temperature change, it will be iterated by the software as well. β was set as a scalar for the model.

3.4 Heat transfer

The equation defining heat transfer through the model differs depending on if the region is porous or free flowing air. By using the module *Heat transfer in porous media* by COMSOL Multiphysics, heat transfer due to convection, conduction and radiation are all included [18]. When including Surface-to-Surface radiation (Q) interface the heat transfer equation over the model becomes

$$(\rho C_p)_{eff} \frac{\partial T}{\partial t} + \rho C_p \boldsymbol{u} \cdot \nabla T = \nabla \cdot \left(k_{eff} \nabla T\right) + Q \tag{3.4a}$$

$$\rho C_p \frac{\partial T}{\partial t} + \rho C_p \boldsymbol{u} \cdot \nabla T = \nabla \cdot (k \nabla T) + Q \quad (3.4b)$$

Which can be identified as equation 2.12 and 2.14.

Since the conduction takes place in series with the heat flux passing one region of the product before entering another, the effective thermal conductivity and heat capacity are given by equation 3.5 and 3.6, respectively [18].

$$\frac{1}{k_{eff}} = \frac{\varphi_s}{k_s} + \frac{\varphi_f}{k_f} \quad (3.5)$$

$$(\rho C_p)_{eff} = \varphi_s \rho_s C_{p,s} + \varphi_f \rho C_p \quad (3.6)$$

Where φ_f and φ_s are the volume fraction of fluid and solid respectively.

The heat transfer was defined as internal, as per definition in section 2.3.1 for porous media. Since the air in the system will change in moisture content as it flows towards the environment, it will affect the thermodynamic properties in the heat equations. To include the changes, different values of moisture content were added to the model. According to a study made by Wang and Sun [13] the relative humidity located at the surface of the skin can be approximated as 60% (domain 1 in Figure 3.2). The surrounding humidity of the air was set to a constant 30% average (domain 2 in Figure 3.2). This is a simplification as the concentration gradient of vapor is not included in the model.

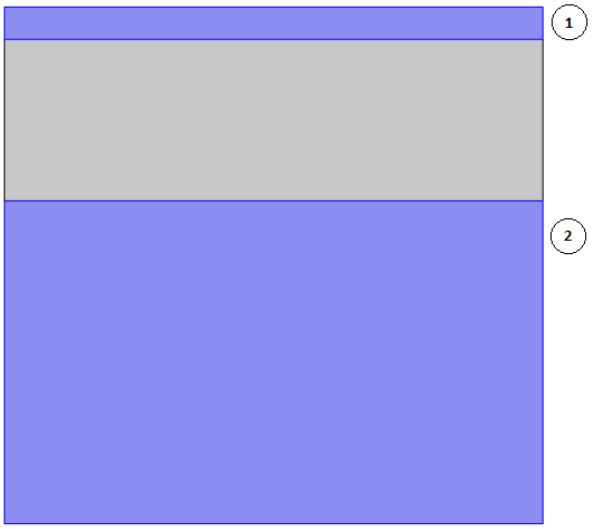

Figure 3.2 Fluid domains

3.4.1 Diffuse surface

To include surface-to-surface radiation to the heat transfer in the model, diffusive surface boundary conditions were added. This includes a view factor in calculations (Equation 2.17) [18]. As the porous domain was defined as opaque, the radiation direction could be set as opacity controlled instead of a specific direction. In this way any possible counter radiation will be accounted for.

The radiative heat source is defined as follow

$$Q = G - \varepsilon n^2 \sigma T^4 \tag{3.7}$$

$$(1 - \varepsilon)G = J - \varepsilon n^2 \sigma T^4 \tag{3.8}$$

This node was defined on the inner and outer boundary of the porous domain. The ambient temperature was defined as the variable T for layer 1 and 2 and 20˚C in the surrounding air. This was done in order to account for the temperature changes within the system. To define how much energy is emitted from the body of the wearer, a third diffuse surface was added at the surface of the skin. The surface is approximated as a black body, hence the emissivity was set to 1.

3.4.2 Thin layer

To imitate the outer film of the product, a conductive thin layer was added to the boundary between pulp and surrounding air in the heat transfer equation. The layer specifies a thickness of 20µm and highly conductive properties, with parameters given in Table 3.2. The equation for the thin layer is defined as

$$-\boldsymbol{n} \cdot \boldsymbol{q} = d_s Q_s - d_s \rho_s C_{p,s} \frac{\partial T}{\partial t} - \nabla_{\boldsymbol{t}} \cdot \boldsymbol{q_s} \tag{3.9}$$

$$\boldsymbol{q_s} = d_s k_s \nabla_{\boldsymbol{t}} T \tag{3.10}$$

Where d_s is the thickness of the layer.

3.5 Boundary conditions

Determining the correct boundary conditions for the model has proven to be crucial in order to obtain a correct simulation.

The boundary conditions at the interface between a clear fluid and a porous media is usually straight forward according to Nield, Bejan [5]. Continuity of temperature at the interface can usually be considered applicable, assuming there is a local thermodynamic equilibrium present. Therefore, variables for temperature and volume force were used through the system. As a simplification in the system, the surface temperature of the skin was set to 30˚C at all times.

A no-slip boundary condition was defined on the surface of the skin, prescribing $\boldsymbol{u}$ = 0 at the wall. This is a common and well suited condition at a stationary solid wall [18]. As the heat emitted from the body is assumed to be constant, a fixed temperature boundary of 30°C was set on the same wall.

Since the film on the outer layer of the product should be resistive for any mass transfer convection, a pointwise constraint was defined on the boundary. The constraint expression was set as $\boldsymbol{u}$, indicating that the fluid velocity is constrained to zero at the boundary.

The two ends of the product were set to symmetric both in the fluid flow and the heat transfer node, as the system only considers a small part of the real product. This prescribes no penetration or vanishing of sheer stresses and creates a mirror effect of the model [18]. By using this symmetry node, the model can be seen as axisymmetric.

For fluid flow:

$$\boldsymbol{u} \cdot \boldsymbol{n} = 0 \tag{3.11}$$

$$\boldsymbol{K} - (\boldsymbol{K} \cdot \boldsymbol{n})\boldsymbol{n} = 0 \tag{3.12}$$

$$\boldsymbol{K} = [\mu(\nabla \boldsymbol{u} + (\nabla \boldsymbol{u})^T)]\boldsymbol{n} \tag{3.13}$$

For heat transfer:

$$\boldsymbol{n} \cdot (k \nabla T) = 0 \tag{3.14}$$

As the model is observed horizontally without any possibility for the fluid to transport upwards, the different profiles will only have a minor impact on the system. Therefore the boundary conditions on the surrounding air will not affect the gas and heat flow, and could also be set as symmetric to simplify the calculation.

The surrounding environment is assumed to stay constant at a temperature of 20°C and a pressure of 1 atmosphere. These values were also defined as initial values over the whole system. Therefore, the reference temperature in equation 3.3 for volume force is equal to 20°C.

Although pressure is not calculated in the model, it still needs to be defined in order to have continuum over the system. Pointwise constraints are therefore defined on each side of the porous media as 1 atmosphere.

All boundary conditions can be seen in Appendix B1.1.

4

Model 2 – Diffusion model

The second model created in COMSOL was a diffusion model for the outer layer of the product. The potential for vapor transport through the film will be observed and analyzed from the model, in order to obtain a surface area ratio between pores and film.

4.1 Model definition

It was decided to observe 1000 g of vapor per square meter and day, as this is a common vapor flux when analyzing breathable films [2]. The actual amount of vapor emitted by the body will depend on the individual. In order to determine the effect of diffusion through the outer-layer of the product, a diffusion flux will need to be obtained. To achieve this, a micro structure model will be created and analyzed.

The model will be built as a 3D geometry in order to see possible effects in the cylindrical pores within the film. The polymers used in the film are approximated to not interact with the vapor diffusing through the material. The model will therefore only regard the fluids, thus the film itself will not be modelled. A simplified structure with straight cylinders approximated as pores can be seen in Figure 4.1a.

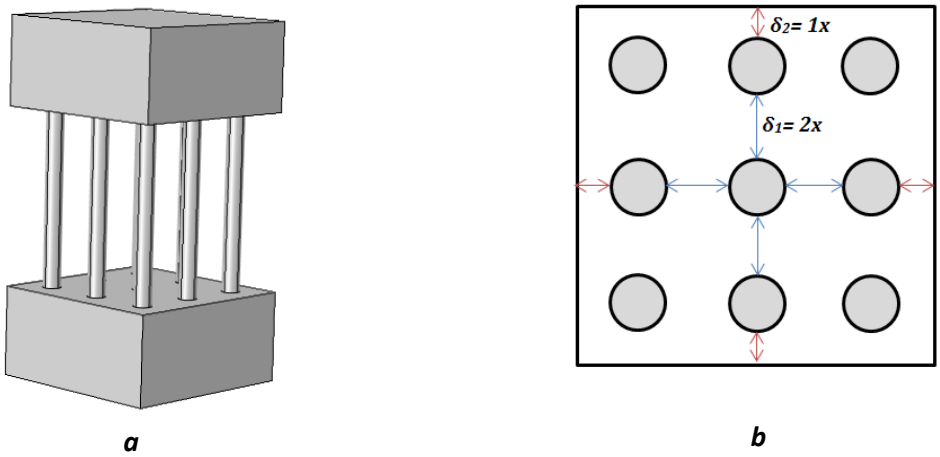

Figure 4.1 a) 3D geometry b) Pore arrangement

The micro model can be viewed as an ideal case regarding the pore geometry. As mentioned in section 2.1.3, the pores are generally much more unevenly distributed, as well as their size and shape. The number of pores included in the model was set to nine, in order to ensure that no possible side effects from the borders of the model disrupt the diffusion flux or concentration gradient. In this arrangement the middle pore can be used as a control surface when retrieving values of the fluxes, hence the focus of the analysis will be in the middle of the model. The arrangement can be seen in Figure 4.1b.

The model will also include a bulk area of saturated air on one side and nitrogen gas with zero water concentration on the other side of the film, in order to account for any possible effects in the out-/inflow of the pores. Only the concentration gradient due to diffusion will be regarded, no flow or heat transfer will be included. To imitate the experimental analysis used for films at SCA, the concentration in the two bulks will stay constant. In physical experiments there is a gas flow on each side of the film providing fresh gas and keeping the concentration constant. As the experimental analysis is made at a temperature of approximately 37.7-37.8˚C, the temperature used in physical data for simulations will be 38˚C [2]. Calculations can be seen in Appendix A4.

Due to a calculation error early in the stage of this project, the vapor concentration defined in the model was miscalculated. This resulted in an overestimation of the required diffusion flux with 15%. The results obtained from the model will however still be used and analyzed, as the effects between pore size and the diffusion flux is the main interest for this thesis, not the numerical values.

4.2 Diffusion

By using the COMSOL interface for *Transport of Diluted Species*, a predefined modelling environment is provided for transport of chemical compounds by diffusion and if wished, convection. The physics interface assumes that all chemical species present are dilute, therefore all mixture properties such as density and viscosity can be assumed to be the same as the solvent [18]. When building Model 2, the *Transport of Diluted Species* module is solely used for examining the diffusion in the outer layer. The convection is therefore neglected and the equation for transport of species becomes

$$\frac{\partial c_i}{\partial t} = \nabla \cdot (-D_i \nabla c_i) = R_i \tag{4.1}$$

$$\boldsymbol{N}_i = -D_i \nabla c_i + \boldsymbol{u} c_i \tag{4.2}$$

A starting concentration of vapor in the bottom bulk would need to be determined. By definition of the apparatus imitated, it could be assumed that RH=100% in this domain would be appropriate. Using the RH, a concentration dependence on the temperature could be calculated and inserted into COMSOL. The diffusion coefficient D_i for water and air has been determined by the use of Lennard-Jones Potential. All calculations are shown in Appendix A3.

4.3 Boundary conditions

The boundaries in the gas bulk on each side of the film was set as Symmetry nodes, hence there will be no mass flux across the boundary ($-\boldsymbol{n} \cdot \boldsymbol{N}_i = 0$). This can be seen as marked blue in figure 4.2a. The concentration was set constant at the top of each bulk, one of the surfaces shown in Figure 4.2b. With these two boundary conditions, the experimental analyses with a constant concentration will be simulated.

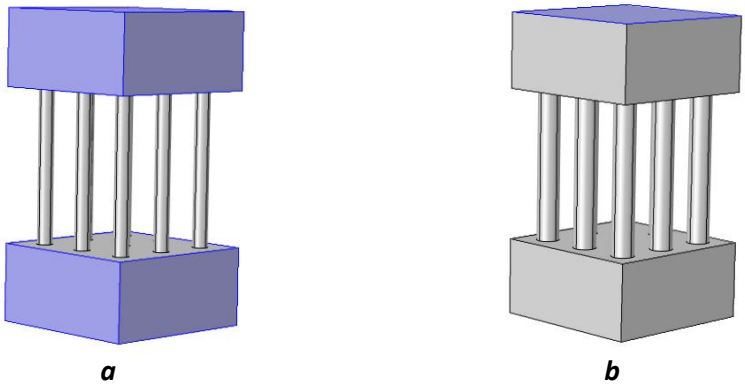

Figure 4.2 a) Symmetry nodes b) Concentration nodes

As the polymers are not supposed to interact with the diffusion, a no slip boundary condition was set on all walls of the pores as well as the bulk surface towards the pore openings, prescribing just as for the symmetry node no mass flux.

5

Model 3 – Macro model

The last model created in this study was a macro model defining a larger part of the diaper. The three layers defined in the sub-model (Figure 3.1) will be used with the same parameters, but in a more versatile geometry. The thickness of the layers will stay the same, except for the domain of surrounding air. This macro model is thought to represent the shape and dimensions of a real life situation to obtain a better overview of the temperature and concentration flux over the product and its closest surroundings.

5.1 Model definition

Figure 5.1a show the model built up in COMSOL. As can be seen, the product is bent in a circular shape with large areas of air in its surrounding. By zooming in on the product itself, the different layers can be observed. In figure 5.1b, it can be seen that the thin layer of air between the skin and the product surface is modelled as well as an additional section of pulp material on top of the product. For extra clarity in the figure, blue domains represent the pulp material. The width and height of the product section observed is 10cm (12cm high including the extra pulp domain). Convection, conduction, surface radiation and diffusion will all be observed.

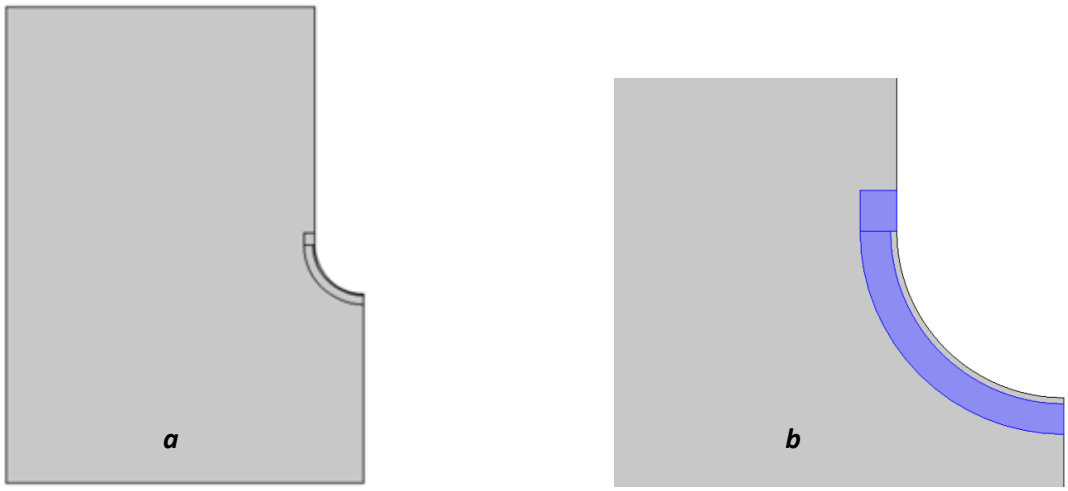

Figure 5.1 Macro model of product a) whole model b) product close up

As layer 1 is very small in comparison to the other domains, the meshing settings are of special importance to define correctly for model 3. A user defined meshing was set up for the system, adding extra cells to the thin layer of air so any interaction inside the layer can be observed. The meshing of the model is showed in Figure 5.2a.

5.2 Fluid flow

As model 3 is larger and has a more complex geometry, some changes from model 1 will need to be made. With permeability decreasing, the Rayleigh number is increasing rapidly indicating that instability is occurring in the fluid flow. Due to the instability, the *Free and Porous Media Flow interface* module was not suitable for the model as it did not support instable or turbulent flow. Instead the *Brinkman Equation interface* for COMSOL 5.1 was acquired, as this version features a function that combines turbulent flow with a porous media domain. By adding domains of free flowing fluid in the air (Figure 5.2b), equations 3.1-2 were built up manually and the momentum equation will be the same as for model 1.

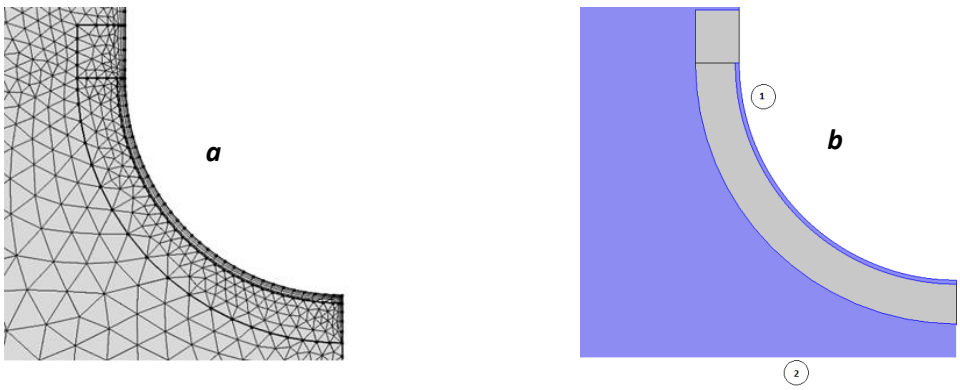

Figure 5.2 a) Mesh b) Fluid domains

5.3 Heat transfer

The COMSOL module *Heat transfer in porous media* for internal heat transfer was used in the same way as in model 1 (Section 3.4). In this way heat transfer due to convection, conduction and radiation will all be included. As diffusion also is included in the system, there will be a concentration vector of vapor present. By using the concentration of vapor instead of a fixed value of relative humidity to define the properties of parameters in humid air, a continuum will be created over the different domains.

Diffuse surfaces were added to each surface of the product as well as for the skin, just as in model 1.

5.4 Diffusion

As convection often is coupled with diffusion, it will be of importance to include the interaction effect when modelling the cross section of the product as it might affect the microclimate. By doing this, a more complete picture over the interactions occurring in the system should be obtained.

When using the *Transport of Diluted Species* module, a convection term is added and the equation is defined as

$$\frac{\partial c_i}{\partial t} = \nabla \cdot (-D_i \nabla c_i) + \boldsymbol{u} \cdot \nabla c_i = R_i \tag{5.1}$$

With the effect of porous material, the transport of gas in the domain is written as

$$\epsilon_p \frac{\partial c_i}{\partial t} + c_i \frac{\partial \epsilon_p}{\partial t} - D_{i,eff} \nabla c_i + \boldsymbol{u} \nabla c_i = R_i + S_i \tag{5.2}$$

With

$$D_{i,eff} = \frac{\epsilon_p}{\tau_i} D_i \tag{5.3}$$

$$\tau_i = \epsilon_p^{-1/3} \tag{5.4}$$

This can be identified as Equation 2.7-2.9 for a porous media with the use of Millington and Quirk model for tortuosity.

As the diffusion coefficient is dependent on the temperature in the system, a variable was calculated from the Lennard-Jones potential and added to the system. Using a variable instead of a fixed value should increase the accuracy of the simulations and make the model more versatile

if different temperature settings would be preferable in future simulations. Complete calculations can be seen in Appendix A3.

A concentration of vapor for 20°C was calculated in Appendix A4 and inserted as the ambient concentration at the open boundaries as well as the initial concentration over the system. In the same way, a starting concentration on the surface of the skin was calculated for 30°C. Due to the same calculation error at early stage as for model 2, the vapor concentration defined in the model was overestimated by 10%. The results obtained from the model will still be used and analyzed, as the values of concentration both on the surface of the skin and in the environment will differ greatly in real life. Also, it is the effects in concentration flux that is of main interest in this study, not the numerical values.

5.4.1 Diffusion barrier

As the outer film of the product is not calculated as a domain in the system, it will be defined as a thin diffusion barrier. This prescribes that transport of vapor through the film can only occur by diffusion. The layer was defined on all boundaries of the product towards the surrounding air, including the additional domain of pulp on top of the product. In order to account for any temperature changes, the previously defined variable for the diffusion coefficient was inserted in the specifications of the layer together with a film thickness of 20µm. The layer was defined as follow on the up and downside of the layer, respectively.

$$-n \cdot D_i \nabla c_{i,u} = \frac{D_i}{d_s}(c_{i,u} - c_{i,d}) \quad (5.5a)$$

$$-n \cdot D_i \nabla c_{i,d} = \frac{D_i}{d_s}(c_{i,d} - c_{i,u}) \quad (5.5b)$$

5.5 Boundary conditions

The temperature and vapor concentration on the surface of the body was set constant to 30°C and RH=100% with a no-slip boundary. The same velocity constraint $\boldsymbol{u}=0$ was set on the thin layer at the outer surface of the product as in model 1.

Just as in model 1, the edges of the product were set as symmetry as the model simulates only a part of the product. Symmetry nodes were also added on the right side borders of the large air domain. This is consistent over all three modules in COMSOL.

As no mirror effects are desired in the surrounding environment, an open boundary condition was set at all other boundaries towards the surrounding air. This condition reduces a part of the Navier-Stokes equation in Equation 4.2, as can be seen in Equation 5.5. The condition is applicable when the boundaries are in contact with a large volume of fluid, as the fluid can both

enter and leave the system. This requires however that the volume using this node is relatively large, hence the air layer in model 3 needs to be large compared to the product itself.

$$\left[-p\boldsymbol{I} + \frac{\mu}{\epsilon_p}(\nabla \boldsymbol{u} + (\nabla \boldsymbol{u})^T)\right]\boldsymbol{n} = 0 \qquad (5.6)$$

The open boundary condition was defined in all tree modules. In heat transfer, the ambient temperature outside the system was set to 20°C and in diffusion the outside concentration was defined as the calculated value for 20°C.

All boundary conditions can be seen in Figure B3.1a-e Appendix B3.1.

6

Results

6.1 Model 1

When simulating the micro climate of the product, 2D surface profiles for temperature and fluid velocity were created together with a line profile for the surface radiation. To analyze the effect convection and radiation have on the microclimate in the system, each phenomenon was separately disabled.

Two parameter studies were also conducted. The permeability was changed from $3.75 \cdot 10^{-9}$ to $3.75 \cdot 10^{-11}$ m^2 in order to observe the effects due to the porosity in the material. Since previous literature research indicates that a change in porosity might cause significant changes in the microclimate, ϵ_p was changed from 0.7 to 0.9 with a constant permeability.

6.1.1 Temperature

Results obtained from simulation with $\epsilon_p = 0.7, \kappa = 3.75 \cdot 10^{-9}$ m^2 (Figure B1.2-3 Appendix B1) show that the temperature gradually decreases in the system, mainly at the higher temperature as it follows the volume force (Figure B1.4). By creating a 1D plot from a cut line over the porous domain, a linear temperature drop could be observed with surface temperatures identified as 29.2 degrees closest to the skin and 24.4 degrees towards the environment. As the micro model was modelled as a horizontal section at the "bottom" of the product, not much will occur with temperature in the large domain of surrounding air.

6.1.2 Fluid velocity

By computing the differential equations 3.1-3.2 for Free and porous media flow, the model shows a small increase of fluid velocity starting close to the surface of the porous material with some wall effects. Inside the porous media the higher fluid velocity continues until it reaches the outer surface and quickly decreases in the surrounding layer of air. Since the surrounding air was approximated to be stagnant in the model, the velocity of the fluid is presumed to go towards 0m/s.

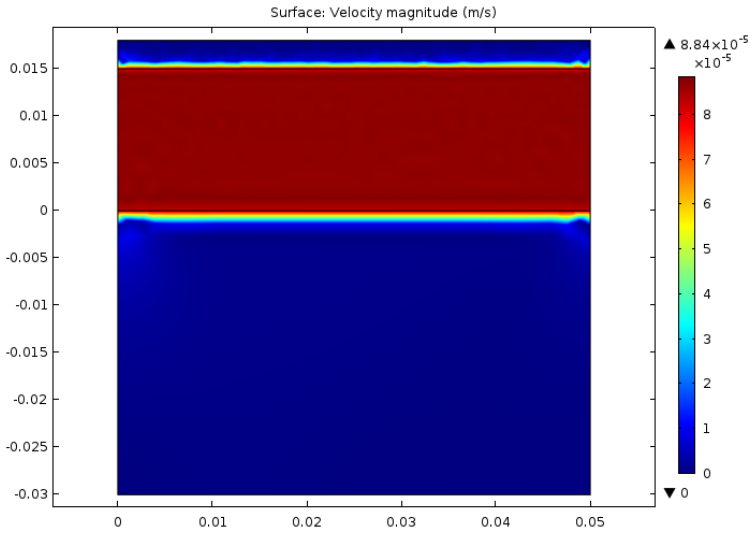

Figure 6.1 Fluid velocity, ϵ_p=0.7 κ=3.75·10^{-9} m^2

6.1.3 Radiation

Surface radiation was observed in a 2D line plot along the three surfaces. As COMSOL treats surface-to-surface radiation as an energy transfer between boundaries, the radiation will contribute to the boundary conditions rather than to the overall heat equation. Therefore only a line plot will be observable.

By observing a 1D plot along all three surfaces (skin, inner surface and outer surface) at time = 0 minutes, an initial radiation value in the system was obtained. When shifting the system to steady state, the resulting radiation from the body and the product could be observed and analyzed.

The amount of energy emitted from the body could be determined as 478.9 W/m^2 when observing a 1D line plot over the surface at steady state, seen in Figure 6.2. From the same plot it can be seen that the energy decreases inside the product with 29.5 W/m^2; from 473.8W/m^2 at the inner surface of the product to 444.4 W/m^2 at the outer layer towards the surrounding.

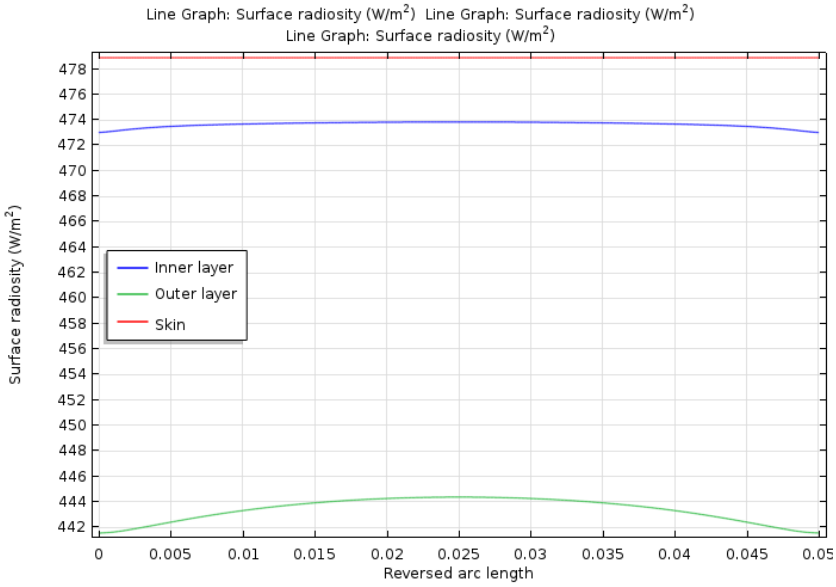

Figure 6.2 Surface-to-surface radiation over the system

6.1.4 Rayleigh effect

The Rayleigh number was calculated over layer 1 and 2 as a variable dependent on the different parameters of Equation 2.15. As can be seen in Figure B1.6ab, decreasing the permeability from $3.75 \cdot 10^{-9}$ to $3.75 \cdot 10^{-11}$ m^2 results in a high Ra-number and the system becomes unstable. To be able to simulate this situation, a turbulence model will need to be included. This is not possible when using *Free and porous media flow* as the model is not yet defined for such conditions. Therefore, the Brinkman equation module used for model 3 will be required for materials with lower permeability than 10^{-9} m^2 for this model as well. The module was defined in the same way as for model 3 with the same boundary conditions. Simulations were made for both for a permeability of $3.75 \cdot 10^{-11}$ and $3.75 \cdot 10^{-9}$ m^2, in order to see any possible changes in result due to different modules used. Mathematically the two different methods do not differ, thus the results should be the same as well.

As explained in section 2.3.1, thermal convection cannot be neglected when observing heat transfer with this high value of Ra-number. Analysis in heat transfer will therefore include conductivity and thermal convection, as well as surface radiation.

6.2 Model 2

When simulating the outer-layer model, 3D plots of the concentration profile and the diffusive flux were obtained. The concentration profile of the model at steady state is displayed in Figure 6.4.

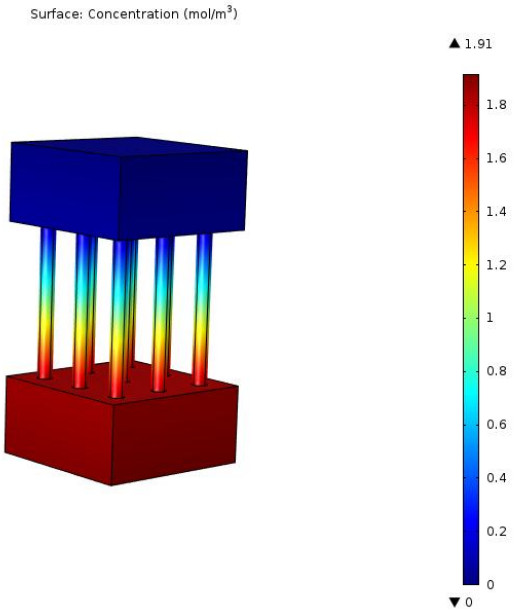

Figure 6.4 Concentration profile Model 2

As defined by the boundary conditions, there will be no mass flux leaving the system at the ends of the two bulks. As a result, the vapor concentration in the bulks will stay close to constant at all times. From Figure 6.4 it can be seen that the concentration gradually decreases as it moves towards a bulk with zero concentration (top bulk area). By computing a 1D line graph along one of the channels, a linear decrease of concentration from 1.9 to 0.1 mol/m^3 could be observed. The plot is displayed in Figure B2.2 Appendix B2.

By slicing the 3D model in to several discs, any possible local channel effects at the in/outflow of the cylinders should be detected. As can be seen in figure 6.5ab, there are no such effects in the concentration profile on the surface or at the cross section of the channels.

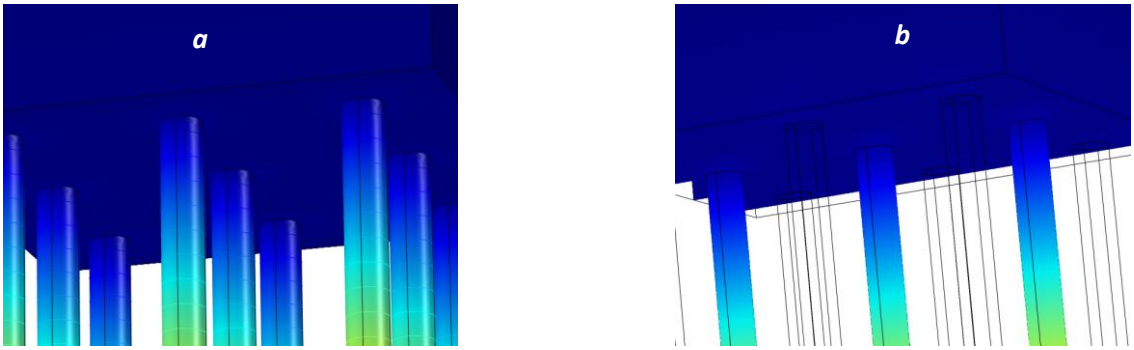

Figure 6.5 Concentration profile towards bulk a) Surface view b) cross section view

When analyzing the profile for diffusive flux in Figure 6.6, several interesting observations could be made: The diffusive flux seems to be constant through the channels but there are indications that some interactions around the channel openings are occurring.

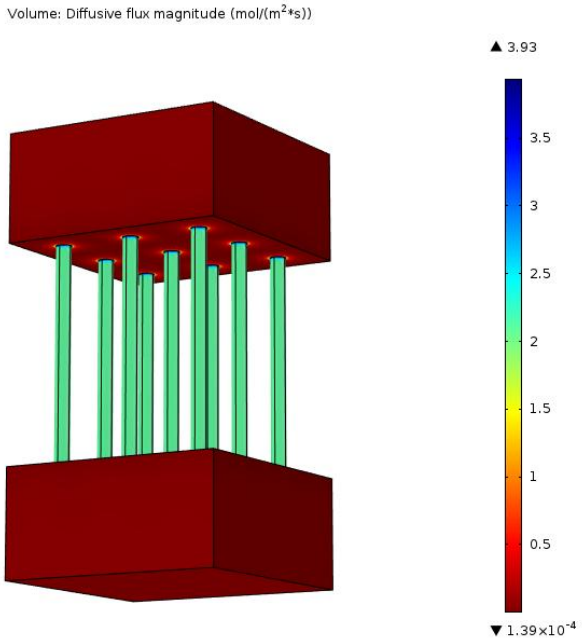

Figure 6.6 Diffusive flux

When zooming in on the pore openings, the diffusive interactions become more noticeable. As displayed in Figure 6.7ab the effects could be observed both on the surface of the model and when slicing the pores. When slicing the model, some clear channel effects can be observed in the bulk area. This indicates that some neighbor effects between the pores do occur for this simulation. Thus in order to maximize the diffusion potential, the positioning of pores should not be too close to each other as it could affect the overall diffusion flux.

However, to make the effects more perspicuous in the report, pores displayed in figures for section 6 are very large, approximate 10-100 times greater than for the analysis in section 7.2. A figure displaying the real pore size can be found in Figure B3.1 Appendix B3. As the channel effects are strictly local (Figure 6.7), the risk of any serious interaction between very small pores might prove to be very low. To be sure that there really are no interactions between the openings, it was decided to conduct some further analysis on the possible neighbor effects.

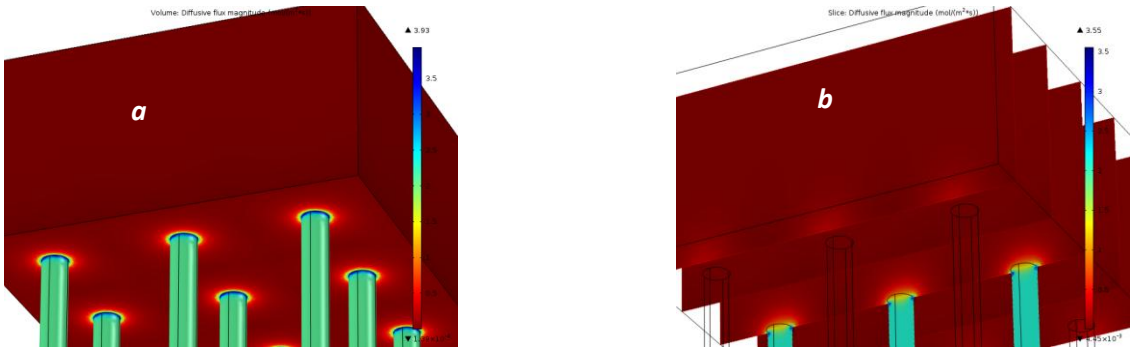

Figure 6.7 Diffusion flux towards bulk a) Surface b) Cross section

6.2.1 Surface area ratio

To find a surface area ratio (SAR) explaining how much of the surface of the film needs to be covered in pores for a diffusion of the required amount of vapor (1000 g H_2O/ (m^2day)) to be possible, a set of simulations were conducted.

For each COMSOL simulation the radiuses of the pores were randomly changed while the bulk area stayed constant, resulting in a re-calculated diffusion flux for each pore size. The fluxes obtained for the nine different pores were close to uniform in all simulation cases. However, for consistency only the middle channel in the model will be considered in the analysis, as it will not be affected by the ends of the bulk areas. The following results were observed.

Table 6.1 Diffusion flux for varying porous radius

Radius pore [µm]	J pore [mol/(m^2·s)]
0.03	2.24
0.05	2.24
0.07	*
0.09	2.23
0.10	2.23
0.12	2.23
0.15	2.22
0.17	2.22
0.19	2.21

**Inconclusive result*

Where J pore is the diffusion flux for the middle pore. The total flow will therefore be nine times the obtained value.

With a model using nine pores and a fixed bulk area, the total diffusion flux ($J_{required}$) will be defined as

$$J_{required} = 9 \cdot \frac{A_{pore} \cdot J_{pore}}{A_{bulk}} \quad (6.1a)$$

By rearranging Equation 6.1a, it is possible to calculate the required pore area (A_{pore}) for $J_{required}$ with the varying J_{pore} as well as the required radius of the pores (r_{pore}). The results can be seen in Appendix B3.

$$A_{pore} = \frac{A_{bulk} \cdot J_{required}}{9 \cdot J_{pore}} \quad (6.1b)$$

As Table 6.1 shows, the diffusion flux is close to uniform for all pore sizes. However, the sizes of pores were chosen randomly for the simulations. Therefore iterations were made, starting with an average value of pore radius from the table. The average value was inserted as a new pore size in the model, resulting in a new diffusion flux from the simulation. The flux obtained was added to Equation 6.1b and a new pore radius could be calculated. As the starting radius ($\bar{r}_{pore}$) was so close to the required radius value at the first run, two other similar values of the radius were simulated as extra confirmation that the result is correct.

$$\bar{r}_{pore} = \frac{\sum r_{pore,i}}{8} \quad (6.2)$$

Table 6.2 Control of required pore area

Radius pore [µm]	J pore [mol/(m^2·s)]	Radius pore required [µm]	Area pore required [$µm^2$]
0.0580	2.24	0.06	0.01
0.0579	2.24	0.06	0.01
0.0578	2.24	0.06	0.01

From the results in Table 6.2 it could be concluded that the required pore area is 0.01 $µm^2$. With the obtained pore size, the ratio between pore and bulk surface area for the required vapor transport could be calculated.

$$\frac{9 \cdot \bar{A}_{pore}}{A_{bulk}} = 0.000214 \qquad (6.3)$$

At least $2.14 \cdot 10^{-2}$ % of the area needs to be covered with pores in order to transport 1000 g $H_2O/(m^2 day)$.

6.3 Model 3

The model was simulated with two different levels of permeability ($3.75 \cdot 10^{-9}$, $3.75 \cdot 10^{-11}$ m^2) and porosities (0.7, 0.9) in order to observe the effects in the system. From the simulations, surface profiles in 2D were obtained for temperature, fluid velocity and concentration of vapor, together with a 2D line profile for surface radiation.

6.3.1 Fluid velocity

As the system involves a Rayleigh number above the critical value, the model will not reach steady state. Instead, a time transient model was created and analyzed. As Figure 6.8 shows, the surrounding velocity is initially stagnant, with only a small movement in layer 1 due to the heat radiated from the body. As the time increases, the surrounding air starts to move due to convection through the product. Figure 6.9 shows the whole system after 60 minutes.

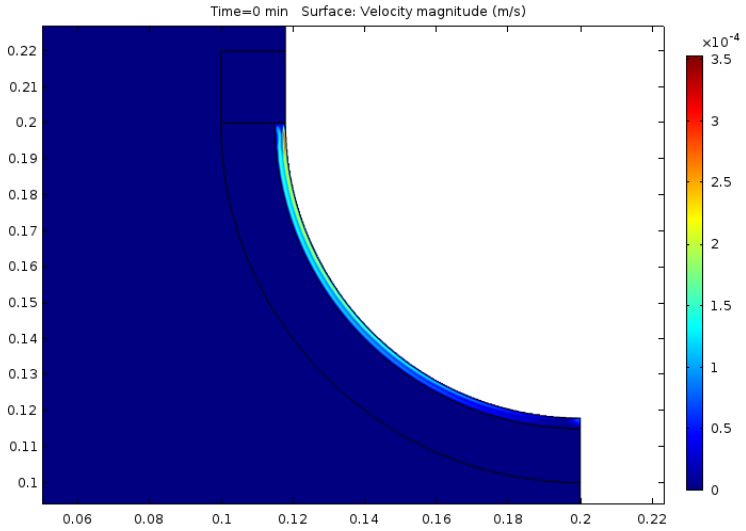

Figure 6.8. Initial fluid velocity, ϵ_p=0.7 κ=$3.75 \cdot 10^{-11}$ m^2

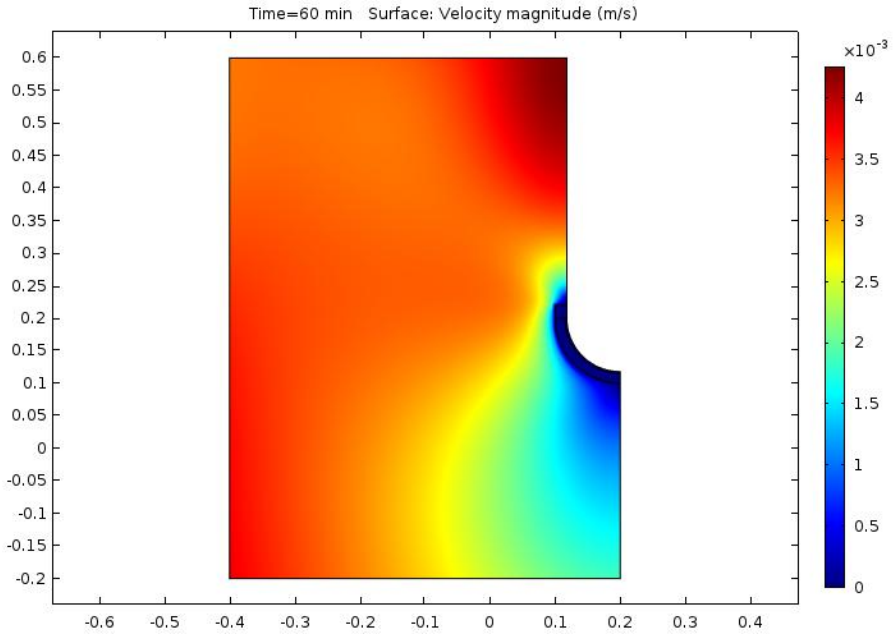

Figure 6.9. Fluid velocity in system after 60min, ϵ_p=0.7 κ=3.75·10^{-11} m^2

As can be seen in Figure 6.9, the velocity of fluid flow is very low at all times with a magnitude of mm/s. However, it can be concluded that there is a velocity effect caused by convective mass transfer. Two different 1D plots were created by adding one cut line through the product and another larger cut line including the thin layer of air and a part of the surrounding air. This method was used in order to observe both heat and mass transfer interactions in the media.

6.3.2 Temperature and concentration

As the surrounding air is close to stagnant, the heat and concentration of vapor emitted from the body is freely spread from the product and rises with temperature and decreasing density of vapor molecules. By using a transient model, the effects as functions of time can be observed in the cross section of the product in the same way as for the velocity. When creating a cut line across the porous domain of the model, it can be seen that the temperature strives towards a linear decrease indicating that the system is close to a steady state after 60 minutes (Figure 6.10).

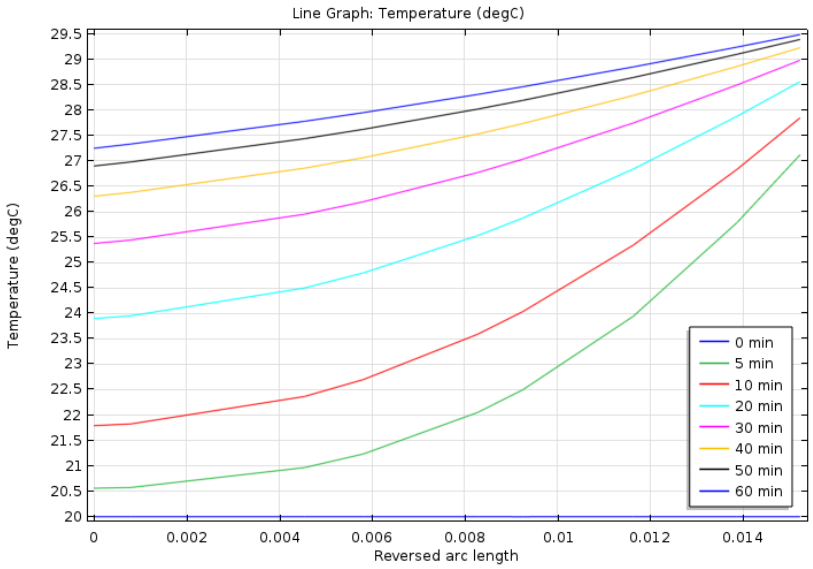

Figure 6.10 Temperature profile over time, cut line 1

By observing the different profiles over the system, it can be seen that the temperature and concentration profiles follow the same outline as the volume force. As ***F*** is a variable dependent on the changing concentration and temperature per definition, this is an expected result. The result after 60 minutes can be observed in Figure 6.11. The coupling between convection (mass and thermal) and diffusion will be further investigated in section 7.3.

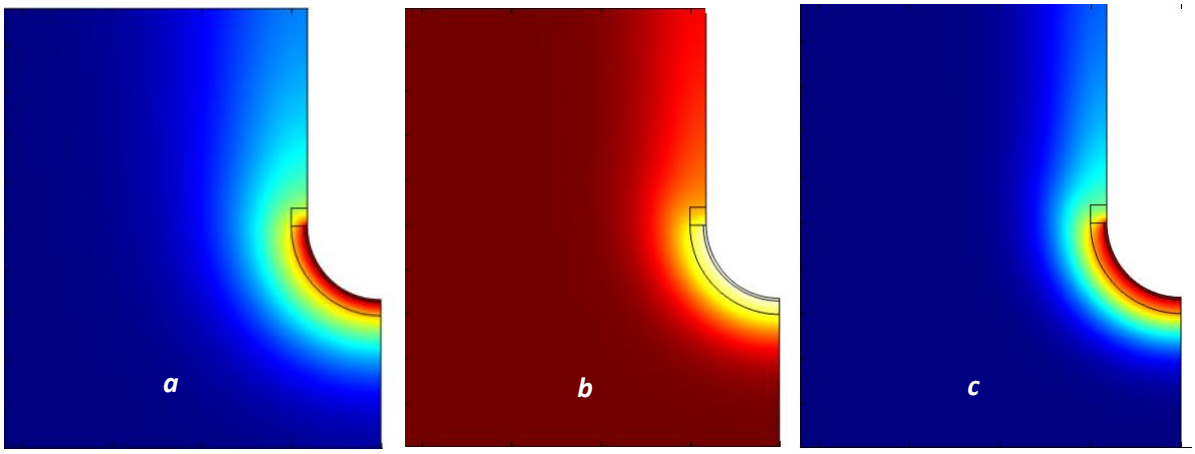

Figure 6.11 System profile, 60min a) Concentration b) Temperature c) Volume force

6.3.3 Surface radiation

When conducting the same 2D line analysis as in model 1, the surface radiation was obtained from time 0-60 minutes. The emitted radiation by the body could be determined as 478.9W/m^2, just as for model 1. Since the system observed is transient, the radiation at the surfaces of the product will increase with time as they are re-calculated for each step. This can be observed in Figure B3.11. Therefore only 60 minutes will be regarded, as the temperature profile showed that this is a time close to steady state.

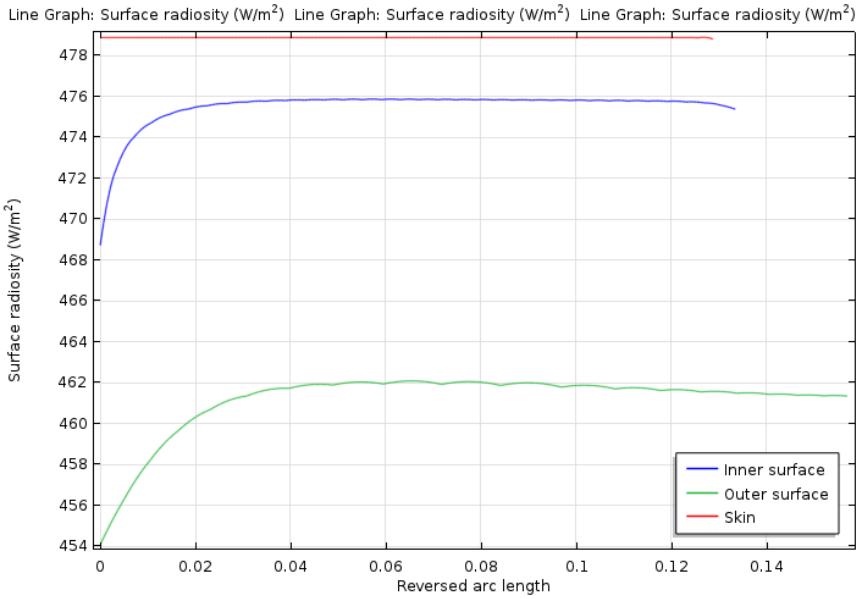

Figure 6.12 Surface radiation over system

As the product is bent, the results are not uniform over the area. At the top section on the product with an additional pulp area, the effect rapidly decreases. This effect can be observed at the left side in Figure 6.11 where the surface radiation in the whole system is displayed. To ensure that the side effects are not included in the results, the numerical values shown in Table 6.3 were extracted at reversed arc length = 0.06.

Table 6.3 Surface radiation results

	S.R Inner surface [W/m^2]	S.R Outer surface [W/m^2]	Radiation emitted from body [W/m^2]	Radiation drop in product [W/m^2]
t= 60 min	475.9	462.0	478.9	13.9

7

Analysis

7.1 Model 1

7.1.1 Free and porous media flow

For the permeability value of $3.75 \cdot 10^{-9}$ m^2 *Free and porous media flow* (Fp) module was used, as discussed in section 6.1.

7.1.1.1 Fluid velocity

When analyzing a cut line over the product, it can be seen that there is a small increase in fluid velocity inside the porous material (10^{-5} m/s). The 1D plot can be observed in Figure B1.5. This increase may be explained by the formation of channels in the medium. With a smaller transport area inside the porous media, the combined velocity will increase compared to the free flow of the surrounding air. This can also be seen in the Hagen Poiseuille's equation in Appendix A1.

By observing the fluid velocity at time = 0 minutes, it can be seen that there exists some initial velocity effects around both surfaces of the product (Figure 7.1a). It seems like the module is starting the motion of fluid around the surfaces between the domains, rather than at the surface of the skin. The effect can be observed as present at all times, and might cause an inaccuracy as it enhances boundary effects around the two surfaces.

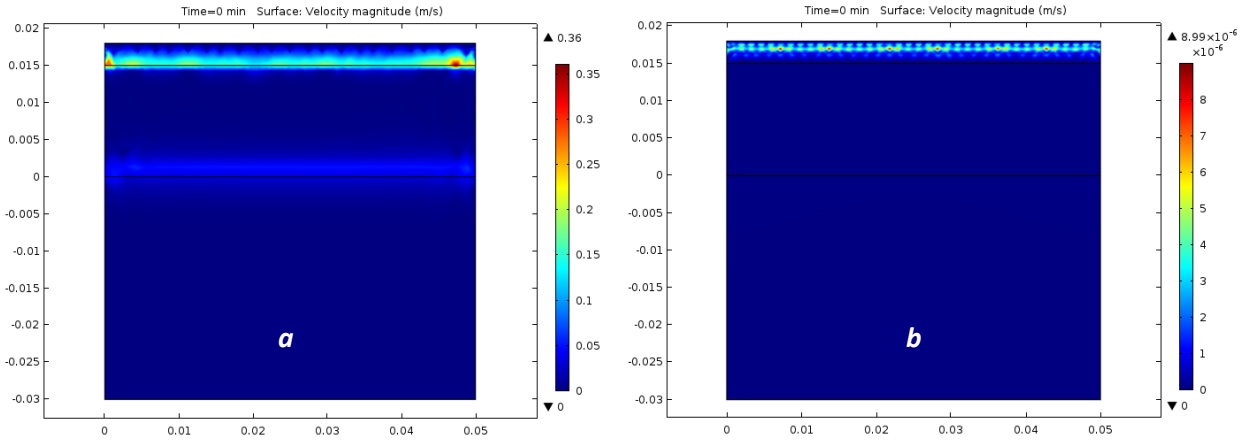

Figure 7.1 Initial velocity field, $\epsilon_p = 0.9$, κ=3.75·10^{-9} m^2 a) Fp-module b) Br-module

7.1.2 Brinkman equation

7.1.2.1 Fluid velocity

As mentioned above, when using the Fp-module an initial velocity around the surfaces of the product could be observed. This is not the case when using the Brinkman equation (Br). From Figure 7.1b it can be seen that there is a small velocity flux close to the hot surface, but none in or around the porous material. As time increases, so does the velocity inside the porous region.

A cut line across the domain shows a very small and irregular rising velocity that seems to become close to constant after approximately 20 minutes (Figure B1.7 Appendix B1). At the end of the domain it can be seen how the convection moves towards zero velocity, as per definition by the boundary condition.

As the system computed by the Brinkman equation is using a turbulence model, the irregularity might be an effect of this definition. The fluid velocity obtained by the Br-module is even lower than the one obtained by using Fp, now in the magnitude of 10^{-6} m/s. Computing such a small flow could be another probable cause for the increasing irregularity, as this effect increased with the lower velocity magnitude. When analyzing the deviation numerically, it can be seen that the irregularity inside the product is in the range of 1-2 µm/s. With such small values, it should not be able to affect the outcome in any significant way. An extensive analysis of the irregularity in convective flow will be made for model 3 in section 7.3.

7.1.2.2 Comparing Br and Fp

In order to keep a consistency in the results for further analysis when using the Br-module instead of Fp, a comparison between the different modules was made. The comparison was conducted by observing results from both modules when using the same values for the parameters. This will also show the validity of the two modules.

As the Br-module requires fewer approximations in the settings due to the turbulence model, it is to be preferred as the results should be more realistic. However, the graphical focus tends to be more on the surrounding air instead of the product itself, as the mass transfer convection in the air domain is included. This can be observed in Figure 6.9. As a consequence, the micro climate might be more difficult to visualize than when the Br-module is used. On the other hand, the numerical values obtained by using a cut line over the product cross section are more essential for the analysis. The graphical effect should therefore become less of importance.

When using the Fp-module, a density of vapor is obtained with a value of 2.4 - 2.3 kg/m^3. Such high value seems to be improbable as the temperature range in the system is between 20-30˚C. When observing the outcome of vapor density in the Br-module, it can be determined as almost half the value as what was acquired by Fp (1.2 kg/m^3). This value is much more probable in the temperature range, thus the credibility of the Br-module increases.

The change in density affects several different profiles in the system. Two of the most important profiles for this study are the ones obtained for temperature and fluid velocity. When using the Br-module, convection is ten times lower compared to using the Fp-module. As both velocities are very small it might be hard to create an opinion of which one is most probable. However, as mentioned in section 7.1.2.1 there is a small existing initial value of velocity in the Fp-module that does not exist in Br. This effect cannot fully be explained and as a consequence the credibility when using the Fp-module decreases even further.

From the comparison analysis between the two different modules, it can be concluded that the Brinkman module is more suitable for this system. For further analysis the Brinkman module will be solely used in order to keep a consistency in the results.

7.1.2.3 Heat transfer

By observing a cut line through the product, the temperature can be seen dropping linearly from 29.2˚C at the inner surface to 24.4˚C at the outer during steady state (Figure B1.8). When comparing conductive and convective heat flux through the product in Figure B1.9-11, the contribution from conductivity could clearly be determined as the greatest.

7.1.2.3.1 Thermal radiation

When observing the effect of radiation using the Br-module, the same values could be obtained as when using the Fp-module (Figure 6.2). As radiation will contribute to the heat transfer in the system, the effect of surface-to-surface radiation was temporarily shut off in order to observe the differences in the temperature profile. To make the system possible to converge, all three diffuse surfaces were temporarily disabled as well.

With radiation present, the temperature drops from 29.2˚C to 24.4˚C. When disabling the effect of radiation, the profile changes and the product becomes cooler inside. It can be concluded that there is a difference of 0.5˚C at the inner surface of the product depending on if radiation is accounted for or not in calculations. As a colder inner surface can be assumed to be more comfortable for the wearer, the radiation can be assumed to be of importance to include when calculating the heat transfer over the product.

Table 7.1 Radiation analysis, ϵ_p=0.7 κ=3.75·10^{-9} m^2

	Temperature inner surface [˚C]	Temperature outer surface [˚C]	Temperature drop [˚C]
Radiation present	29.2	24.4	4.8
Radiation disabled	28.7	24.1	4.6

The results from Figure 6.2 show how the radiative heat flux inside the product drops with 29.5 W/m^2.

Wu, Fan [15] mention how the main contribution for thermal energy flux in a fibrous medium comes from radiation, when the medium is applied on a human body. This statement can be confirmed by this analysis as the body emits almost 480W/m^2. In figure B1.9, the total heat flux including thermal convection and conductivity can be identified as constant at approximately 16 W/m^2 over the porous domain at steady state. In this case, the radiative heat flux will be almost twice as large.

Although absorption is not included in the modelling of the system, its definition will help when investigating the effect of radiation in the product. From equation 2.19ab, it can be seen that the effect of radiation through a medium is dependent on the absorption constant. This constant can be defined as in Equation 7.1, where R is the radius of fiber used.

$$\beta_s = \frac{\varphi\varepsilon}{R} \tag{7.1}$$

The radiation potential can be seen as directly dependent on the radius of the fibers. For a material with a constant fiber fractional volume, an increased radius would result in a decreased absorption constant. This effect is mainly due to a decreased effective surface area in the material, as less thermal energy can be absorbed. As a result the radiation potential through the material would increase, resulting in a cooler product.

7.1.2.4 Effect of convection

By removing the volume force ***F*** from the system, the effects on temperature made by convection could be noticeable. Without the convection present, a much lower driving force is present in the system. Due to the lower driving force, the turbulence model in the system is not required and can be disabled. As the velocity present due to convection was originally very low, not much change in the temperature profile is expected. A transient model was calculated, since a model in steady state would not display much information in the temperature profile.

In Figure B1.13 at t = 60 min, the fluid velocity inside the medium can be seen as non-existing, confirming that convection is not present. The new temperature profile can be observed numerically in Table 7.2. Without convection present, the temperature is decreasing more slowly inside the product as the driving force is much lower. The inner surface of the product is 29.3˚C, 0.1 ˚C warmer than with convection present. In comfortable terms for the wearer, this difference can be questioned if the difference will be important or not as it most likely would not be noticed. It can however be concluded that the temperature drop decreases with more than 1 ˚C.

Table 7.2 Convection analysis, ϵ_p=0.7 κ=3.75·10^{-9} m^2

	Temperature inner surface [˚C]	Temperature outer surface [˚C]	Temperature drop [˚C]
Convection present	29.2	24.4	4.8
Convection disabled	29.3	25.7	3.6

Although convection is not as crucial to include in the heat transfer equation as the effect of radiation, this is an indication that there is a strong connection between the temperature profile and the flow of fluid. Even with a low numerical value of convection as 10^{-6} m/s, the effect is noticeable in the overall microclimate.

7.1.2.5 Parameters

When analyzing the cut line through the porous media, it can clearly be seen that the main contributor of the heat transport inside the domain is thermal conductivity (Figure B1.9-10). The effect of conductivity in the media is close to constant through the whole cross section with a value of approximately 16 W/m^2. In comparison, the effect of thermal convection is approximated 0.1-0.2 W/m^2.

By definition in Equations 2.15-16, the conductive thermal energy flux is solely dependent on the fractional fiber volume and not the radius of the fibers. The porosity and thermal conductivity will therefore be of interest for the heat transfer over the product.

7.1.2.5.1 Porosity

Although the permeability is dependent on the porosity, the effect is not included in this analysis. From the correlation between Darcy's law and Hagen Poiseuilles' equation (Equation 2.23) it can be seen that the size of the pores inside the material highly affects the value of permeability. As the porosity is directly connected to the size of pores, the connection between porosity and permeability is palpable. However, as this is only a parameter analysis this effect will not be observed.

By increasing the porosity of the porous material from 0.7 to 0.9 with a constant value of permeability, it can be seen that the temperature on the outer surface of the product decreases from 24.4˚C ($\epsilon_p = 0.7$) to 21.8 ($\epsilon_p = 0.9$) ˚C. This is an indication that the heat transport process is significantly improved (Figure B1.15).

As increased porosity implies a larger area for the fluid to flow through, the local velocity will slightly decrease. This is observed in the cut line through the medium where the decrease can be approximated to $0.1 \cdot 10^{-6}$ m/s, or 3%. As previously discussed in section 7.1.2.3, even small changes in the convection for mass transfer will be able to affect the temperature flux over the product. In this case the temperature drop over the product increases as the convection decreases, opposite from that previously observed. As defined in Equation 2.16-17, a lower volume of material will result in a lower conductivity potential. From the same cut line as previously observed, the changes can clearly be seen (Figure B1.14). The new effect of conductivity is observed to approximately 14.5 W/m^2 with a flux from one surface to the other of 2.2 W/m^2, hence the increased temperature drop does not originate from the conductivity of the material.

The explanation for changing temperature profile comes from the effect of radiation. By increasing the porosity the thermal radiation flux increases with 2.9 W/m^2 (Figure B1.16). Equation 7.1 shows how the absorption factor is just as dependent on the fractional volume of fibers as on the fiber radius. As the porosity increases, the fractional volume will decrease and as a consequence so will the absorption constant making it possible for more thermal energy to pass through the product. This results in a higher value on the inner side of the product and a lower value on the outer surface. As the effect of radiation is strongly dependent on the temperature (T^4), the temperature profile follows the radiation potential. As a result the inner surface of the product will be warmer and the outer surface cooler than in the case of a more dense material.

Table 7.3 Porosity analysis, $\kappa=3.75\cdot10^{-11}\ m^2$

Porosity	Temperature drop[˚C]	Radiative flux [W/m^2]	Conductive flux [W/m^2]
0.7	6.7	41.3	2.6
0.9	6.7	44.2	2.2

7.1.2.5.2 Permeability

To observe the effect in the microclimate due to permeability, κ was changed from $3.75\cdot10^{-9}$ m^2 to $3.75\cdot10^{-11}$ m^2, with a constant porosity of 0.7.

For the temperature profile in the product a close to identical profile can be observed, from 28.8˚C to 22.2˚C. The main difference can be observed in the fluid velocity. As a lower value of permeability indicates a more impermeable material, convection is decreasing almost linearly to the increased value of κ. This can be observed in Figure B1.17. Although, the main heat transfer phenomenon inside the product is conductivity that stays unchanged, the effect will only be minor.

As the part of the product observed is horizontal, not much impact of convection and in extension permeability is expected. To observe the changes in microclimate due to the fluid flow, model 3 will need to be observed.

7.2 Model 2

7.2.1 Diffusion flux

When observing the diffusive flux profile in Figure 6.6, it could be concluded that the flux was constant through the channel. As the flux is directly proportional to the concentration gradient of vapor, this can easily be explained mathematically by Fick's first law (Equation 2.5). Figure B2.2 in Appendix B2 showed that the concentration drop is linear, therefore the gradient will stay the same for each grid inside the mesh and there will be no change in the diffusion.

When analyzing the diffusion fluxes obtained in Table 6.1, it can be concluded that the flux varies only slightly when changing the size of the pores. By converting the table into a 1D plot (Figure 7.2), the drop of diffusion flux can be seen as linear. This indicates that something is happening systematically in Fick's law ($J_{ij} = D_{ij} \frac{\partial c_i}{\partial x}$). As the diffusion is dependent on the concentration flux, the concentration profile was examined more closely. Due to the fact that the simulation is observing pores on the micro scale, the changes made in the pore radius are very small (0.02-0.2µm).

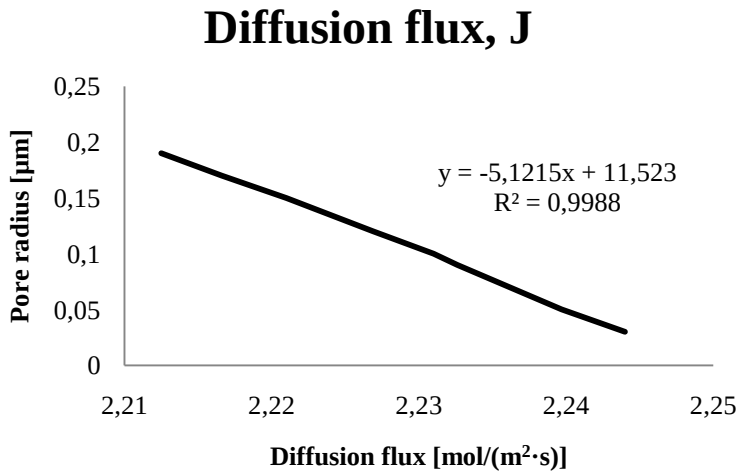

Figure 7.2 Diffusion flux obtained from results

From figure B2.2 in Appendix B2 it could be seen that the concentration of vapor for a pore with a radius of 0.0578 µm decreased from 1.907 mol/m^3 to 0.004 mol/m^3, a difference of 1.903 mol/m^3. If the radius of the pore is increased to 0.1 µm, the concentration could be seen decreasing from 1.904 to 0.007, a difference of 1.897 mol/m^2.

By definition of Fick's law, a decreased concentration flux would result in a decreased overall diffusion flux. It seems there is a small effect on the bulk concentration depending on the size of the pores; when the pore area is large, the concentration in the bulk decreases slightly as there are no in- or outflow from the two bulks. If the concentration inside the bulks were defined as constant at all time, there would most likely not be any changes in the diffusion flux.

7.2.2 Neighbor effects

Since Figure 6.6ab indicated that some possible neighbor effects existed, the size of the bulk areas and the distance between pores were changed. By changing the distances but keeping the same proportion of the model, it should be possible to see if the surface area ratio (SAR) between bulk and pore will be affected. The distance was decreased by 28.6% ($L_{bulk} = 21\ \mu m \rightarrow L_{bulk} = 15\ \mu m$) and the numerical results can be seen in Table B2.2-3 Appendix B2.

To ensure that this ratio is somewhat valid over a wide range of pore sizes, additional simulations were made with pore radiuses in the range of 0.5-0-9 µm.

Table 7.4 Required parameters for radius 0.5-0.9 µm

Radius pore [µm]	J [mol/(m^2·s)]	Radius pore required [µm^2]	Area pore required [µm^2]
0.5	2.143	0.059	0.011
0.7	2.094	0.060	0.011
0.9	2.041	0.060	0.012

It can be seen from table 7.4 that the required radius of the pore is still in the same range as in Table 6.2, hence the SAR will not vary significantly with different pore sizes ($\pm 0.065\%$ of original SAR value).

7.2.3 Surface area ratio

From Equation 6.3 it can be seen that at least $2.14 \cdot 10^{-2}$ % of the area needs to be covered with pores in order to transport 1000 g H_2O/(m^{2}day). By changing the size of the bulk area and the distance between pores, it can be concluded that the diffusion fluxes are approximately the same for the decreased area ($7.05 \cdot 10^{-5}$% difference), hence the neighboring effects of the pores will not have any significant impact over the SAR.

Although pore size and distribution do not affect the diffusion flux inside the pores significantly, the concentration will as it is proportional to the flux. If the temperature of the film would decrease to 37.0˚C, it would change the concentration of the vapor in the bulk and affect the overall diffusion flux required. Simulations for this case were made and the results can be seen in Table B2.4-5 in Appendix B2.

As the results show, the diffusion fluxes in the pores decrease as well as the SAR. By changing the temperature from 38.0˚C to 37.0˚C in the bulk, the SAR changed with 0.001%, which is a hundred times greater change than changing the space between pores with 28.6%. Although the change in ratio is small percentagewise with only one degree difference, the effect of temperature has proven to be far more significant to the outcome than any other factor observed in the simulation.

7.2.4 Film thickness

The model describes an ideal situation with straight cylindrical pores, hence the obtained SAR might be practically impossible as no films like this exist today. However, the model conducted can be used for various lengths of channels to approximate a possible length of the path the water molecules need to be transferred in the film. Simulations with a gradually expanding imaginary film were made in an attempt to find a relationship between diffusion flux and the length of the channels. As can be seen in Figure 7.3-4, there are clear relations both for the diffusion flux and SAR in regard to the length of the pores.

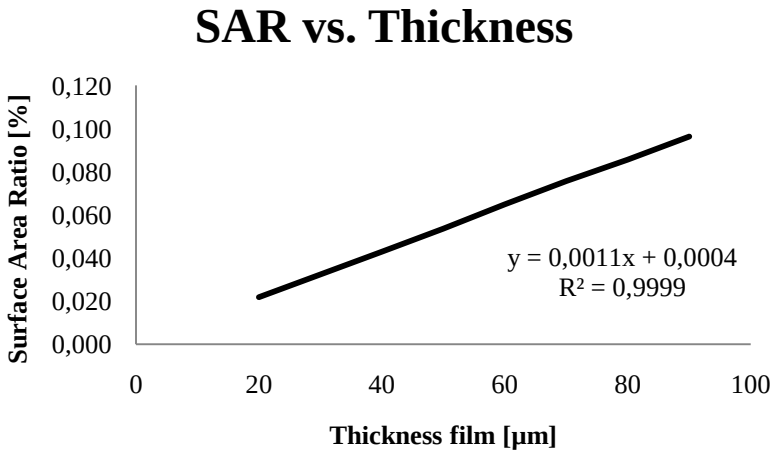

Figure 7.3 SAR vs Thickness of film

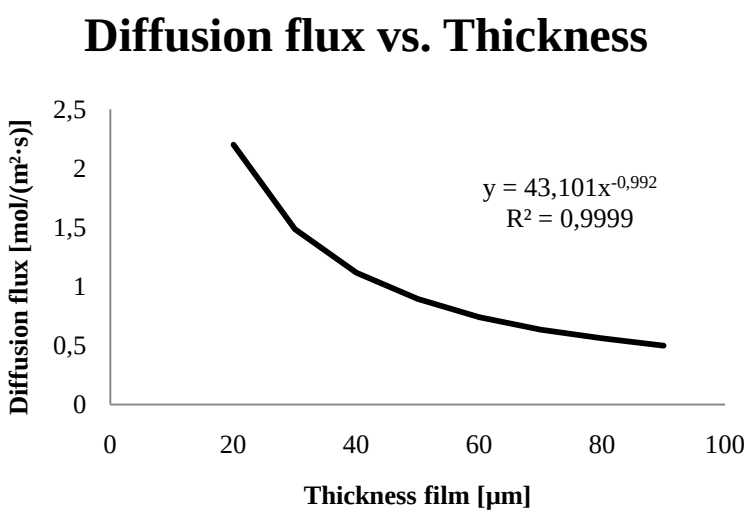

Figure 7.4 Diffusion flux vs Thickness of film

By using the equations obtained by the trend lines for each plot, the size of pores and SAR can easily be calculated for any film as long as pathway data is known and the film consists of non-reacting surfaces. By using the correlations obtained by the trend lines, an unlimited number of different films can be applied and controlled experimentally in order to be used in various hygiene products, not only diapers. The data for various film thicknesses can be seen in Table B2.6 Appendix B2.

7.3 Model 3

The standard settings for the third model analysis was set to $\kappa = 3.75 \cdot 10^{-11}$ m^2 and $\epsilon_p = 0.7$, as this lower value of permeability is more realistic for the actual product. However, using a hundred times lower value of permeability will result in a different profile for temperature and concentration than obtained in model 1. Therefore a comparison between the different models will be unsuitable. As the intention of the macro model is to simulate a realistic situation for the product and not compare the different models, no comparison analysis will be made in this section of the report. A small validity analysis will however be regarded in section 7.4, comparing the two models when using the same parameters.

7.3.1 Cut lines

From Figure 7.5a it can be seen that the temperature is decreasing at the top surface of the product, mainly due to the additional section of pulp. A 1D line plot along the outer surface of the product was created in order to make this decrease in surface temperature more visible, shown in Figure 7.5b. From the plot, the area with highest temperature can be identified as the middle part of the product, as it is the furthest away from the ends of the product. This is also true for concentration of vapor as they follow the same curve, seen in Figure 7.6. Therefore the numerical values will only be observed in the middle section of the product, inside the green boxes in Figure 7.5-6ab, in order to minimize any end effects.

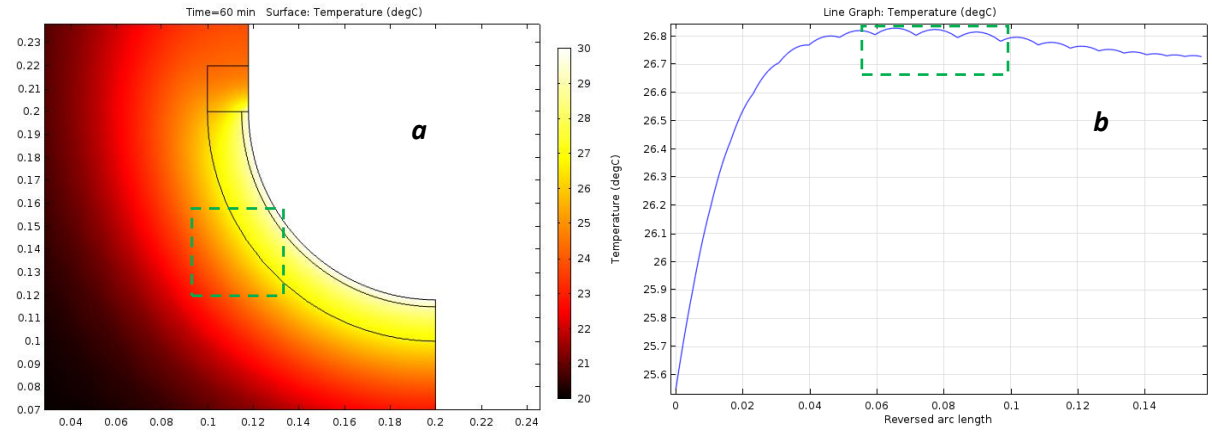

Figure 7.5 a) System temperature profile **b) Temperature profile on the outer layer of product**

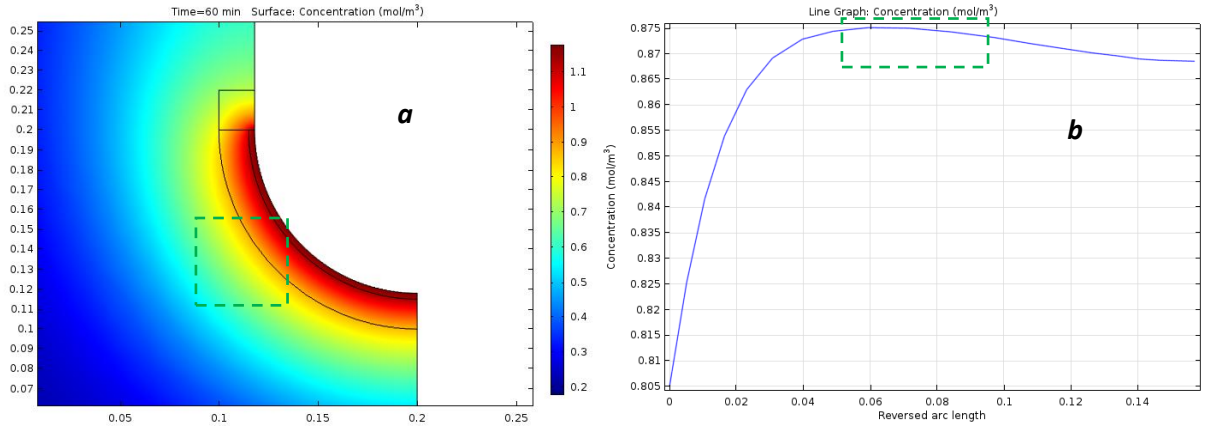

Figure 7.6 a) System concentration profile **b) Concentration profile on the outer layer of product**

When creating the cut lines across the domains, the middle section of the product was used. One line for the porous domain was constructed, seen in Figure 7.7a. A second line including the thin layer of air and parts of the surrounding air was created as well, in order to create a more complete overview of the microclimate for the analysis.

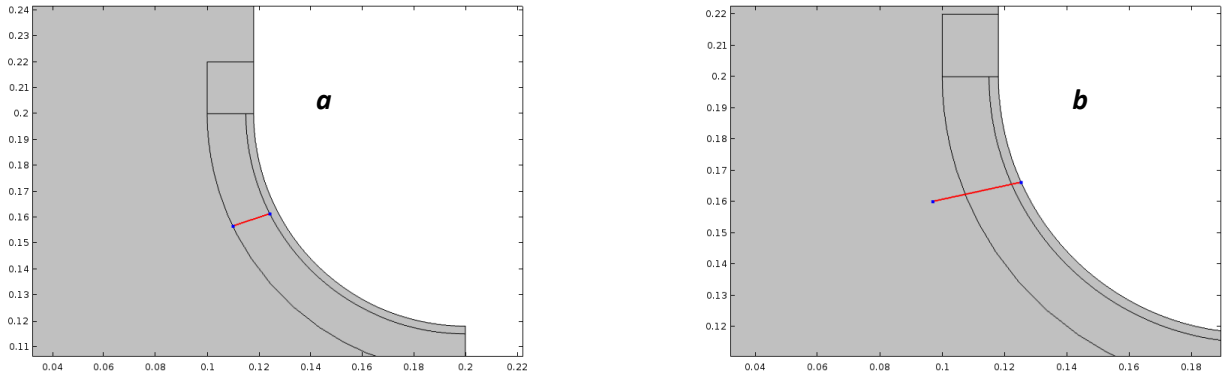

Figure 7.7 Cut line a) Cut line 1, porous domain **b) Cut line 2, all domains**

The temperature profile from cut line 1 (Figure 6.10) shows how the temperature drop decrease inside the product, going from 29.5˚C to 27.3˚C for a product with porosity of 0.7 and permeability of $3.75 \cdot 10^{-11}$ m^2. When observing the right bottom end of the product where the product is starting to become horizontal, only a small temperature change (29.3˚C-27.8˚C) compared to cut line 1 could be observed. The decrease of temperature seems to be close to constant over the whole product, if the top section is excluded. Hence only cut line 1 and 2 will be observed in future analysis.

7.3.2 Fluid flow

When observing the first minutes in the system, two pathways can be identified inside the thin layer of air closest to the human body. In figure 7.8a, the first minute is observed from which the paths can clearly be seen, especially as the product becomes more vertical in shape. A hypothesis was made that the warmer fluid close to the heat source would rise to the top of the product and from there fall down along the product surface, creating the irregularity that demanded a turbulence model in the computing. By adding arrows in the air domain, this effect could be established, shown in figure 7.8b. The flow of fluid becomes irregular in the top section of the product as it starts to flow downwards again; this is possibly one of the areas where turbulence will occur in the system.

As the time passes, the thin layer of air is heated up to an almost uniform temperature. As a result, the circulating effect decreases and becomes close to zero, as a transient cut line through the small domain show in Figure B3.2. Since the model don't reach steady state, t=60min is assumed to be close to steady state (Section 6.3.2). From the cut line in Figure B3.2, it can be seen that the velocity has decreased significantly and is close to uniform during this time.

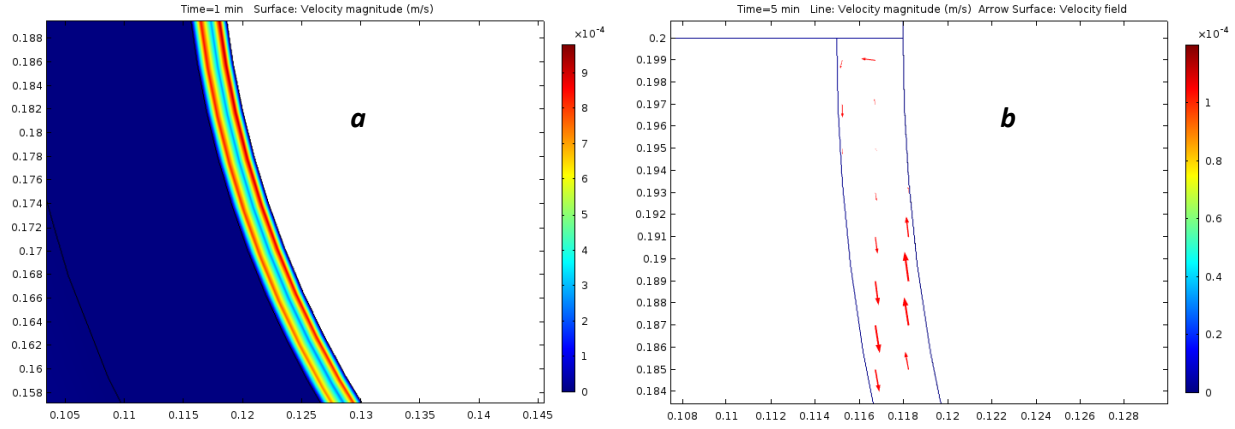

Figure 7.8 a) Velocity pathways inside the air domain, t=1 min.

b) Proportional velocity arrows inside the air domain, t=5min.

By normalizing the arrows, the flow through the porous domain could be analyzed as well. It is however worth mentioning that as the arrows are normalized, they are not proportional to the velocity magnitude.

A series of times were observed in the system, showing how the fluid flow starts without any turbulence at time 0 minutes (Figure 7.9a). In the first minutes it can be observed how the outer layer is resisting convection to pass through, resulting in a tendency for turbulence to arise along the outer surface inside the product. The formation of a vortex inside the product as the product turns more horizontal can also be observed, as it becomes more and more distinguished as the minutes pass. Figure 7.9b shows the system after 3 minutes where the occurrence of a vortex can clearly be seen. As the system gets closer to steady state at time 60 minutes, a clear turbulence in the convective flow inside the product can be observed (Figure 7.9c). The vortex has disappeared and been replaced by an increase of random irregularities and a flow of fluid going backwards. The backwards flow is in reality very low but do exist, as a consequence of the resistive outer layer of the product and the rising hot fluid. This fluid goes back to the thin layer of air and rises to the top before falling down and through to the porous media again, creating a large circulation in the system. This occurrence of turbulence inside the porous media might be the greatest reason for the model to demand a turbulence model during the model stage.

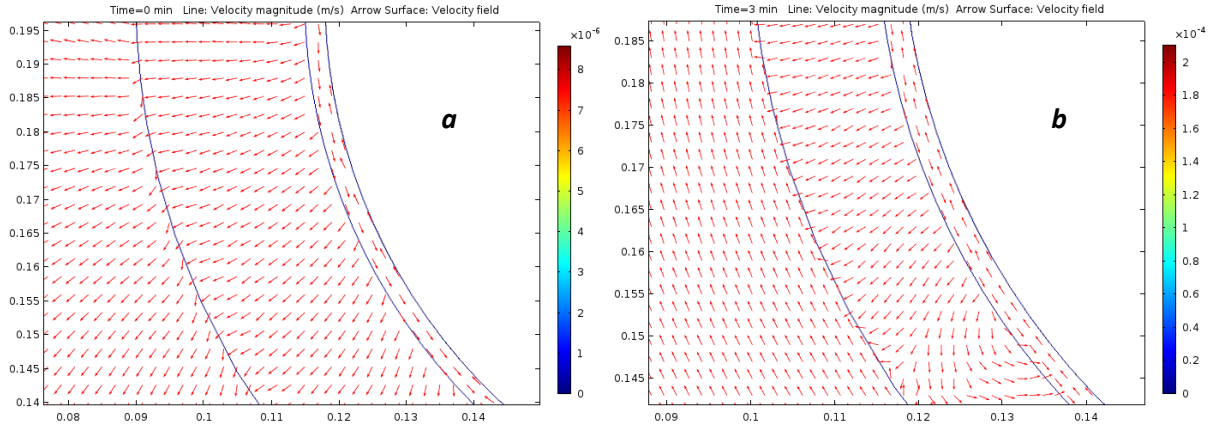

Figure 7.9 a) Normalized velocity arrows over the whole system, t = 0min **b) Normalized velocity arrows over the whole system, t = 3min**

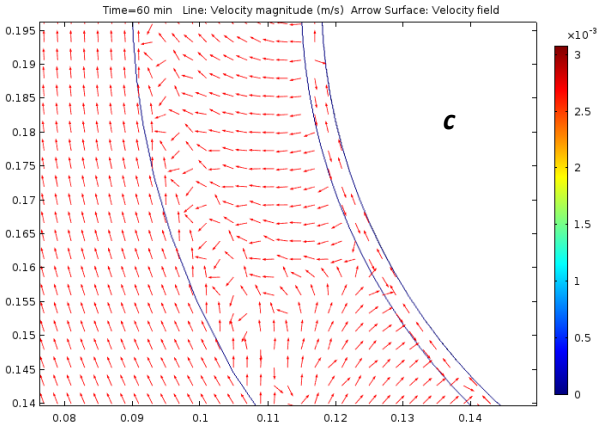

c) Normalized velocity arrows over the whole system, t= 60 min

7.3.3 Heat transfer

From cut line 1, it can be seen that the main contribution of heat transfer over the porous domain comes from conductivity (Figure B3.3-6), just as for model 1. Convective heat transfer is mainly present at the surface closest to the body and rapidly decreases as it moves in to the product, away from the heat source.

When observing all three domains in cut line 2 (Figure B3.7-9), it can be concluded that the main contributor in the air domains is convective heat transfer. The ambient air generates by far the largest effect of heat transfer due to its large domain size and the relatively high temperatures emitted from the product.

7.3.3.1 Radiation

As the results in section 6.3.3 shows, the surface radiation decreases from 475.9 W/m^2 on the inner surface of the product to 462.0 W/m^2 on the outer layer towards the surrounding. To investigate the effect radiation has on the temperature in the system, the same analysis as in model 1 was conducted by disabling the radiation and the diffuse surfaces, in order to observe a new temperature profile.

From Table 7.5 it can be seen that the temperature drops on each side of the product. As the body radiates heat to the system, a lower temperature on the inner surface of the product is reasonable. The table shows how the drop of temperature through the product stayed the same as when radiation was present. This is an indication that the loss of energy on the inner surface lags through the whole system. In this case, the radiation will have an effect of the temperature profile with 0.4˚C. No effect on the mass transfer of vapor through the system could be observed.

Table 7.5 Radiation analysis, ϵ_p=0.7 κ=3.75·10^{-11} m^2

	Temperature inner surface [˚C]	Temperature outer surface [˚C]	Temperature drop [˚C]
Radiation present	29.5	27.3	2.2
Radiation disabled	29.1	26.9	2.2

7.3.3.2 Effect of convection

The same analysis of the effect in heat transfer due to convection in model 1 was conducted in model 3. When removing the volume force ***F***, the effect made by convection is disabled. From cut line 1, a velocity of the same magnitude as in model 1 could be observed (10^{-8} m/s). In the porous domain, higher temperatures than with convection present could be seen as the temperature drops from 29.6˚C on the inner surface to 27.9˚C towards the surrounding air. Since diffusion is affected by the temperature profile, the cut line showed a similar effect on the concentration profile as well, shown in Table 7.6.

Table 7.6 Convection analysis cut line 1, ϵ_p=0.7 κ=3.75·10^{-11} m^2

	Temperature inner surface [˚C]	Temperature outer surface [˚C]	Concentration inner surface [mol/m^3]	Concentration outer surface [mol/m^3]
Convection present	29.5	27.3	1.1	0.8
Convection disabled	29.6	27.9	1.2	1.0

When analyzing cut line 2, the boundary between porous media and surrounding air becomes less distinctive in the total heat flux profile (Figure B3.14). When the convection was present it could clearly be seen that the dominating heat transport phenomenon inside the product was conductivity, whereas the main driving force in the air domains were due to convection. As convection in the outer air domain could be determined to be many times larger than the conductivity inside the porous media, a sharp boundary could be noted in Figure B3.7. By removing the effect of convection, fewer differences between the two domains in the temperature profile are now observed. The effect can be seen in figure B3.14, which is identical to the conductive heat transfer profile.

7.3.3.2.1 Porous media size

As convective mass and heat transport is a function of temperature and concentration in the system, the fluid velocity may be manipulated by changing the thickness of the product. Temperature drop occurs most rapidly in the fluid domains, where convection is the dominating transport phenomenon. By increasing the thickness of the product with 1 cm and keeping the thin air layer constant, transport due to conductivity should increase in the microclimate and convection should decrease. The volume force is present at all times.

In figure 7.10a it can be seen that the velocity of the fluid is close to zero inside the product and rapidly increases close to the outer surface. As the 1D plot shows the absolute value of velocity,

this increase in convection actually shows the turbulence due to the resistive outer layer of the product. By observing the normalized velocity arrows in Figure 7.10b, it can be seen that the counter flow at the outer surface is more evident with a thicker product as more fluid is able to accumulate inside the media.

Increasing the product with 1 cm should therefore make the convection negligibly small for heat transport, whereas the effect of conductivity increases significantly. As can be seen in Figure B3.15, the conductive heat transfer is observed to increase from 7.3 W/m^2 in the thinner product to 11.7 W/m^2, an increase of 38%. One possible explanation for the increase of conductivity flux is the higher potential for energy transport, as the temperature inside the product increases with a lower contribution from convection.

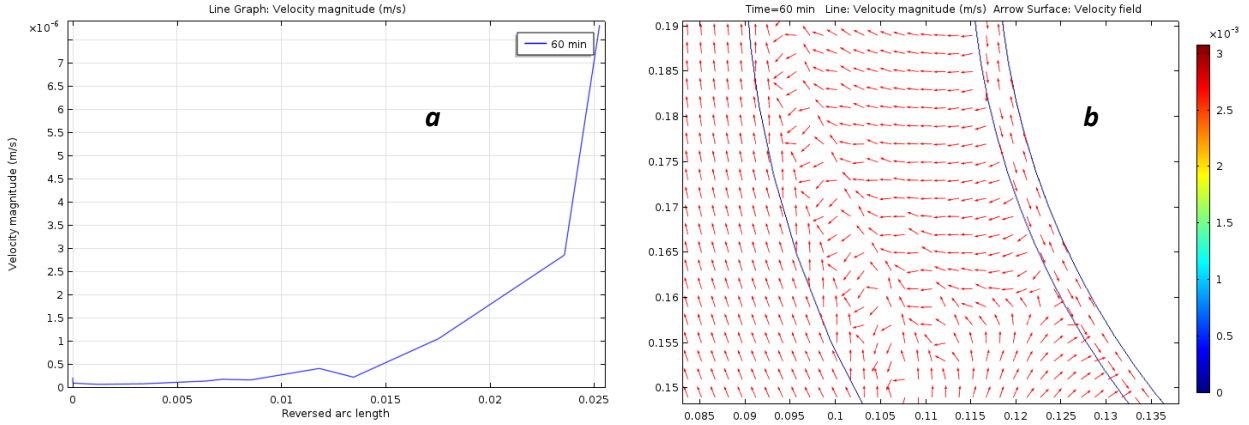

Figure 7.10 2.5 cm thick product a) Convection 1D plot, cut line 1 b) Normalized velocity arrows over the whole system

The temperature profile becomes less linear inside the product as its size increases, with a temperature decreasing from 28.6˚C to 24.1˚C mainly due to the increased effect by conductivity (Figure B3.16). Even though the cooler inner surface of the product might be preferable, an analysis on the effect of vapor concentration showed a negative trend. It can be seen that the concentration of vapor on the inner side of the product has increased to 1.2mol/m^3 by using a thicker product. As the diffusion transport is much slower in a porous media compared to free flowing air, so is the concentration flux. By observing an extended version of cut line 1, the outer surface of the product can be observed to 0.8mol/m^3.

Creating thicker products in order to remove the small effect of convection will not be recommended, as the climate around the product would increase in vapor concentration. This would be especially true closest to the body, where the humidity will be most noticeable and create an uncomfortable feeling.

7.3.4 Diffusion

When observing cut line 2, it can be seen that the concentration of vapor decreases from 1.1 mol/m^3 to 0.8 mol/m^3 inside the product. As the diffusion coefficient (obtained in Appendix A3) is dependent on the temperature profile it follows the same curve. In figure B3.17, the diffusion coefficient can be observed.

From Figure 7.12a, the diffusive flux can be seen decreasing over the whole system, gradually reducing the diffusion potential as the temperature decreases. When creating a small cut line just over the outer surface of the product, an increase in the diffusion flux was observed at the porous media closest to the surface (Figure B3.18). As the outer layer is defined as a diffusion barrier, the only way for the fluid to pass the surface is by diffusion. Hence the potential increases slightly.

As mentioned in section 2.2.2.1, diffusion coupled with convection is sometimes of importance for the transfer of species. To investigate the effect, the coupled convection was removed from the model. The results can be seen in figure 7.11b and 7.12b.

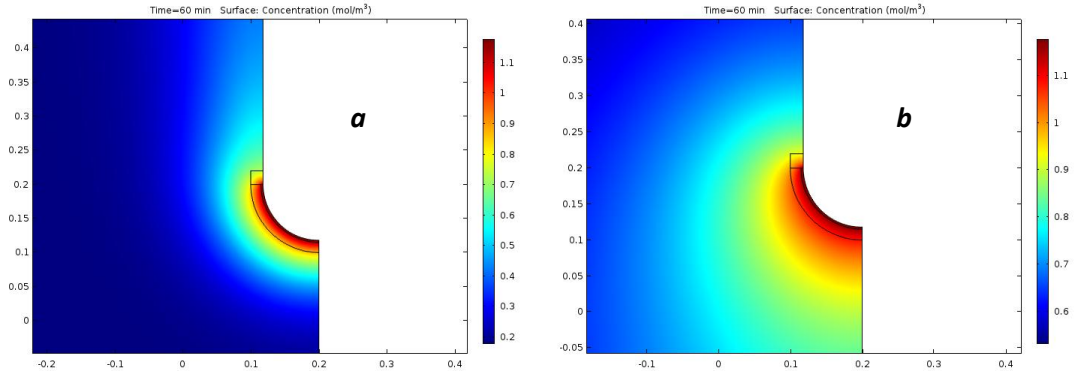

Figure 7.11 Concentration profile a) Convective coupledb) No convection

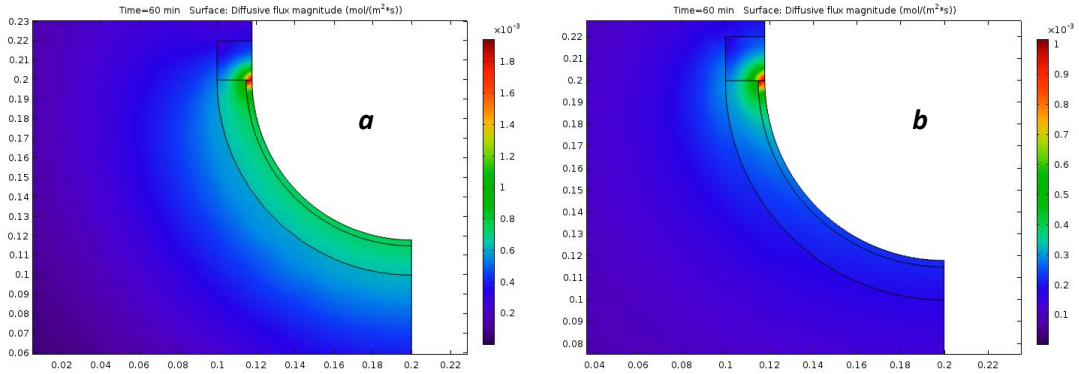

Figure 7.12 Diffusion flux a) Convection coupled b) No convection

As the system profiles show, the diffusion flux rapidly decreases inside the product since it is not defined to diffuse anywhere. As the diffusion coefficient is only dependent on the temperature it will not change from the case with convection coupled. With no convection present, the vapor is free to flow no matter what direction, as a result the concentration profile changes significantly, as can be seen in Figure 7.11b.

Coupling diffusion with convection can from the analysis be concluded to be very mathematically important when creating these kinds of models.

7.3.5 Parameters

7.3.5.1 Porosity

Just as in model 1, when increasing the porosity of the material from 0.7 to 0.9 with a constant value of permeability, the heat transport is improved (29.7-27.4˚C) as well as the effect of radiation (476.8-462.8 W/m^2), by the same way as explained in model 1. The resulted difference between surfaces can be observed in Table 7.7.

Table 7.7 Porosity analysis, ϵ_p=0.7 κ=3.75·10^{-11} m^2

Porosity	Temperature drop [˚C]	Concentration drop [mol/m^3]	Radiative flux [W/m^2]
0.7	2.2	0.3	13.9
0.9	2.3	0.2	14.0

What has not previously been observed is the effect on vapor concentration in the system. With a higher porosity in the material, it can be seen that less vapor is diffused through the product. The diffusion flux decreases compared to the case with a porosity of 0.7. With the diffusion coefficient not changing numerically in cut line 2, the concentration gradient will decrease as it follows Fick's law. By using cut line 1, it could be seen that the concentration went from 1.1mol/m^3 on the inner surface of the product to 0.9 mol/m^3 on the outer surface (Figure B3.19). With a higher concentration on the outer side of the product compared to a material with porosity = 0.7, this is an indication that the diffusion transport is much slower that before.

7.3.4.2 Permeability

When increasing the permeability from $3.75 \cdot 10^{-11}$ to $3.75 \cdot 10^{-9}$ m^2, the convective resistance inside the product decreases. As concluded in section 7.1.2.4 and 7.3.3.2, convection is very important for the temperature profile. By changing the permeability it should be possible to see large differences in the temperature profile and in extension in the radiation and concentration.

Table 7.8 Permeability analysis, ϵ_p=0.7 κ=$3.75 \cdot 10^{-11}$ m^2

K [m^2]	Temp. inner surface [˚C]	Temp. outer surface [˚C]	SR. inner surface [W/m^2]	SR. outer surface [W/m^2]	Conc. inner surface [mol/m^3]	Conc. outer surface [mol/m^3]
$3.75 \cdot 10^{-9}$	29.4	26.8	475.5	456.0	1.1	0.8
$3.75 \cdot 10^{-11}$	29.5	27.3	475.9	462.0	1.1	0.8

From Table 7.8 it can be concluded that a higher value of permeability is to be preferred in order to keep a desirable environment over the system. The material becomes less resistive to convective flow, hence the overall microclimate improves. This effect can be related to the effect previously observed by convection in section 7.3.3.2, where the surface temperature increased as a result of no convection present. By definition of Equation 2.24, an increased size of the channel areas inside the porous media would increase the permeability significantly. Therefore an increased porosity would improve the permeable effects of a material as well.

7.4 Validity analysis

7.4.1 Model 1 and 3

When all parameters for both of the models were set the same, the results were compared. As a diffusion process is included to the system in model 3, any transport processes that might be highly affected by mass transfer, such as convection, will not be regarded. Therefore only the temperature and radiation profiles will be observed in this analysis.

Table 7.9 Validity analysis, model 1 and 3

	Temperature inner surface [K]	Temperature outer surface [˚C]	Radiation inner surface [W/m^2]	Radiation outer surface [W/m^2]
Model 1	302.3	297.5	473.8	444.4
Model 3	302.6	300.4	475.9	462.0

As Table 7.9 shows, there is a difference of 1% in outer surface temperature and a 3.8% difference in outer surface radiation. If a robustness level of 5% would to be used, the differences between models could be accepted. However, it is worth mentioning that the temperature on the outer surface differs with approximately 3˚C, a high enough value that any potential future add-ons in the models might be affected. It will therefore be recommended that only model 3 is used for future research, as the model has been proven to be more robust overall and includes transport by diffusion as well.

7.4.2 Model 2

To validate model 2, a regular sensitivity analysis was conducted as there is no second model to compare with as for model 1 and 3. Just as in the analysis for model 1 and 3, a robustness level of 5% was considered acceptable. By increasing the starting concentration with 10 and 20%, the diffusion flux obtained in the pores was observed.

Table 7.19 Validity analysis, model 2

	Original	**+10%**	**+20%**	**Difference [%]**
Model 2	J = 2.31 mol/(m^2s)	J = 2.45 mol/(m^2s)	J = 2.68 mol/(m^2s)	9.99, 19.99

As can be seen in Table 7.19, the changes inside the pores are close to linear regarding concentration defined in the bulk air. Hence the model can be assumed to be valid for various concentrations added to the system.

7.5 Conclusions

7.5.1 Convection

Over all, the velocity of convection tends to be very low (10^{-8}-10^{-6} m/s) inside the product. This is not unexpected, as the convection occurring is natural without any other driving forces than the temperature gradient. By disabling the convective effect on the microclimate, both the temperature and concentration of vapor in the fluid increased. This is shown in Table 7.20-21. Wearing a warmer and more moist product would not be comfortable, thus the effect of convection is very important both for the mass and heat transfer in the microclimate.

One of the central parameters to define correctly when observing the effect of convection is the permeability of the porous material. It has been proven that the value highly affects the convective flow in the system and influences the mass and heat transfer. As larger porosity in the material increases the value of permeability, it would improve the convective properties in the microclimate observed.

Table 7.20 Heat transfer in manipulated systems, model 3

	Temperature inner surface [˚C]	Temperature outer surface [˚C]	Temperature drop [˚C]
Original settings	29.5	27.3	2.2
Radiation disabled	29.1	26.9	2.2
Convection disabled	29.6	27.9	1.6
Porosity +0.2	29.7	27.4	2.3

Table 7.21 Mass transfer in manipulated systems, model 3

	Concentration inner surface [mol/m^3]	Concentration outer surface [mol/m^3]	Concentration drop [mol/m^3]
Original settings	1.1	0.8	0.3
Radiation disabled	1.1	0.8	0.3
Convection disabled	1.2	1.0	0.2
Porosity +0.2	1.1	0.9	0.2

7.5.2 Radiation

Thermal radiation has been proven to be one of the main contributors in the heat transfer equation and will be important to include when observing the microclimate of a hygiene product. It has been shown that the effect rapidly drops with increasing distance from the heat source. As the design of diapers tends to strive towards a thinner product, the contribution of radiation will be even bigger. Thus it will be even more important to include this effect in future analysis.

With such a large effect from radiation, there is a positive effect on using larger fibers in the thermal climate of the product just as for convection. However, it should be noted that a larger fiber most likely will affect the possibility of absorbing liquid in a similar way as discussed for the absorption constant in Equation 7.1. As this study only focus on the dry state of the product, further analysis will have to be made for a liquid phase to observe the effect and weigh pros and cons against each other.

7.5.3 Surface area ratio

It could be concluded that when using an ideal microporous film, at least $2.14 \cdot 10^{-2}$ % of the area needs to be covered with pores in order to transport 1000g $H_2O/(m^2 day)$. This film is however not realistic in real life, thus the numerical value will not be reliable. However, by using the model created in this thesis, different pore sizes and lengths can be tested in order to approximate a real layer.

As the model is simulating an experiment conducted at SCA, an application app of the model was created to further simplify the simulations in the experiments. By using the app the parameters can easily be changed in boxes next to the model in question. No requirements of understanding the program in detail will be needed to conduct analysis in this way, and may be a helpful tool in comparing simulation results with experimental ones.

8

Future research

The models created in this thesis are very versatile and all the dimensions and parameters of the product can easily be alternated for future research.

By using model 2, different lengths of the pores can be determined as well as the closeness and thickness of the openings in order to simulate different layers for hygiene products. If a different amount of vapor is wished to be observed, this can easily be changed just by inserting the new amount of vapor concentration in the system. To make the parameter changes more easy to execute for a person with no background in the software, the application app included in the thesis may be used.

In model 3, and if wished model 1, different thickness of the product and the layer of air close to the body may be changed in order to find an optimum combination for the micro climate. As the size of the layer of air has not been analyzed in this thesis, this will likely be an area of interest for further analysis. As previously mentioned, all the parameters in the system can be changed to observe different effects and combinations in the microclimate for a specific product. All parameters used in this thesis are general and not brand specific. As a result, alterations will therefore be necessary in order to make the model fit the actual product in question. However, this means that the range of product applications for the model is quite wide. Hence the product can possibly be used for several different hygiene products, not only baby diapers.

A possible absorption effect in the product was noted, especially when observing the radiation. To include the effect of absorption would therefore be suggested as the next step to develop the model further. This study only observes the product in a dry state. To observe the full life time of

the product, a liquid phase should be added to the system in order to get a more complete understanding of what parameters in the product are of most importance.

To further investigate the thermal effect by radiation, a box of air in the surrounding domain could be added. This could be done to investigate how much the outer surface of the product radiates to the surrounding where the temperature is approximated 20°C.

Bibliography

1. Hossain, M.A., et al., *Conduction-radiation effect on natural convection flow in fluid-saturated non-Darcy porous medium enclosed by non-isothermal walls.* Applied Mathematics and Mechanics, 2013. **34**(6): p. 687-702.

2. Charlotta Hanson, S., *Personal correspondence*.

3. Madsen, B., A. Thygesen, and H. Lilholt, *Plant fibre composites – porosity and stiffness.* Composites Science and Technology, 2009. **69**(7): p. 1057-1069.

4. Wu, P.C., et al., *Novel Microporous Films and Their Composites.* JOURNAL OF ENGINEERED FIBERS AND FABRICS, 2007. **2**(1): p. 49-59.

5. Nield, D.A., A. Bejan, and SpringerLink, *Convection in porous media*. 2013, New York: Springer.

6. Ho, C.K., S.W. Webb, and SpringerLink, *Gas transport in porous media*. Vol. 20. 2006, Dordrecht; London: Springer.

7. Hsu, C.-T., *Dynamic modeling of convective heat transfer in porous media*, in *Handbook of porous media*. 2005, Taylor & Francis Boca Raton, FL. p. 39-80.

8. Millington, R.J., *Gas Diffusion in Porous Media.* Science, 1959. **130**(3367): p. 100-102.

9. Shiina, Y. and M. Hishida, *Critical Rayleigh number of natural convection in high porosity anisotropic horizontal porous layers.* International Journal of Heat and Mass Transfer, 2010. **53**(7): p. 1507-1513.

10. Glomski, M. and M.A. Johnson, *A precise calculation of the critical Rayleigh number and wave number for the Rigid-Free Rayleigh-Benard problem.* Applied Mathematical Sciences, 2012. **6**(103): p. 5097-5108.

11. Yang, Y., *Thermal Conductivity*. 2007, Springer New York: New York, NY. p. 155-163.

12. Farnworth, B., *MECHANISMS OF HEAT-FLOW THROUGH CLOTHING INSULATION.* Textile Research Journal, 1983. **53**(12): p. 717-725.

13. Wang, J. and W. Sun, *Heat and sweat transport in fibrous media with radiation.* European Journal of Applied Mathematics, 2014. **25**: p. 307-327.

14. Siegel, R. and J.R. Howell, *Thermal radiation heat transfer*. 2002, New York: Taylor & Francis.

15. Wu, H., J. Fan, and N. Du, *Thermal energy transport within porous polymer materials: Effects of fiber characteristics.* Journal of Applied Polymer Science, 2007. **106**(1): p. 576-583.
16. Bedane, A.H., H. Xiao, and M. Eić, *Water vapor adsorption equilibria and mass transport in unmodified and modified cellulose fiber-based materials.* Adsorption, 2014. **20**(7): p. 863-874.

17. Mörtstedt, S.-E. and G. Hellsten, *Data och diagram: energi- och kemitekniska tabeller*. 1999, Stockholm: Liber.

18. Multiphysics, C., *Heat Transfer Module User's Guide.* 2012. **4.3**.

19. Montiel Gonzalez, M., J. Hinojosa Palafox, and C. Estrada Gasca, *Numerical study of the Boussinesq approach validity for natural convection and surface thermal radiation in an open cavity.* Revista Mexicana De Fisica, 2013. **59**(6): p. 594-605.

20. Welty, J.R., *Fundamentals of momentum, heat, and mass transfer*. 2008, Chichester; Hoboken, N.J: Wiley.

21. Poling, B.E., J.M. Prausnitz, and J.P. O'Connell, *The properties of gases and liquids*. 2001, New York: McGraw-Hill.

Appendix
A1

Permeability

According to Hagen Poiseuille's equation, the pressure drop in one single channel in the porous material can be defined as follow [20]

$$-\frac{\partial P}{\partial L} = \frac{32 \cdot \mu U}{d_p^2} \tag{A1.1}$$

Where (∂P/∂L) is the pressure drop, U the average fluid velocity, μ the dynamic viscosity of the fluid and dp the diameter of the channel.

As the permeability should define the whole media it is assumed that there exist *n* numbers of channels.

$$n = \frac{V_{tot} \cdot \epsilon_p}{V_{single}} = \frac{A \cdot L \cdot \epsilon_p}{\frac{\pi}{4} \cdot L \cdot d_p^2} = \frac{4 \cdot A \cdot \epsilon_p}{\pi \cdot d_p^2} \tag{A1.2}$$

Where A is the cross section area.

Following Poiseuille's equation (A4.1), the flow rate Q can be determined through a single channel as follow

$$Q_{single} = \left(\frac{\partial P}{\partial L}\right) \cdot \frac{\pi \cdot d_p^4}{128 \cdot \mu} \tag{A1.3}$$

And

$$Q_{tot} = Q_{single} \cdot n = \left(\frac{\partial P}{\partial L}\right) \cdot \frac{\epsilon_p \cdot A \cdot d_p^2}{32 \cdot \mu} \tag{A1.4}$$

According to Darcy's law (Equation 2.2):

$$\boldsymbol{u} = \frac{Q_{tot}}{A} = -\frac{\kappa}{\mu} \cdot \left(\frac{\partial P}{\partial L}\right) \tag{A1.5}$$

Combining equation B4 and B5 gives a correlation for the permeability of the porous media.

$$\kappa = \frac{\epsilon_p \cdot d_p^2}{32} \quad \text{(A1.6)}$$

As the porosity is supposed to stay constant in the material

$$\kappa \propto dp^2 \quad \text{(A1.7)}$$

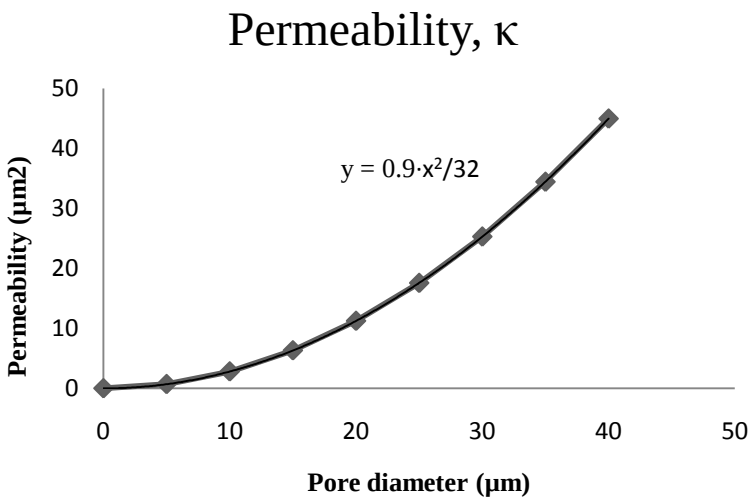

Figure A1.1 Pore diameter influence of permeability, porosity =0.9

A2

Table A2.1 Physical data for saturated air [17]

Temp [C]	P [bar]	ρ* [g/m^3]	X* [g/kg]
10	0.01227	9.39	7.79
11	0.01312	10.00	8.27
12	0.01403	10.66	8.85
13	0.01497	11.30	9.45
14	0.01599	12.03	10.10
15	0.01704	12.79	10.79
16	0.01817	13.60	11.50
17	0.01937	14.52	12.30
18	0.02064	15.41	13.12
19	0.02197	16.36	14.00
20	0.02337	17.34	14.88
21	0.02486	18.38	15.86
22	0.02644	19.47	16.89
23	0.02809	20.62	17.98
24	0.02984	21.82	19.13
25	0.03166	23.09	20.34
26	0.03361	24.42	21.63
27	0.03565	25.81	22.99
28	0.0378	27.28	24.44
29	0.04005	28.81	25.95
30	0.04242	30.37	27.55
31	0.04493	32.09	29.26
32	0.04754	33.85	31.06
33	0.05030	35.70	32.94
34	0.05319	37.64	34.94
35	0.05622	39.63	37.05
36	0.05941	41.75	39.27
37	0.06275	43.96	41.64
38	0.06625	46.12	44.13

X = relative amount of vapor g/kg of dry air
ρ = amount of vapor g/m^3 in moist air
P = vapor pressure

**Total pressure = 1bar*

Concentration

From Table A2.1 the concentration of steam in saturated humid air (RH=100%) for T=30˚C can be obtained.

$\varrho_{30} = 30.37\ g/m^3$

With

$M_{30} = xM_{H2O} + (1-x)M_{air} = 0.02755 \cdot 18 + (1 - 0.02755) \cdot 28.97 = 28.67\ g/mol$

The concentration becomes

$C_{30C} = \frac{\varrho_{30}}{M_{30}} = 1.06\ mol/m^3$

A3

Diffusion coefficient

Lennard-Jones Potential

Correlations obtained from Poling, Prausnitz [21] Chapter 11.

$$D_{AB} = \frac{0{,}00266T^{3/2}}{PM_{AB}^{1/2}\sigma_{AB}^{2}\Omega_D}$$

$$\Omega_D = \frac{A}{(T^*)^B} + \frac{C}{\exp(DT^*)} + \frac{E}{\exp(FT^*)} + \frac{G}{\exp(HT^*)}$$

Constants	
A	1.06036
B	0.15610
C	0.19300
D	0.47635
E	1.03587
F	1.52996
G	1.76474
H	3.89411

For T =20˚C:

Index A = air B = water

$$\sigma_{AB} = \frac{\sigma_A + \sigma_B}{2} = 3.176\ \text{Å}$$

$$\varepsilon_{AB} = (\varepsilon_A \cdot \varepsilon_B)^{1/2} = 252.181 \cdot k$$

$$T^* = \frac{kT}{\varepsilon_{AB}} = 1.166$$

$$M_{AB} = 2 \cdot \left(\frac{1}{M_A} + \frac{1}{M_B}\right)^{-1} = 22.213 g/mol$$

➔ $\Omega_D = 1.3386$

$$D_{AB} = \frac{0.00266(293.15)^{3/2}}{(1.01325)(22.213)^{\frac{1}{2}} \cdot (3.176)^2(1.3386)} = 0.2109\ cm^2/s$$

When repeating the calculations for several different temperatures, a relationship is determined

T [°]	D_{ij} [cm^2/s]
20	0.210875
25	0.216535
27	0.219389
37	0.233907
38	0.235381

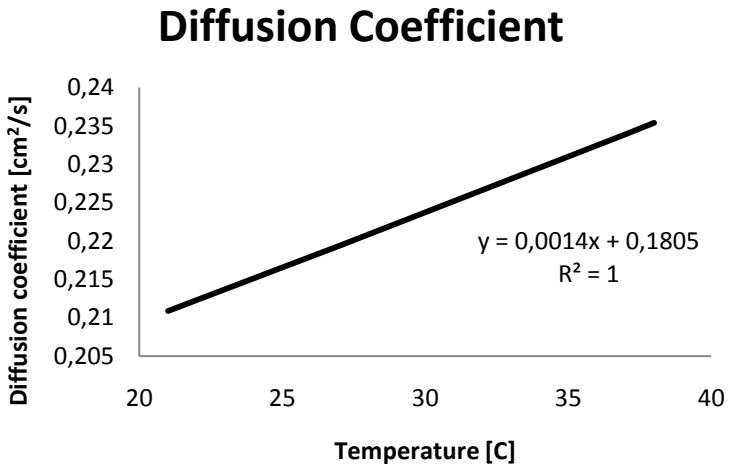

A4

Diffusion flux

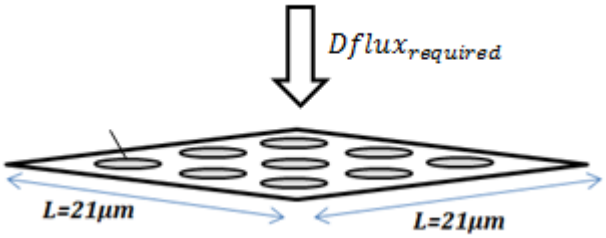

A fixed size on the bulk area (A_{bulk}) was
decided as $21 \times 21\ \mu m^2$. To calculate how much of the bulk area that needs to be covered by pores (A_{pore}) in order to obtain the required flow of vapor (1000g $H_2O/(m^2 day)$) following calculations were made.

$$\dot{m} = 1000 \cdot \frac{1}{24 \cdot 3600} = 0.01157\ g/(m^2 s)$$

As defined in the apparatus used at SCA, the temperature over the film is 37.7-37.8˚C.
With T =38˚C, *x* can be obtained from Table A2.1.

$$M_{38} = xM_{H2O} + (1-x)M_{air} = 0.04413 \cdot 18 + (1 - 0.04413) \cdot 28.97 = 28.48\ g/mol$$

Hence the required diffusion flux over the surface is

$$Dflux_{required} = \frac{\dot{m}}{M_{38}} = 4.0625 \cdot 10^{-4}\ mol/(m^2 s)$$

The diffusion coefficient was calculated using Lennard-Jones potential for 38˚C
$D_{AB} = 0.2354\ cm^2/s$

Concentration of vapor for T=22˚C RH =100% were made using Table A2.1

$$\varrho_{38} = 46.12\ g/m^3$$

$$\rightarrow C_{38} = \frac{\varrho_{38}}{M_{38}} = 1.619\ mol/m^3$$

In the same way, calculations for diffusion coefficient, required diffusion flux and concentration of vapor for T=37˚C RH =100% were made

$$M_{37} = 28.51\ g/mol$$

$$\varrho_{37} = 43.96\ g/m^3$$

$\rightarrow C_{37} = \frac{\varrho_{37}}{M_{37}} = 1.54\ mol/m^3$

$\rightarrow Dflux_{required} = 4.058 \cdot 10^{-4}\ mol/(m^2 s)$

$\rightarrow D_{AB} = 0.2339\ cm^2/s$

B1

Model 1

1. Boundary conditions

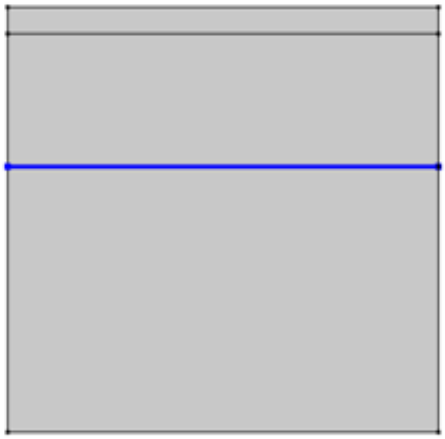

Figure B1.1a Thin layer (Ht), Thin diffusion barrier (Tds), Pointwise constraint (Fp, Br)

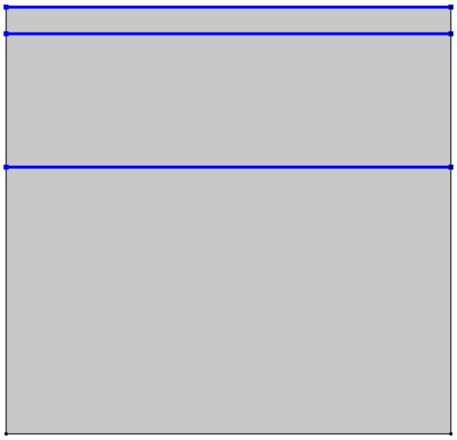

Figure B1.1b Diffuse surface (Fp, Br)

Figure B1.1c Temperature (Ht), Concentration (Tds), No slip wall (Fp, Br)

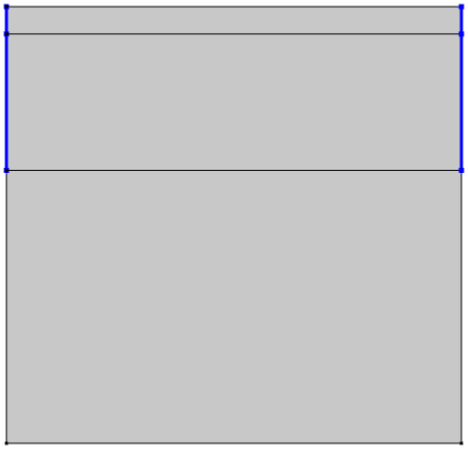

Figure B1.1d Symmetry boundaries (Ht, Br, Tds)

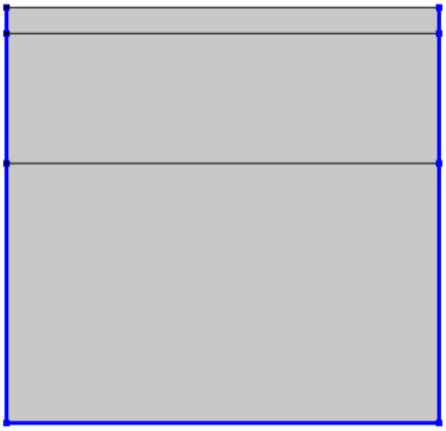

Figure B1.1e Symmetry (Fp)

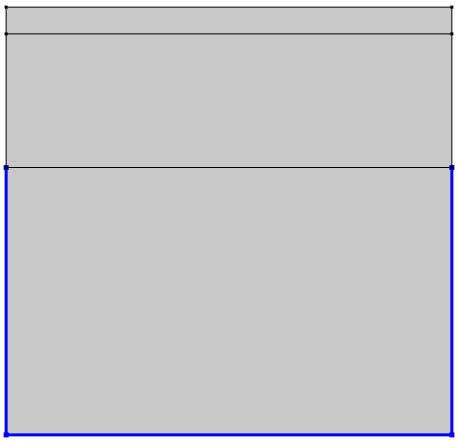

Figure B1.1f Open boundary (Br)

Ht = Heat transfer in porous media module
Fp = Free and porous media flow module
Br = Brinkman module
Tds = Transport of diluted species module

2. Results

Free and porous media flow module

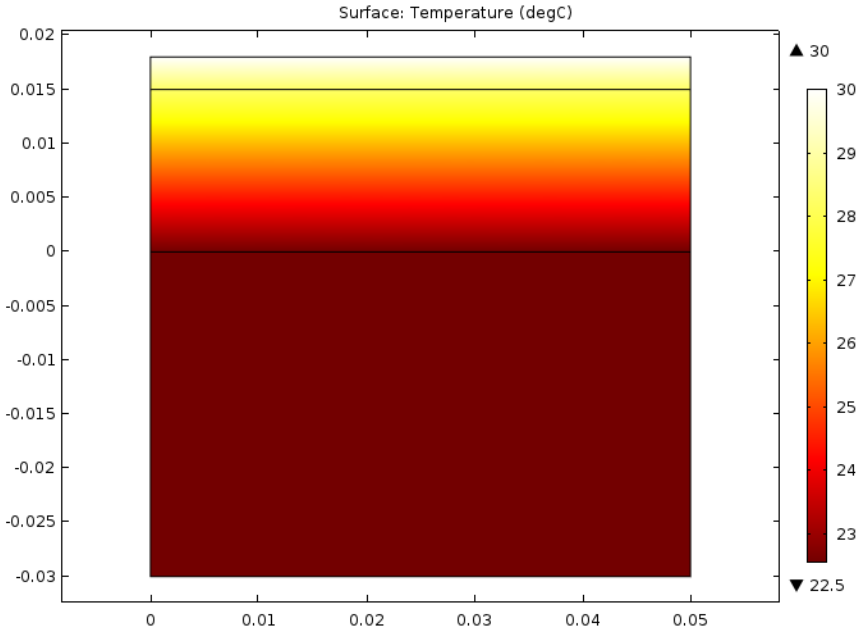

Figure B1.2 Temperature profile (Fp), $\epsilon_p = 0.7$, κ=3.75·10^{-9} m^2

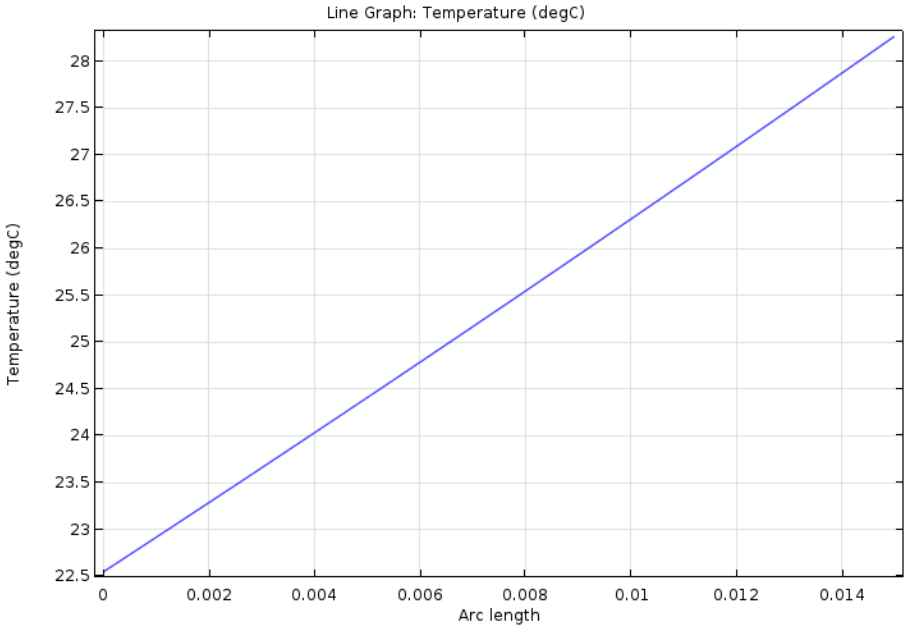

Figure B1.3 Temperature plot over porous domain (Fp), $\epsilon_p = 0.7$, κ=3.75·10^{-9} m^2

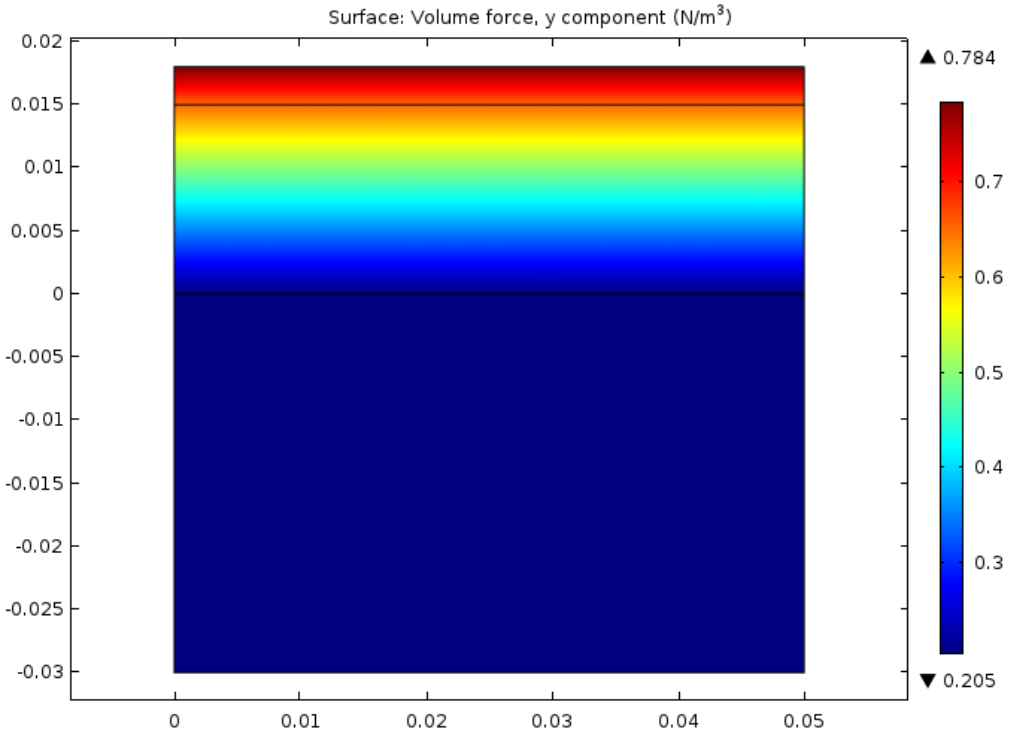

Figure B1.4 Volume force of vapor (Fp), $\epsilon_p = 0.7$, κ=3.75·10^{-9} m^2

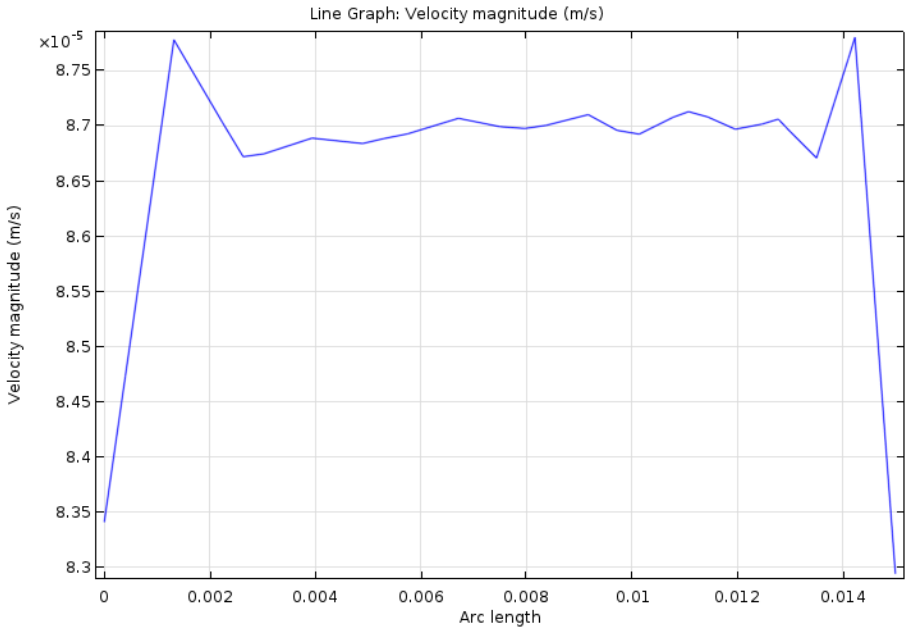

Figure B1.5 Fluid velocity over porous domain (Fp), $\epsilon_p = 0.7$, κ=3.75·10^{-9} m^2

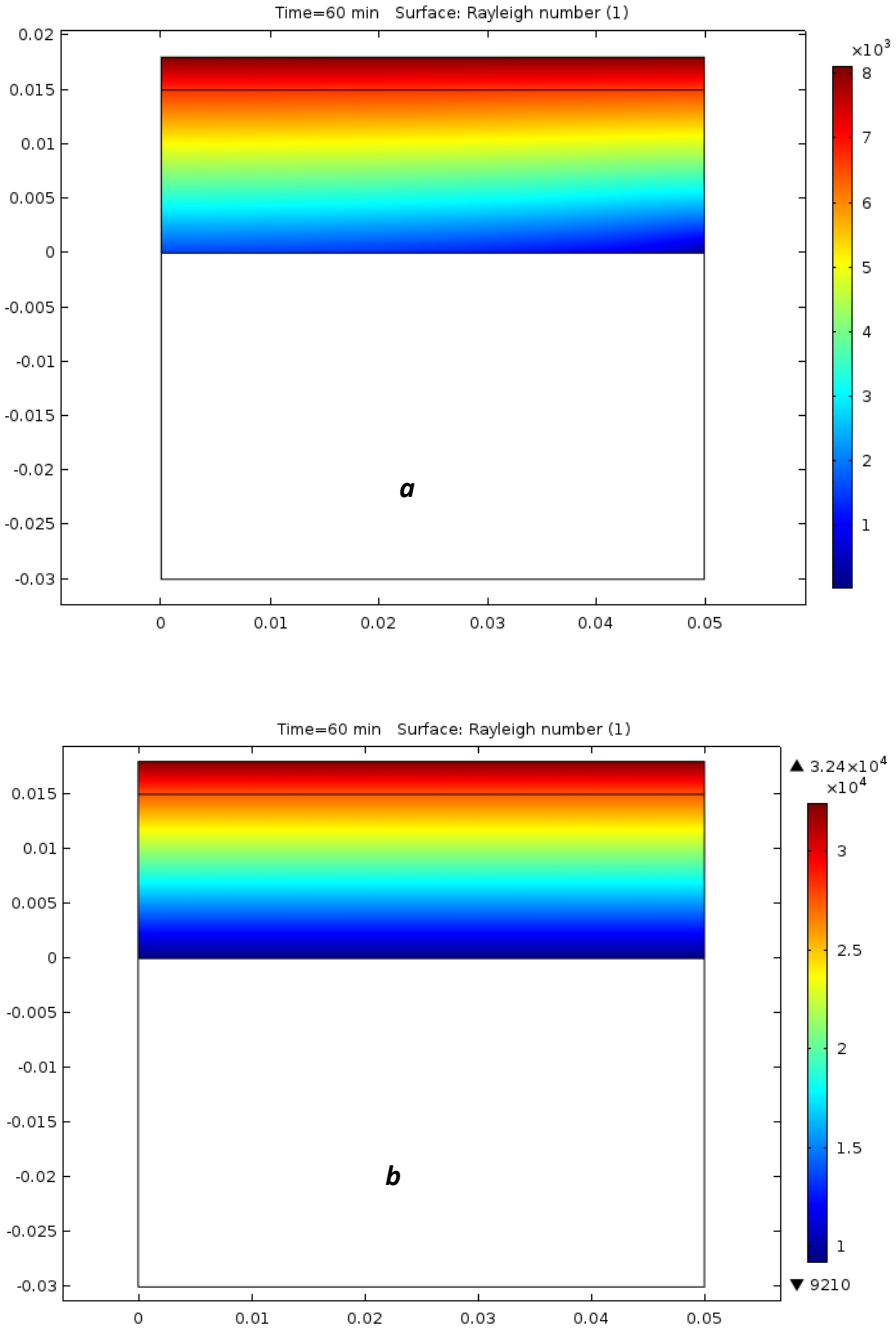

Figure B1.6 Rayleigh number 60min $\epsilon_p = 0.7$, a) κ=3.75·10^{-9} m^2 b) κ=3.75·10^{-9} m^2

Brinkman module

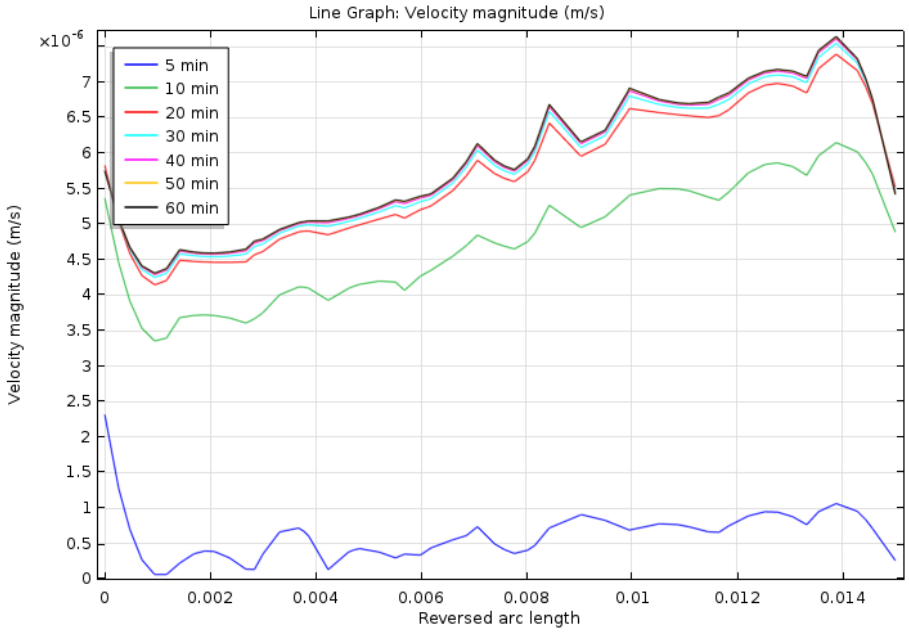

Figure B1.7 Fluid velocity over porous domain $\epsilon_p = 0.7$, κ=3.75·10^{-9} m^2

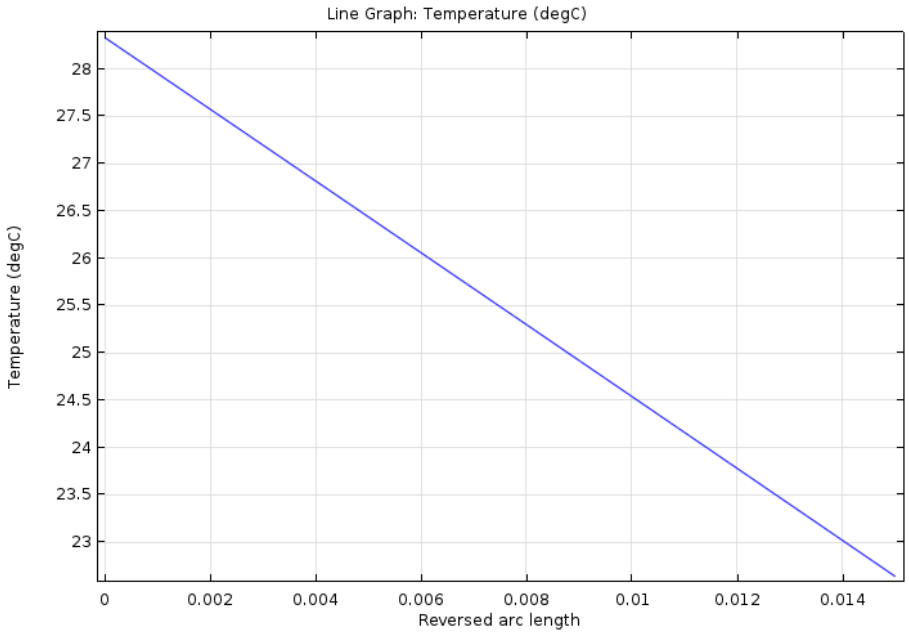

Figure B1.8 Temperature profile over porous domain $\epsilon_p = 0.7$, κ=3.75·10^{-9} m^2

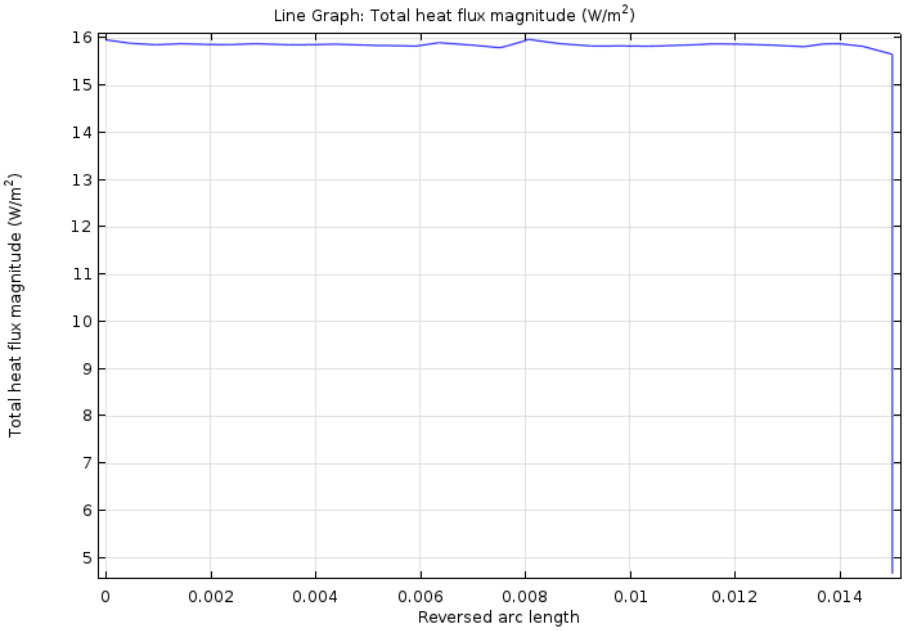

Figure B3.9 Total heat flux through the porous domain $\epsilon_p = 0.7$, κ=3.75·10^{-9} m^2

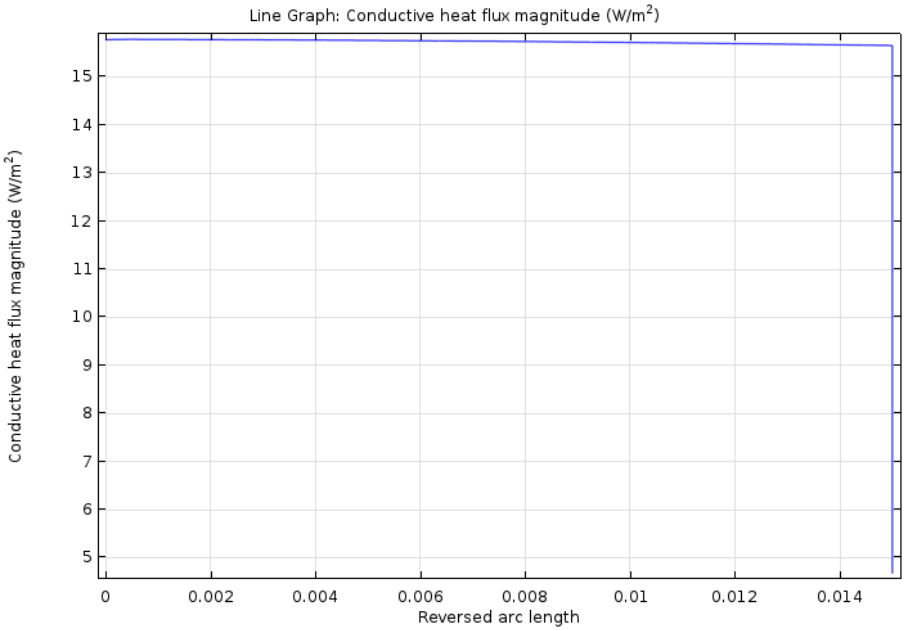

Figure B2.10 Conductive heat flux through the porous domain $\epsilon_p = 0.7$, κ=3.75·10^{-9} m^2

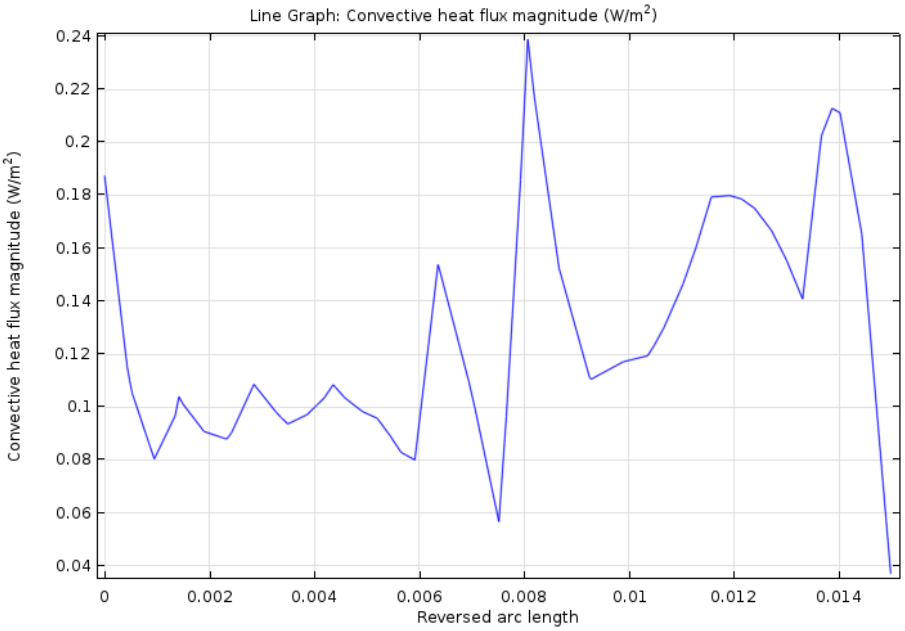

Figure B1.11 Convective heat flux through the porous domain $\epsilon_p = 0.7$, κ=3.75·10^{-9} m^2

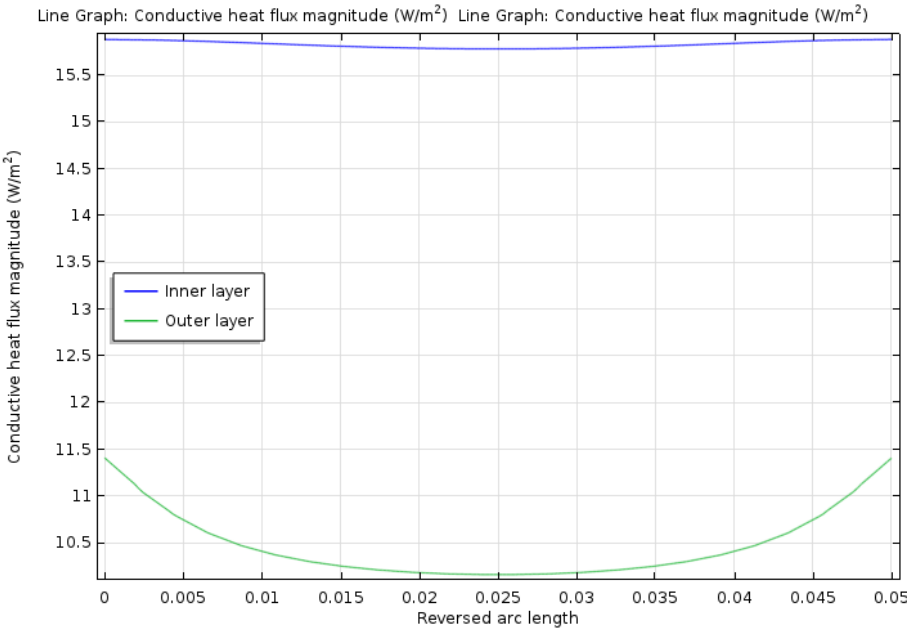

Figure B1.12 Conductive heat flux on inner and outer surface of the porous domain $\epsilon_p = 0.7$, κ=3.75·10^{-9} m^2

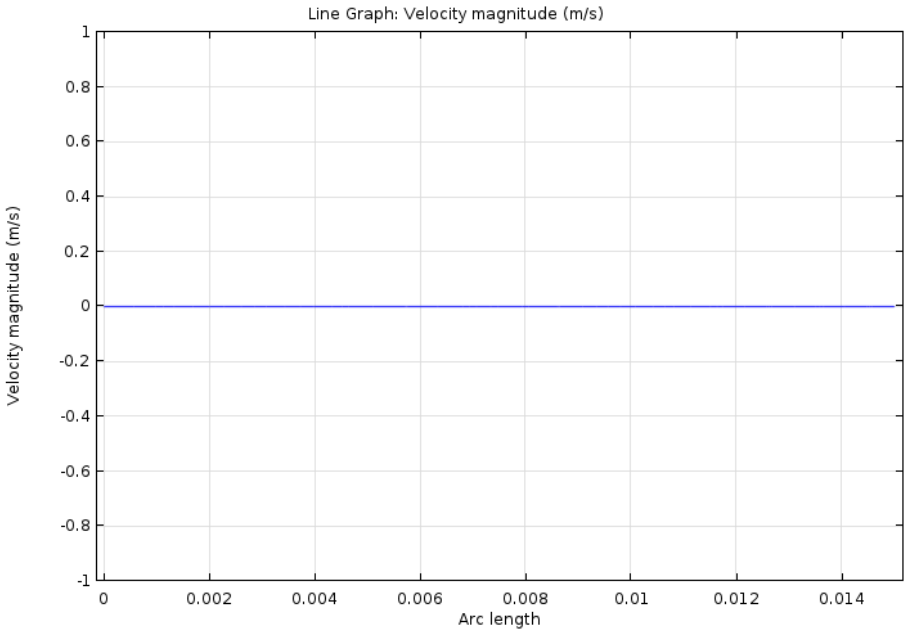

Figure B1.13 Fluid velocity in convection analysis, $u=0$, $\epsilon_p = 0.7$, $\kappa=3.75\cdot10^{-9}\ m^2$

Porosity = 0.9

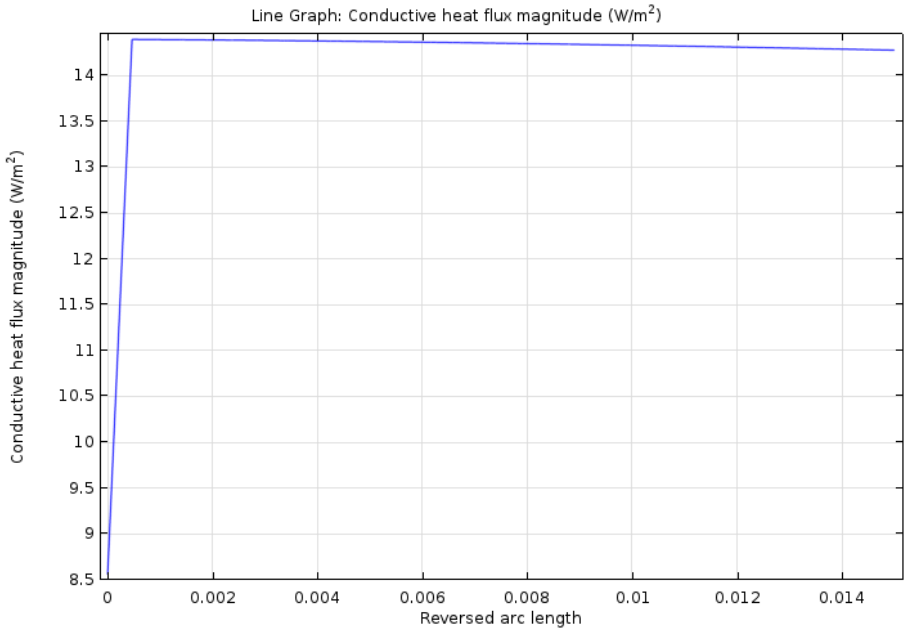

Figure B1.14 Conductive heat flux through the porous domain $\epsilon_p = 0.9$, $\kappa=3.75\cdot10^{-9} m^2$

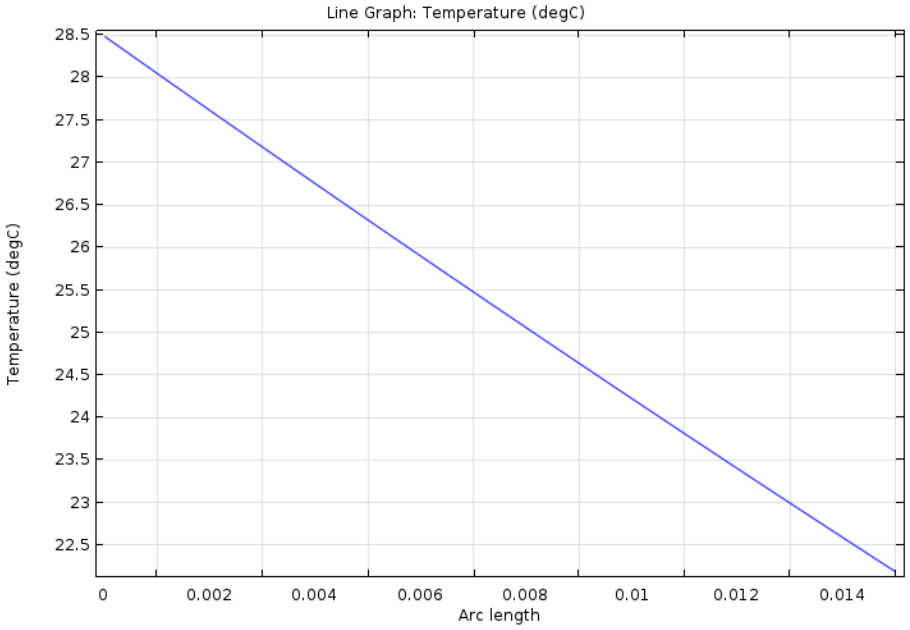

Figure B1.15 Temperature profile through porous media $\epsilon_p = 0.9$, κ=3.75·10^{-9} m^2

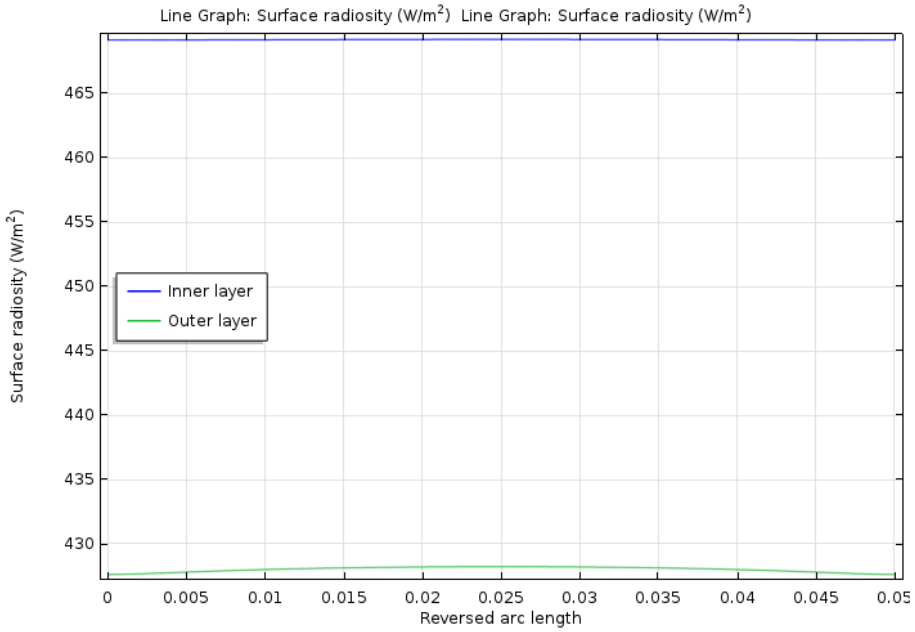

Figure B1.16 Thermal radiation on each surface of porous media $\epsilon_p = 0.9$, κ=3.75·10^{-9} m^2

Permeability = $3.75 \cdot 10^{-11}\ m^2$

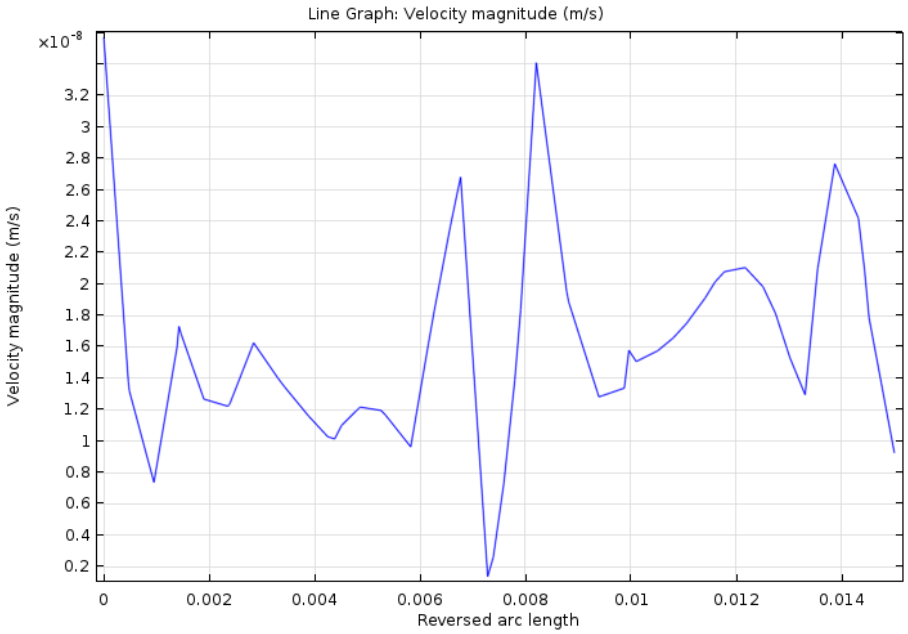

Figure B1.17 Convective heat flux through the porous domain $\epsilon_p = 0.7$, $\kappa = 3.75 \cdot 10^{-11}\ m^2$

B2

Model 2

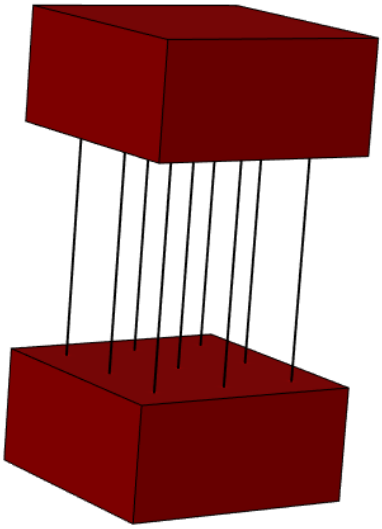

Figure B2.1 Model 2, real size pores

1. Results

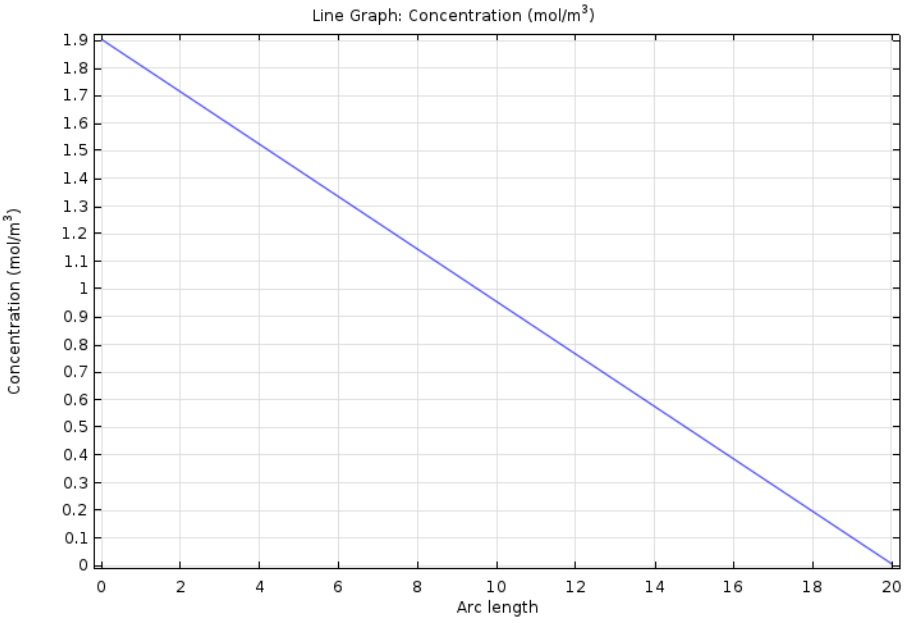

Figure B2.2 Concentration profile over centrum pore

Table B2.1-5 show results from simulations on model 2 with changing pore distance and temperature.

Table B2.1 Required pore area and radius. Pore distance 7µm, Temperature 38˚C

Radius pore [µm]	J pore [mol/(m^2·s)]	Area pore, required [µm^2]	Radius pore, required [µm]
0.03	2.244	0.01047	0.0577
0.05	2.240	0.01049	0.0578
0.09	2.233	0.01052	0.0579
0.10	2.231	0.01053	0.0579
0.12	2.227	0.01055	0.0580
0.15	2.221	0.01058	0.0580
0.17	2.217	0.01060	0.0581
0.19	2.213	0.01062	0.0581

Table B2.2 Required pore area and radius. Pore distance 5µm, Temperature 38˚C

Radius pore [µm]	Jpore [mol/(m^2·s)]	Radius, required [µm]	Area, required [µm^2]
0.03	2.244	0.0412	0.00534
0.05	2.241	0.0413	0.00535
0.07	2.237	0.0413	0.00536
0.09	2.233	0.0413	0.00537
0.10	2.228	0.0414	0.00538
0.12	*	*	*
0.15	2.219	0.0415	0.00540
0.17	2.214	0.0415	0.00541
0.20	2.207	0.0416	0.00543

**Inconclusive result*

$$\text{SAR: } \frac{9 \cdot \bar{A}_{pore}}{A_{bulk}} = \frac{9 \cdot 0.0054}{225} = 0.000215$$

Table B2.3 Required pore area and radius. Pore distance 5µm, Temperature 38˚C

Radius pore [µm]	J pore [mol/(m^2·s)]	Radius, required [µm]	Area, required [µm^2]
0.50	2.117	0.0425	0.00566
0.70	2.094	0.0427	0.00572
0.90	2.041	0.0432	0.00587

$$\text{SAR: } \frac{9 \cdot 0.00575}{225} = 0.000230$$

Table B2.4 Required pore area and radius. Pore distance 7µm, Temperature 37˚C

Radius pore [µm]	J [mol/(m^2·s)]	Radius, required [µm]	Area, required [µm^2]
0.03	2.102	0.0592	0.01100
0.05	2.099	0.0592	0.01102
0.07	2.096	0.0593	0.01103
0.09	2.093	0.0593	0.01105
0.10	2.090	0.0594	0.01107
0.12	2.087	0.0594	0.01108
0.15	2.081	0.0595	0.01112
0.17	2.077	0.0595	0.01114
0.20	2.071	0.0596	0.01117

$$\text{SAR: } \frac{9 \cdot \bar{A}_{pore}}{A_{bulk}} = \frac{9 \cdot 0.0111}{441} = 0.000226$$

Table B2.5 Required pore area and radius. Pore distance 7µm, Temperature 37˚C

Radius pore [µm]	J [mol/(m^2·s)]	Radius, required [µm]	Area, required [µm^2]
0.50	2.007	0.0606	0.01152
0.70	1.960	0.0613	0.01180
0.90	1.911	0.0621	0.01210

$$\text{SAR: } = \frac{9 \cdot 0.0118}{441} = 0.000241$$

Table B2.6 Varying film thickness. Pore distance 7µm, Temperature 38˚C

Thickness film [µm]	J [mol/(m^2·s)]	Radius, required [µm]	Area, required [µm^2]	SAR [%]
20	2.199	0.0583	0.01068	0.02181
30	1.485	0.0710	0.01582	0.03229
40	1.116	0.0819	0.02105	0.04297
50	0.894	0.0915	0.02628	0.05364
60	0.740	0.1005	0.03175	0.06480
70	0.634	0.1086	0.03706	0.07563
80	0.560	0.1156	0.04196	0.08563
90	0.498	0.1225	0.04718	0.09629

B3

Model 3

1. Boundary conditions

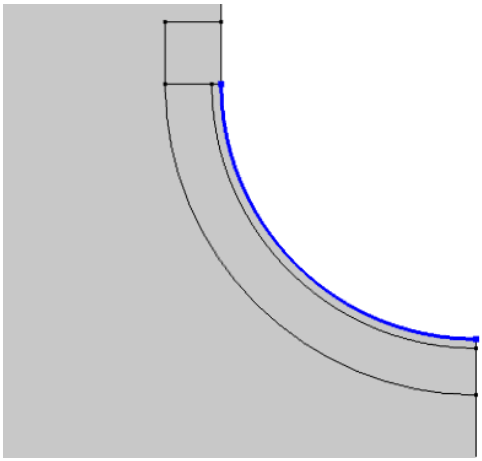

Figure B3.1a Fixed temperature (Ht), fixed concentration (Tds), No-slip (Br)

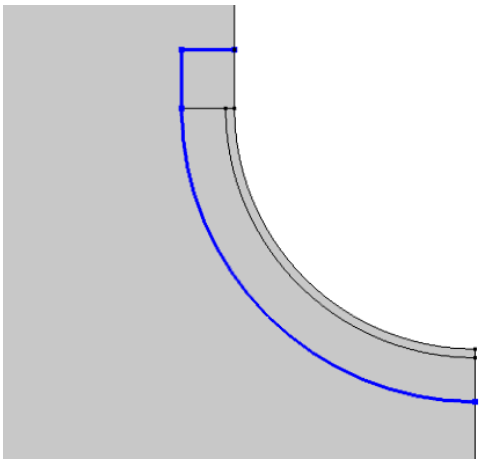

Figure B3.1b Thin layer (Ht), Thin diffusion barrier (Tds) Pointwise constraint (Br)

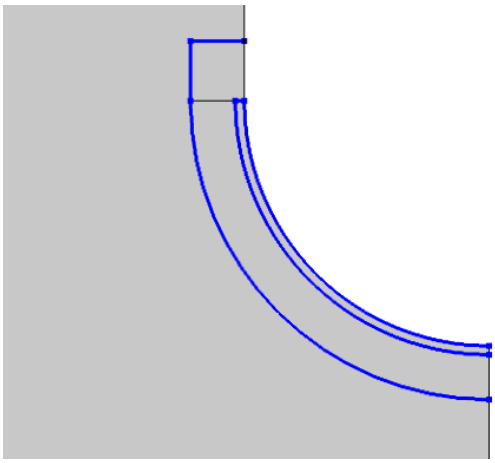

Figure B3.1c Diffusive surface (Ht)

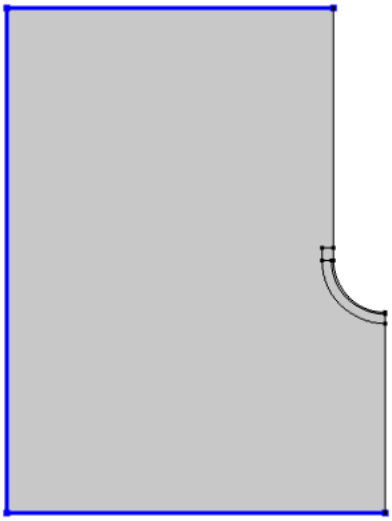

Figure B3.1d Open boundaries (Ht, Br, Tds)

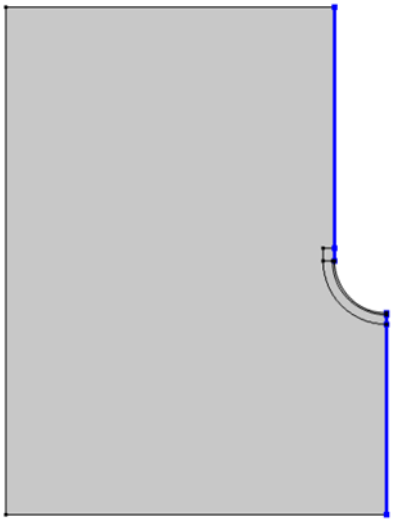

Figure B3.1e Symmetry boundaries (Ht, Br, Tds)

Ht = Heat transfer in porous media module
Br = Brinkman equation module
Tds = Transport of diluted species module

2. Results

Fluid flow

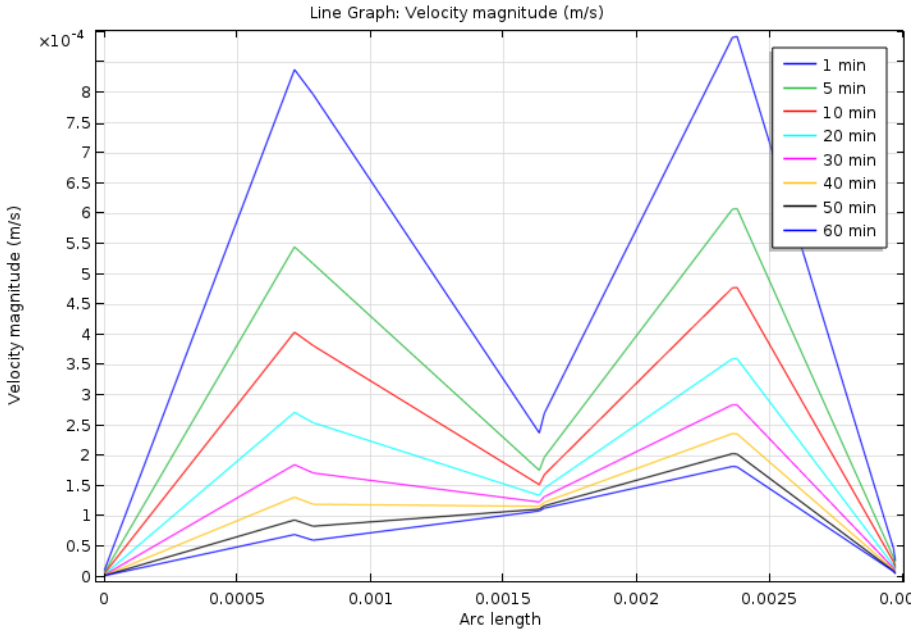

Figure B3.2 Velocity plot over thin layer, $\epsilon_p = 0.7$, κ=3.75·10^{-11} m^2

Heat transport

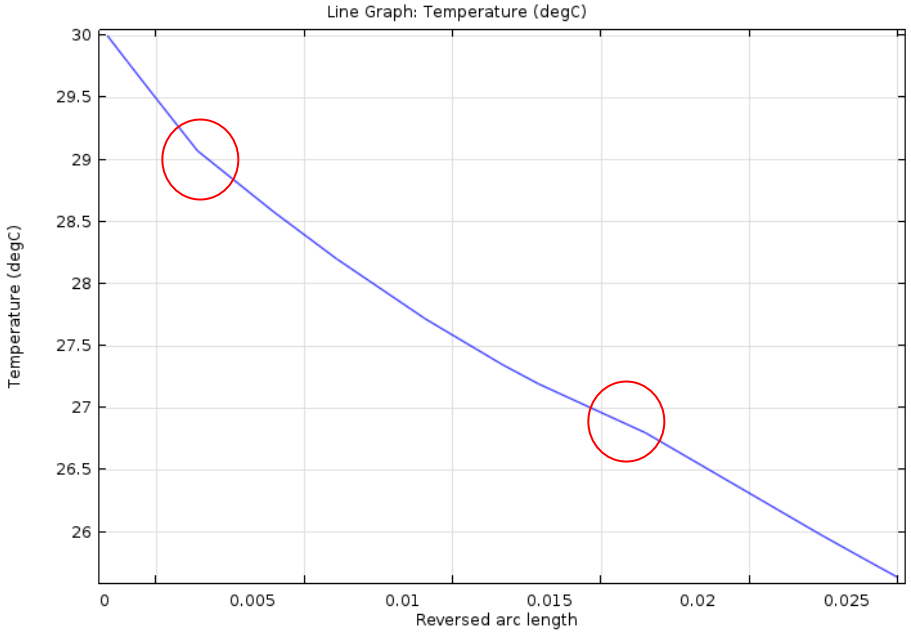

Figure B3.3 Temperature profile, cut line 2, ϵ_p=0.7 κ=3.75·10^{-11} m^2

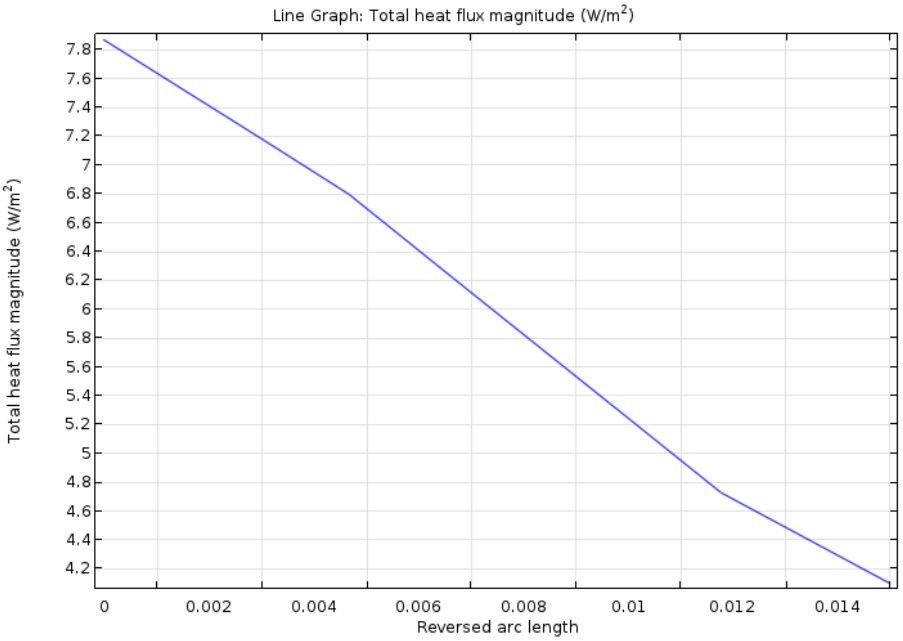

Figure B3.4 Total heat flux cut line 1, ϵ_p=0.7 κ=3.75·10^{-11} m^2

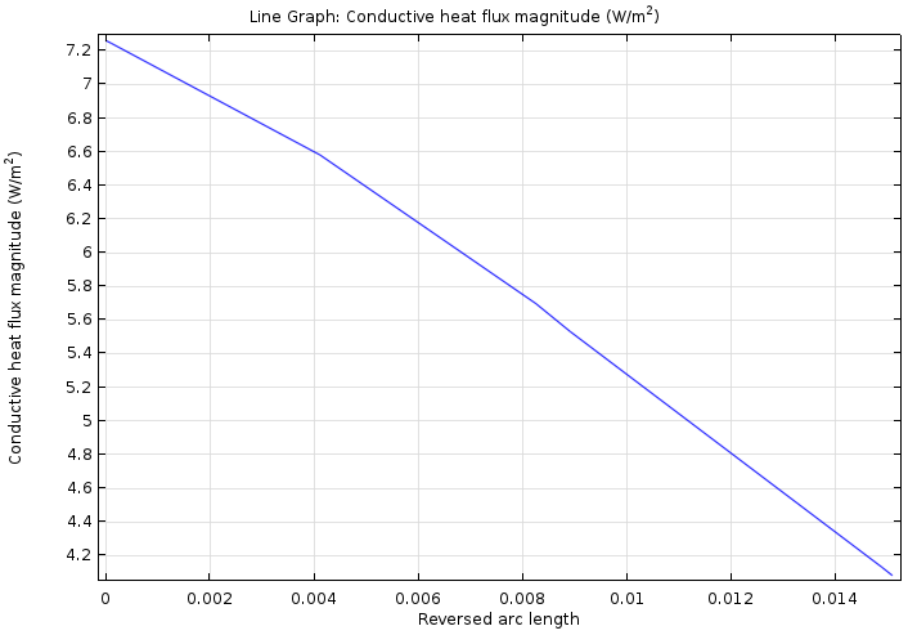

Figure B3.5 Conductive heat flux cut line 1, ϵ_p=0.7 κ=3.75·10^{-11} m^2

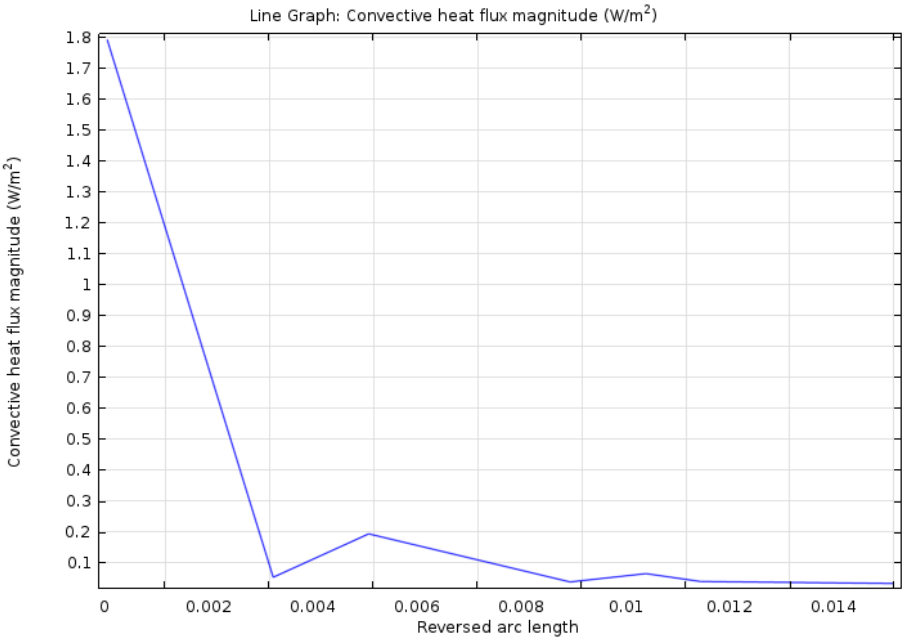

Figure B3.6 Convective heat flux cut line 1, ϵ_p=0.7 κ=3.75·10^{-11} m^2

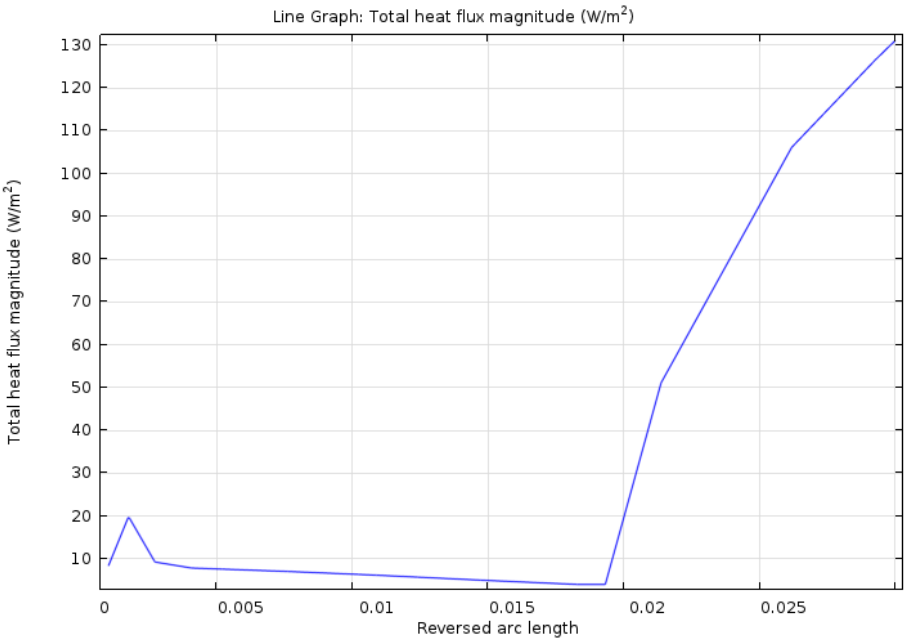

Figure B3.7 Total heat flux cut line 2, ϵ_p=0.7 κ=3.75·10^{-11} m^2

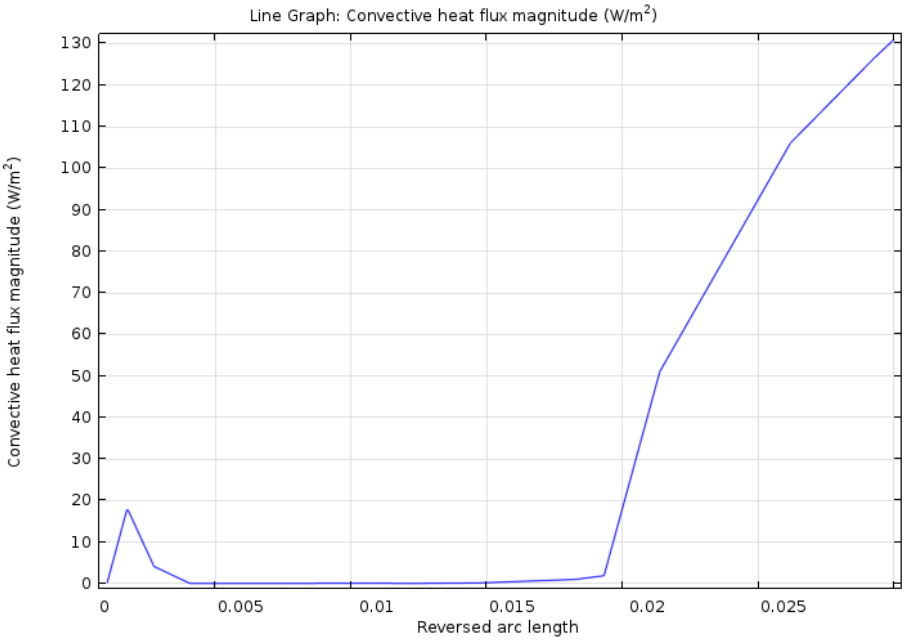

Figure B3.8 Convective heat flux cut line 2, ϵ_p=0.7 κ=3.75·10^{-11} m^2

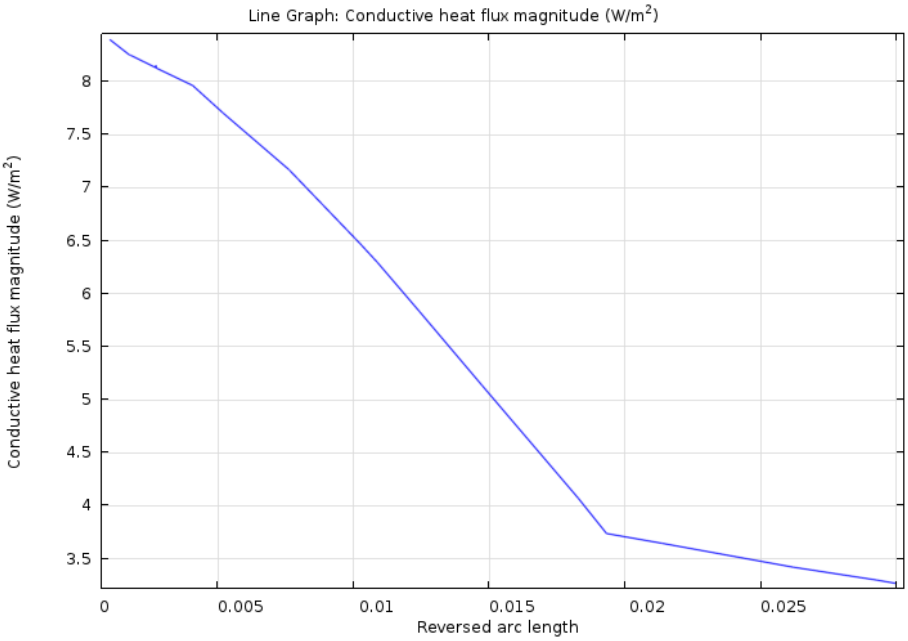

Figure B3.9 Conductive heat flux cut line 2, ϵ_p=0.7 κ=3.75·10^{-11} m^2

Surface radiation

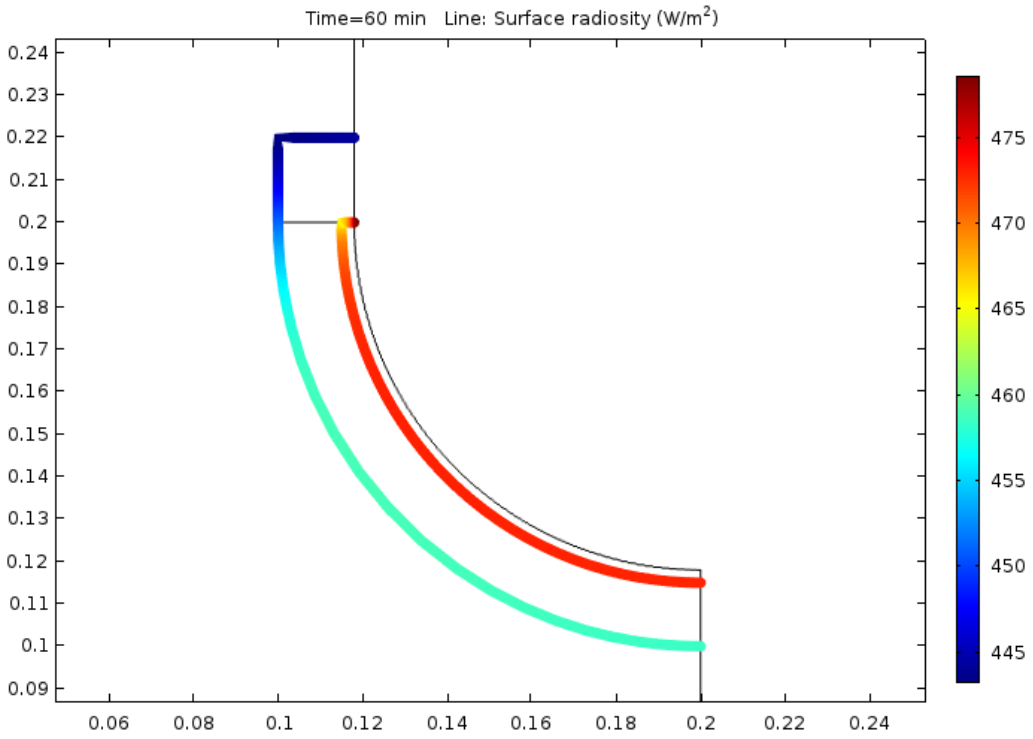

Figure B3.10 Surface radiation, ϵ_p=0.7 κ=3.75·10^{-11} m^2

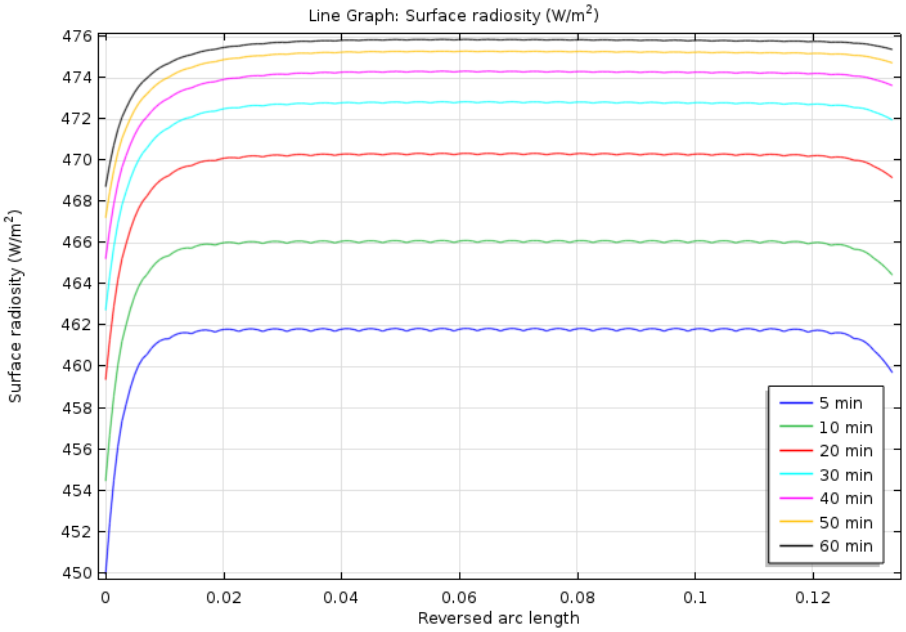

Figure B3.11 Surface radiation on inner surface of the product, ϵ_p=0.7 κ=3.75·10^{-11} m^2

Convection analysis

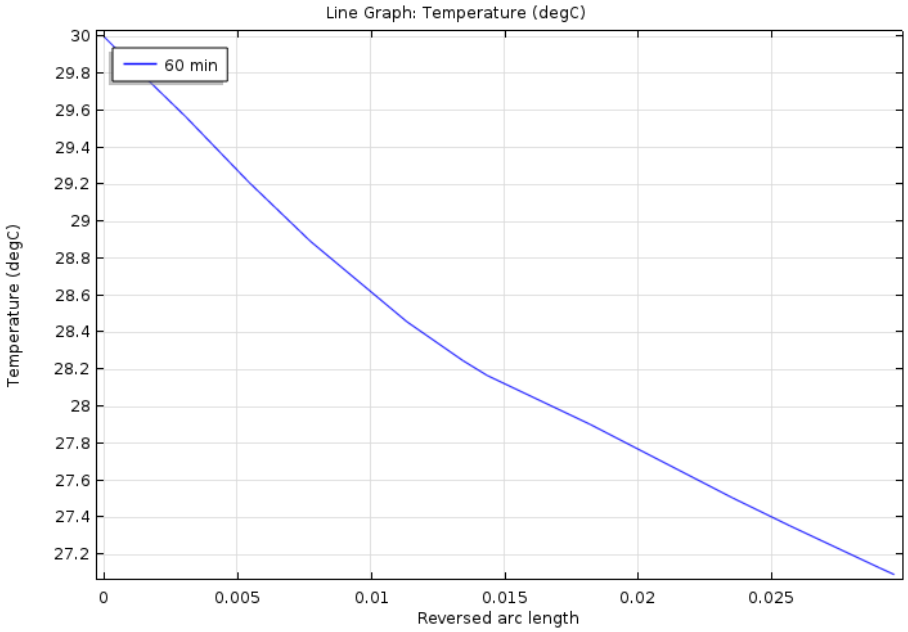

Figure B3.12 Temperature profile cut line 2, $u=0$, $\epsilon_p=0.7$ $\kappa=3.75\cdot10^{-11}$ m^2

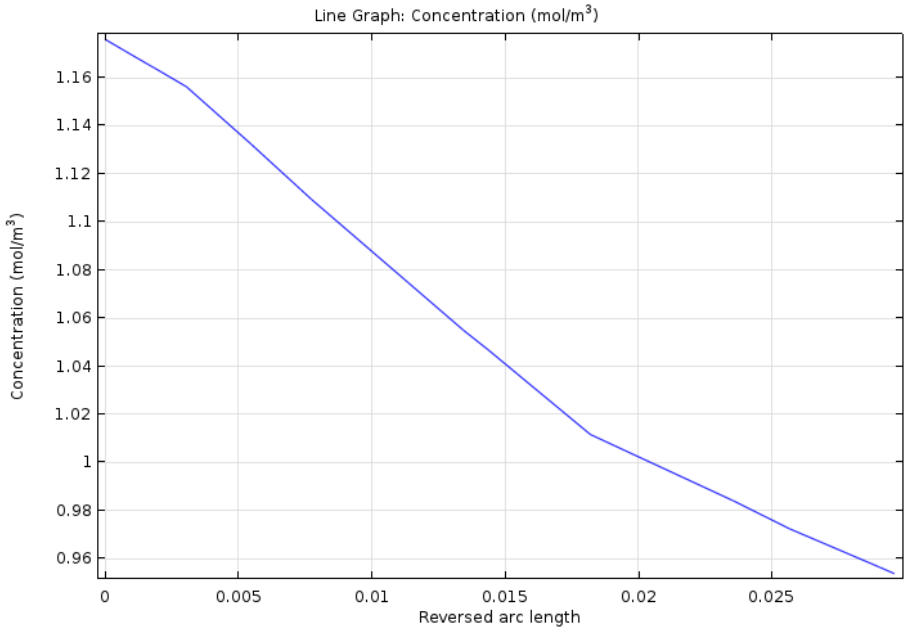

Figure B3.13 Concentration profile cut line 2, $u=0$, $\epsilon_p=0.7$ $\kappa=3.75\cdot10^{-11}$ m^2

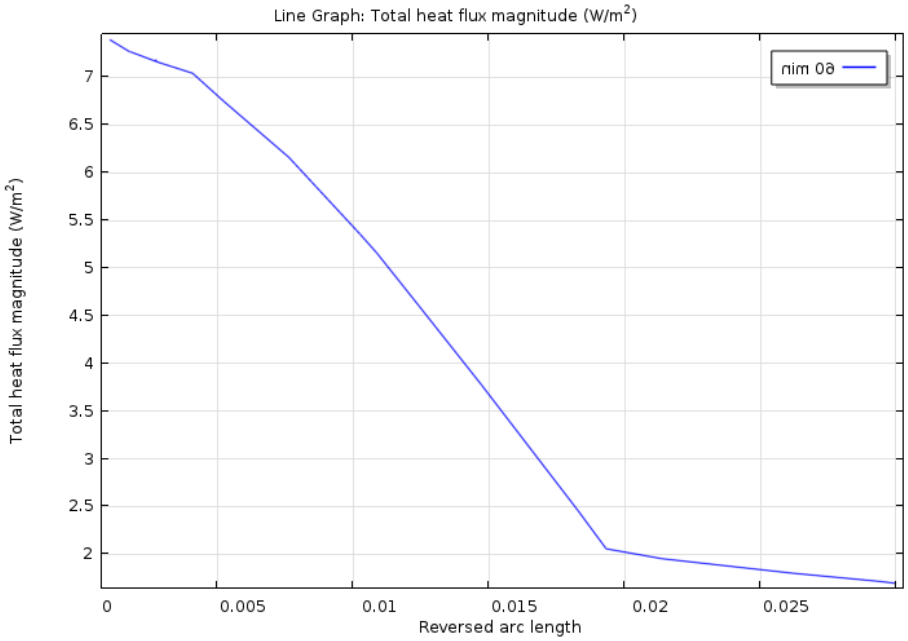

Figure B3.14 Figure B3.7 Total heat flux cut line 2, $u=0$, $\epsilon_p=0.7$ $\kappa=3.75\cdot10^{-11}$ m^2

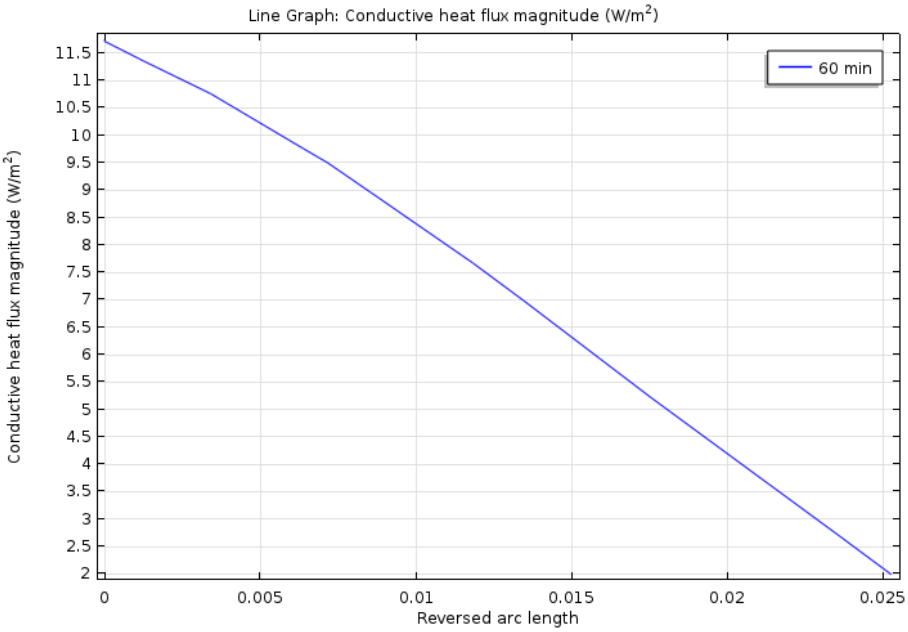

Figure B3.15 Conductive heat flux cut line 1, $u=0$, $\epsilon_p=0.7$ $\kappa=3.75\cdot10^{-11}$ m^2

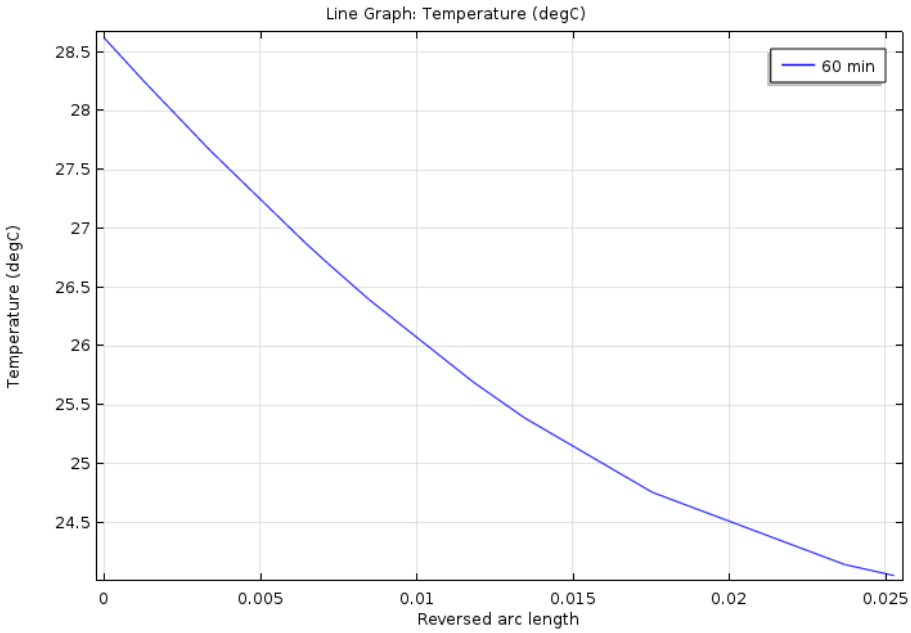

Figure B3.16 Temperature profile cut line 1, *u=0*, ϵ_p=0.7 κ=3.75·10^{-11} m^2

Diffusion

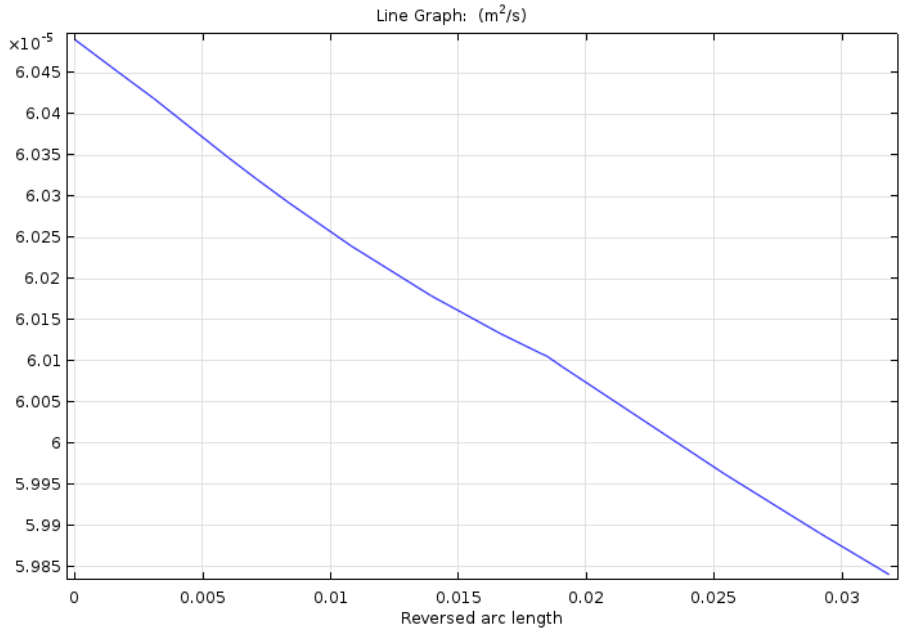

Figure B3.17 Diffusion coefficient cut line 2, ϵ_p=0.7 κ=3.75·10^{-11} m^2

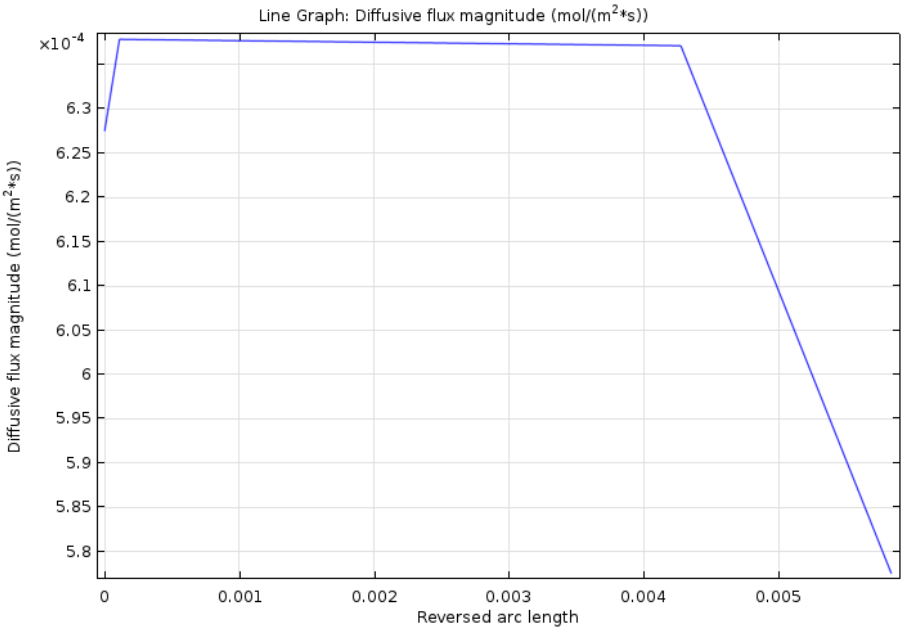

Figure B3.18 Diffusion flux over outer layer, ϵ_p=0.7 κ=3.75·10^{-11} m^2

Porosity = 0.9

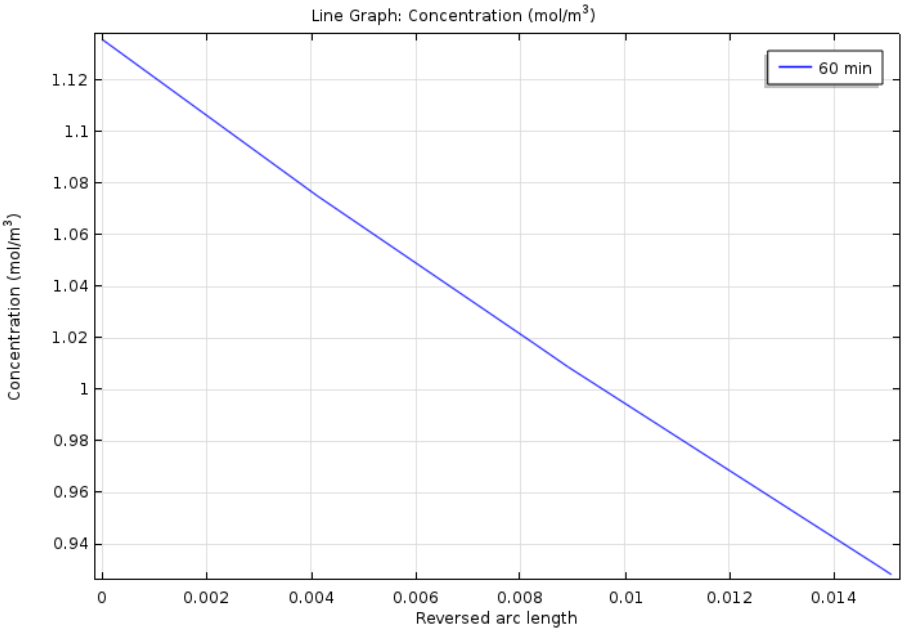

Figure B3.18 Concentration profile cut line 1, ϵ_p=0.9 κ=3.75·10^{-11} m^2